https://doi.org/10.1070/RCR5023

High-entropy alloys: properties and prospects of application as protective coatings

Boris R.Gelchinski, Ilya A.Balyakin, Anatoly A.Yuryev, Andrey A.Rempel

Institute of Metallurgy, Ural Branch of the Russian Academy of Sciences, ul. Amundsena 101, 620016 Ekaterinburg, Russian Federation

Alloys with high configurational entropy fundamentally differ from traditional alloys as they contain not one, but five or more basic elements with concentrations of 5 to 35 at.% each. Owing to the unique elemental composition, high-entropy alloys can have unusual functional properties such as high strength and wear resistance, exceptional heat resistance, good structural stability and good resistance to corrosion and oxidation. The review considers methods of synthesis of high-entropy alloys, methods and results of computer simulation of the high-entropy alloy structures and applications of such alloys as corrosion-, heat- and radiation-resistant materials and biomedical materials. Particular attention is paid to the prospects for the use of such alloys as protective coatings.
The bibliography includes 352 references.

Contents

1. Introduction 1
2. Methods of synthesis 4
2.1. Mechanical alloying 5
2.2. Spark plasma sintering 7
2.3. Bridgman method 8
2.4. Vacuum arc melting 8
2.5. Additive manufacturing 9
3. Methods and results of computer simulation 10
3.1. General statements of thermodynamics 10
3.2. Semiempirical criteria 11
3.3. Density functional theory calculations at 0 K 12
3.4. Special quasi-random structures 12
3.5. *Ab initio* molecular dynamics 13
3.6. Classical molecular dynamics 14
3.7. Cluster expansion method 16
3.8. Free energy calculation 16
3.9. Monte Carlo method 17
3.10. Phase diagram calculation method 18
4. Heat-, corrosion- and oxidation-resistant materials and coatings 18
4.1. Phase composition and microstructure 19
4.2. Mechanical characteristics 19
4.3. Corrosion resistance 20
5. Radiation-resistant materials and coatings 21
6. Materials and coatings for biomedicine 22
7. Properties and applications of protective coatings based on high-entropy alloys 24
8. Note added in proof 25
9. Conclusion 26
10. List of abbreviations and symbols 26
11. References 27

1. Introduction

Metallic materials are traditionally developed starting with the choice of the basic element, which is then doped to obtain the desired combination of performance characteristics in a new product. However, another approach is also possible, namely, fabrication of alloys from approximately equal amounts of several basic elements. According to this idea, in the early 2000s, two research groups headed by Yeh [1–5] and Cantor,[6] working independently in China

B.R.Gelchinski. Doctor of Physics and Mathematics, Head of the Department of Materials Science, Chief Researcher at the Laboratory of Powder and Composite Materials, IMET UrB RAS.
E-mail: brg47@list.ru
Current research interests: computer simulation of topologically disordered systems, nanomaterials, high-entropy alloys, plasma methods for the formation of protective coatings.
I.A.Balyakin. Post-graduate of UrFU, Junior Researcher at the Laboratory of High-Entropy Alloys of IMET UrB RAS.
E-mail: i.a.balyakin@gmail.com
Current research interests: high-entropy alloys, *ab initio* calculations, molecular dynamics, machine learning, artificial neural networks.
A.A.Yuryev. PhD in Physics and Mathematics, Senior Researcher at the Laboratory of Powder and Composite Materials of IMET UrB RAS, Associate Professor at the Department of Metallurgy, Iron and Alloys of the Institute of New Materials and Technologies, UrFU.
E-mail: yurev_anatolii@mail.ru
Current research interests: electronic and atomic structure and properties of disordered systems, *ab initio* calculations, molecular dynamics, high-entropy alloys, melts.
A.A.Rempel. Academician, Doctor in Physics and Mathematics, Director of IMET UrB RAS, Head of the Laboratory of High-Entropy Alloys of IMET UrB RAS, Professor at the Department of Physical Methods and Instruments of Quality Control, UrFU.
E-mail: rempel.imet@mail.ru
Current research interests: high-entropy alloys, structural defects, disorder – order phase transitions, quantum size effects, nanomaterials, nanotechnologies.

Translation: Z.P.Svitanko

Received 1 May 2021

© 2022 Uspekhi Khimii, ZIOC RAS, Russian Academy of Sciences and IOP Publishing Limited

(Taiwan) and UK, respectively, developed almost simultaneously a conceptually new type of materials — high-entropy alloys (HEAs).†

It is of noteworthy that actually the first mention of HEAs was made in a paper called Multimetal Cocktail by Ranganathan,[7] who noted that Yeh *et al.*[1] (the paper was accepted for publication in 2003) proposed a new approach to the fabrication of alloys with desired functional properties. Yeh and co-workers noted in a review[8] that they proposed this new concept for the first time in 1996.[9] Meanwhile, Cantor *et al.*[10, 11] claimed that the pioneering detailed investigation of alloys consisting of multiple main components was undertaken in 1981 by Vincent[12] and was continued in 1995 by Knight.[13]

In recent years, the number of studies of multicomponent high-entropy alloys has increased, because specialists have realized the potential of these alloys for the design of materials with enhanced performance characteristics. The multicomponent alloys containing a large number of components in equal (or nearly equal) concentrations and possessing very high performance characteristics have been called high-entropy alloys. It is believed that high mixing entropy is the major factor responsible for the fact that multicomponent alloys are formed as single-phase solid solutions. Depending on the chosen alloying system, the HEA matrix phase may be represented by a simple solid solution or by a more complex system consisting of several phases (ordered or intermetallic phases). High-entropy alloys substantially differ from known materials or conventional alloys. The properties of equiatomic HEAs are determined by the presence of atoms with different size and electronic structure in the crystal lattice, which gives rise to a considerable lattice distortion. This favours pronounced strengthening and stability of properties of HEAs. The reduced Gibbs free energy ensures the stability of a solid solution during the subsequent high-temperature treatment.

A US patent[14] granted to Chinese scientist Yeh describes the key principles and methods for the fabrication of HEAs that comprise 5–10 major chemical elements (in concentrations from 5 to 30 at.%) and some minor components (in concentrations <3.5 mol.%). The alloys existing in the following systems were initially chosen for investigations:[1, 14–19] Al–Co–Cr–Cu–Fe–Ni, Co–Cr–Cu–Fe–N–Ti, Al–Ti–V–Fe–Ni–Zr, Mo–Ti–V–Fe–Ni–Zr and Cu–Ni–Al–Co–Cr–Fe–Si. Some authors (see, *e.g.*, Refs 1 and 6) synthesized and studied even 16- and 20-component systems.

The studies showed that the entropy of these materials increases with increasing number of elements; nanostructures and even amorphous phases can form due to substantial lattice distortions caused by different atomic radii of substitutional elements. This is accompanied by a decrease in the diffusion and crystallite growth rates.[20–26]

It is presumed that apart from usual properties of metallic alloys, HEAs would possess unusual properties inherent in metal ceramics such as high hardness and durability, age hardening, positive hardening temperature coefficient, high-level strength characteristics at elevated temperatures, wear and corrosion resistance and some other properties. The publication activity on this subject is increasing from year to year (Fig. 1), indicating high promise of this research field.

† Intensive studies carried out during the last ~20 years have not yet confirmed the high-entropy effect for this type of alloys; therefore, the name multi-principal element alloys was proposed for them. However, the original term high-entropy alloys is still widely used.

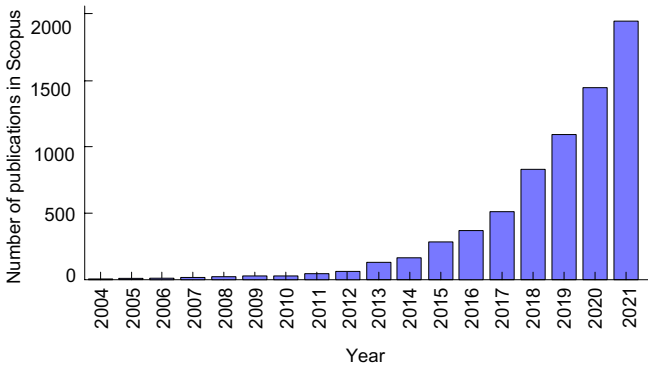


Figure 1. Number of publications on HEAs from 2004 to 2021. The Figure was created by the authors using Scopus database.

It is pertinent to consider the position of HEAs among the sorts of condensed matter, the range of which is permanently extended. Initially, it was enough to classify the physical state of any matter as solid (crystalline), liquid or gas, but in the last decades, quite a few compounds existing between the solid and liquid states were discovered and synthesized. The general classification of such compounds in the order of decreasing short- and long-range order was proposed by Wang and Fernandez-Matrinez.[27] A variant of this classification extended by adding HEAs is depicted in Fig. 2. These alloys are located between amorphous solids and nanocrystals, since nanocrystals still have small areas (1–100 nm size) in which a repeated unit cell can be distinguished. Apparently, HEAs do not have such areas, but the degree of ordering in them is higher than in amorphous solids, as there are regularly (according to the crystal lattice) arranged units with disordered atoms of various elements.

Considerable research attention is drawn to the polyfunctional nature of these multicomponent metallic systems and their applicability for studying fundamental problems related to the formation and stability conditions of solid solutions. Initially, it was assumed that the formation of solid solutions is due to high configurational entropy of equiatomic alloys. However, it was found experimentally

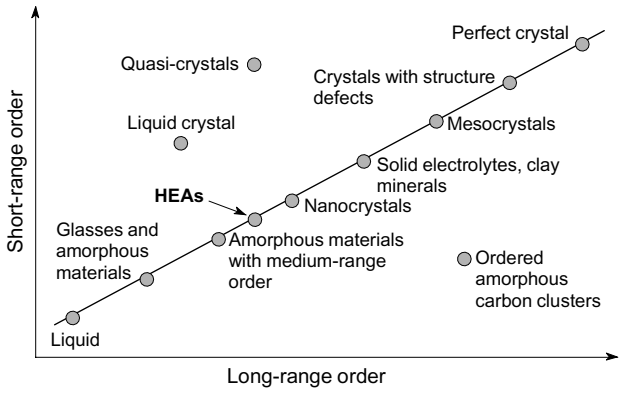


Figure 2. Classification of types of condensed matter. The Figure was created by the authors using published data.[27]

that not any multicomponent system can produce a single-phase solid solution.[8, 18, 28–36] Furthermore, an increase in the number of components in an alloy promotes the formation of numerous intermetallic compounds and deteriorates the performance.[6, 10, 29] A large number (several hundred) of HEA compositions have been studied to date; their structures and some properties (mainly mechanical) were determined. Numerous reviews (see, for example,[8, 37–44]) and monographs[45, 46] on this subject appear.

These reviews and chapters of monographs differ in the number of covered issues and in the level of detail of discussion. Some reviews[8, 37–39] comprehensively analyze the problems of HEA synthesis and properties, while the paper by Pogrebnjak *et al.*,[40] in addition, comprehensively describes the preparation methods, studies of functional properties and applications of nitride coatings. More specialized reviews concentrate on films and protective coatings, considering their preparation, properties and applications. Perhaps, the most comprehensive review[37] is devoted to analysis of the concept of HEAs and related notions. In particular, it was noted that the studies of HEAs stimulated new ideas and investigation of compositionally diverse materials covered by the notion multi-principal element alloys (MPEAs). The authors analyzed this notion, carried out a thermodynamic investigation of complex concentrated alloys (CCAs), and thus made the following important conclusions. Although the classical thermodynamic laws are invariable, the patterns of application of these laws to MPEAs may differ from those for conventional alloys. There are several factors that are responsible for the presence of a multitude of alloys that have different compositions without any consequences for the entropy or types of existing phases. Thus, the authors assigned materials corresponding to the above definitions (MPEAs and CCAs) to the HEA-like category; this alsop applies to concentrated ternary and quaternary alloys that do not correspond to the definition of HEAs, but still have features that promote research into MPEAs and CCAs.

Tsai and Yeh[8] gave a brief account of some aspects of HEA properties, *e.g.*, basic effects, phases and crystal structures, mechanical and high-temperature properties, structural stability and corrosion resistance. The authors discussed some unsolved issues and possible applications of HEAs as hydrogen storage materials, radiation and electromagnetic shielding materials, antibacterial agents, *etc*. It is noted that researchers of HEAs have, metaphorically speaking, a plethora of new alloys opened for them; however, the understanding of the nature of these new materials is still superficial. In order to evaluate the potential of HEAs, it is necessary to know the properties of the constituent elements and to study the possible combinations of these elements. Zhang *et al.*[38] considered the physical, magnetic, chemical and mechanical properties of HEAs. Examples of alloys with promising properties were presented and discussed. For example, high wear resistance was found for the $Co_{1.5}CrFeNi_{1.5}Ti$ and $Al_{0.2}Co_{1.5}CrFeNi_{1.5}Ti$ high-entropy alloys; high strength at room temperature was characteristic of AlCoCrFeNi and high strength at elevated temperatures was inherent in NbMoTaV. The overall corrosion resistance of $Cu_{0.5}NiAlCoCrFeSi$ was markedly higher than that of stainless steel 304.

The concept of high entropy opens up a new way for the design of upgraded materials with unique properties that cannot be attained by microdoping of only one major element. A review by Pickering and Jones[39] is devoted to analysis of the proper notion of high-entropy alloys; the authors gave a critical evaluation of the principles of their formation and investigation prospects. The authors claim that evaluation of these principles with allowance for obtained experimental data and the use of classical physicochemical approach led them to the conclusion that effects caused by high entropy may be less pronounced than initially believed: it appears that the effect of entropy stabilization is not universal, evidence for the HEA lattice deformation is insufficient, and the diffusion kinetics is not necessarily abnormally slow compared to the kinetics typical of conventional alloys.

Nevertheless, it is clear that studies of HEAs stimulate development of materials science. Valuable data were reported by Pogrebnjak *et al.*[40] The authors analyzed and summarized the data on different preparation methods and properties of HEAs, which are most often single-phase solid solutions, and carried out comparative analysis of the properties of protective coatings with different elemental compositions deposited by various methods. It was noted that unique physicochemical properties of HEAs such as corrosion resistance, high thermal stability, wear resistance, strength, *etc*., extend the scope of applicability of these systems. Lewin[41] reported in-depth, comprehensive data devoted to a relatively narrow topic: new functional materials based on multicomponent nitrides. The author summarized data on multicomponent nitrides that form coatings comprising solid solution phases together with simple crystalline structures. The research problems that can be solved by combining the methodology of materials science with modern analysis and control methods are discussed. The latter implies advanced processing of big data arrays using elements of artificial intelligence and machine learning, which help to evaluate experimental and theoretical results. This methodological change is necessary in order to take full advantage of the potential of multicomponent materials.

The surface doping of materials reduces the consumption of rare and expensive chemical elements in comparison with their consumption in the case of bulk doping. Li *et al.*[42] critically considered the state-of-the-art concepts, design principles and microstructural and mechanical changes that take place during the manufacture and post-treatment of HEA-based coatings. In addition to anticorrosive properties and radiation resistance, other surface properties of HEAs were also analyzed. The trends of development of fundamental studies of HEA-based coatings are discussed, including the preparation methods, functional properties and possible applications. A review by Li *et al.*[43] is devoted to methods of development and analysis of available data on the properties of HEA coatings and films. The basic definitions of thin films and coatings are formulated and their production processes, microstructure and functional properties are discussed. In addition, the possible approaches and criteria for the design of alloys with enhanced properties are considered and the directions for future research of HEA-based films and coatings are outlined.

A small review paper[44] considers data on HEA films. Methods for their synthesis, selection of the elemental composition, structure, phase composition and various performance properties are described and prospects for practical application of the films are discussed. Some chapters of multi-author books[45, 46] are devoted to deposition methods and performance characteristics of coatings.

Murty *et al.*[45] considers a rather narrow subject matter concerning coatings for building structures, with emphasis being placed on their mechanical properties and oxidation resistance.

Gao *et al.*[46] discussed not only the properties of HEA coatings, including ceramic ones, but also preparation methods. The discussion covered typical thick and thin layered coatings made of HEAs and HEA-based materials. These coatings are deposited using appropriate techniques and may improve the quality of parts or products by increasing their thermal stability and wear and corrosion resistance. The thermal spraying technique can be used to deposit HEA layers with a thickness from tens to hundreds of micrometres and even to a few millimetres, while sputtering technology produces thin films that are submicrometre to a few micrometres thick. If an appropriate reaction gas is used during the deposition, it is possible to produce HEA films containing nitrogen or carbon (or nitrogen and carbon) or oxygen. The authors noted good prospects for HEA application as biomedical, antibacterial, anti-sticky, hydrophilic and hydrophobic coatings, as well as for protection against electromagnetic interference.

In recent years, numerous national and international conferences devoted to HEAs have been held.[47–51] In Russia, the first conference [51] on HEAs took place in 2019 (the conference became annual). Conferences under the name *World Congress on High Entropy Alloy*s were held in the USA in 2019 and 2020.[49, 50] The *International Conference on High Entropy Materials* and the *International Conference on High Entropy Alloys* took place in Germany (Berlin) [47] and in Austria (Graz) [48] in 2020 and 2021, respectively. However, no systematic research of the physicochemical and physicomechanical properties of HEAs over broad concentration and temperature ranges has been carried out as yet and specific features of the formation of protective HEA coatings have not yet been elucidated. However, it is understood that the problem of thermodynamic stability of a single-phase multicomponent solid solution is very complicated and requires thorough integrated investigations.[29, 36, 52]

The structure of this review is dictated by its subject matter. As follows from the title, the review is devoted to analysis of studies of HEAs and the possibility of HEA application as protective coatings. The fabrication of protective coatings is the most promising and economically viable practical use of HEAs owing to their good performance characteristics. The first three Sections address the general views on HEAs, methods for their synthesis and computer simulation of their structure. Analysis presented in Section 2 demonstrates that ~40 elements in various combinations (of five and more elements) can potentially be used to prepare HEAs; this opens up the possibility of preparing numerous HEAs with exceptional characteristics. Section 3 successively considers the general thermodynamic issues, semiempirical criteria, density functional theory (DFT), a method for generating a correct arrangement of atoms that is used to study special quasi-random structures (SQS), and classical molecular dynamics (MD) and *ab initio* MD (AIMD) methods. The contribution of machine learning techniques to the generation of potentials for classical MD is indicated. Among statistical mechanics approaches, cluster expansion, Gibbs energy calculation, Monte Carlo method and calculation of phase diagrams (CALPHAD) are discussed.

Section 4 deals with the application of HEAs as heat-resistant and corrosion- and oxidation-resistant materials and coatings. A Table summarizing data on refractory alloys obtained in recent years is given. It is noted that, despite the statements of many authors about the good prospects for HEA application as heat-resistant materials, by no means all of them address the high-temperature strength of the alloys. Coatings based on HEAs are considered and data on substrate–coating combinations, with indicated methods of synthesis and properties of the coatings are given. High interest of specialists in this research area is emphasized.

Section 5 is devoted to the radiation resistance of HEAs and coatings based on them; specialists in nuclear and nuclear fusion energy put a lot of hope on these systems. Materials and coatings for modern biomedicine are characterized in Section 6. This application of HEAs is one of the most important and promising; therefore, it receives particular attention here. In Section 7, we give a brief review of the properties of HEA-based protective coatings.

2. Methods of synthesis

The preparation of high-entropy alloys, which are multicomponent solid solutions without long-range order and with pronounced lattice distortions, is a complicated task. Depending on the composition and desired characteristics of the alloy, various approaches are used for the preparation. The variety of methods for HEA synthesis can be classified in terms of the initial physical state of substances — gaseous, liquid or solid. The following main methods are used:

— mechanical alloying (MA) based on the use of dynamic strain of mixtures of powdered components in high-energy ball mills with various power density and milling time; this ensures mass transfer and chemical reaction between the powders. For increasing the sample uniformity and density, hot-pressing sintering (HPS) is additionally performed at a temperature equal to 0.5–0.8 of the melting point of the major component, which ensures good sintering;[53–68]

— spark plasma sintering (SPS); this method is an alternative to hot pressing; in this case, sintering and compaction are provided by the current passed through the sample;[69–84]

— Bridgman method is the earliest one; it is based on heating of the starting materials above the melting point and slow cooling in a special container; the alloy is gradually formed along the whole length of the container (in the horizontal or vertical orientation), which is usually rotated; this method is less popular than other methods, but it has been used to prepare HEAs, *e.g.*, by Zhang and co-workers;[85, 86]

— vacuum arc melting (VAM) method according to which the heat for metal heating and melting is provided by an electric arc compressed in the transverse direction;[87–91]

— additive method that consists in layer-by-layer fabrication of any product from powders on the basis of a computer 3D model.[92–95]

The results of HEA syntheses performed in recent years by the methods listed above are summarized in Table 1. A more detailed analysis of HEA synthesis and properties that were improved is given below.

Table 1. High-entropy alloys and their structures synthesized by various methods.

Alloy	Method of synthesis	Structure	Ref.
$FeCoCrNiMnTi_{0.1}C_{0.1}$	MA + HPS	FCC and minor amount of M23C6, M7C3 phases	53
CoCrFeMnNi	MA (deformation under pressure)	Single-phase nanocrystalline alloy	54
	MA + vacuum HPS	Nanocrystalline FCC powders	61
	MA + shock wave compaction	FCC phase	62
	MA (drawing on a steel substrate)	FCC phase	63
CoCrFeMnNi + Y_2O_3 nanoparticles	MA	FCC phase + uniform oxide inclusions	64
CoCrFeMnNi + SiC nanoparticles	MA + HPS		65
FeCoNiMnV	MA	FCC + BCC phases	66
MoNbTaTiV	MA	Nanopowder with uniform chemical distribution	67
CoFeNiCrMnAl	MA		68
CoFeNiCrMnAl	MA + HPS	FCC + BCC phases	55
CuNiCoZnAl	MA	FCC phase	56
$AlCoCrCuFeZn_x$	MA	Nanocrystalline alloy	57
$Fe_{18}Ni_{23}Co_{25}Cr_{21}Mo_8WNb_3C_2$	MA + HPS	Austenite and carbide phases	58
WMoNbZrV	MA	BCC nanocrystals	59
FeSiBAlNi	MA	FCC nanocrystals + amorphous phase	60
$B_4C - 5\%$ CrMnFeCoNi	SPS	Compacted ceramic composite + HEA and BCC phase	69
$Nb_{25}Mo_{25}Ta_{25}W_{25}$ and $Ti_8Nb_{23}Mo_{23}Ta_{23}W_{23}$	SPS	BCC phases	70
CoCrFeMnNi	SPS	FCC phase	77
TiAlMoSiW	SPS	BCC + FCC phases	78
$Ni_{1.5}Co_{1.5}CrFeTi_{0.5}$	SPS	FCC phase	79
$AlFeCuCrMg_x$	SPS	Two BCC phases	80
CoCrFeNiMn	SPS	FCC phase	81
AlCuNiFeCr	SPS + annealing	FCC and two more phases	82
TiAlMoSiNi	SPS	BCC + FCC phases	83
WC-AlCoCrCuFeNi	SPS	HEA as a binder for composite material	84
$Al_{0.3}CoCrFeMnNi$	SPS	FCC phase	71
$(AlCoCrFeNi)_{100-x}Fe_x$	SPS	BCC + FCC phases	72
AlCoCrFeNi	SPS	FCC + BCC + σ phases	73
MoNbTaTiV	SPS	Nanocrystals with BCC phase	74
$Ti_xWTaVCr$	SPS	BCC phase	75
CoCrFeMnNi	SPS	FCC phase	76
$CoCrFeNiAl_{0.3}$	Bridgman	FCC phase	85
FeCoNiAlSi	Bridgman	FCC phase	86
$Cr_xAlFeCoNi$	VAM	FCC + BCC + σ phases	87
$Al_xFeNiCrCo$	VAM	FCC + BCC + σ phases	88
$Al_{0.4}CoCu_{0.6}NiSi_x$	VAM	BCC + FCC + L12 phases	89
$AlFeCoNiB_x$	VAM	FCC + B2 phases	90
NbZrTiCrAl	VAM	BCC phase	91
AlCrFeCoNi	Additive	BCC phase	92
$AlCoFeNiV_{0.9}Sm_{0.1}$,	Additive	FCC phase	93
$AlCoFeNiSm_{0.1}TiV_{0.9}$	Additive	FCC phase	93
$AlCoFeNiSm_{0.05}TiV_{0.95}Zr$	Additive	FCC phase	93
$AlCoFeNiTiV_{0.9}Sm_{0.1}$	Additive	FCC phase	94
$AlCoFeNiV_{0.9}Sm_{0.1}$	Additive	FCC phase	94
$Ni_6Cr_4WFe_9Ti$	Additive	FCC phase	95

Note. The Table and the text give generally accepted designations for crystal lattices: FCC is face-centred cubic, BCC is body-centred cubic, HCP is hexagonal close-packed.

2.1. Mechanical alloying

Mechanical alloying is the key method for the synthesis of alloys. As a rule, this method is used as the first stage of HEA preparation; additional treatment is subsequently performed in order to improve their properties.

Liu *et al.*[53] prepared the $FeCoCrNiMnTi_{0.1}C_{0.1}$ high-entropy alloy by combining MA and vacuum HPS methods at temperatures of 850, 900, 950 and 1000 °C. During the MA, the elements were gradually fused together, and the microstructure of the obtained bulk alloy consisted of an FCC matrix phase composed of Fe, Co, Ni and Mn and minor amounts of $M_{23}C_6$, M_7C_3 and $TiMnO_3$ phases. This alloy exhibited good mechanical properties upon sintering at 900 °C: the yield strength and hardness reached 1652 MPa and 461 HV, respectively. A relationship between the microstructure and mechanical properties was found: strengthening of grain boundaries was the dominating strengthening mechanism.

The high-entropy equiatomic CoCrFeMnNi alloy is one of most promising among the studied alloys. Kilmametov *et*

al.[54] obtained a dense bulk sample of this alloy by high-pressure torsion deformation. Metal powders consisting of micrometre-sized particles were successively mixed in equimolar proportions, compacted and deformed at a pressure of 5 GPa. The evolution of microstructure obtained by MA was studied by transmission electron microscopy, X-ray diffraction and three-dimensional atom probe tomography. The single-phase nanocrystalline alloy with a grain size of ~50 nm showed the highest hardness for this composition equal to 6700 MPa.

Cheng *et al.*[61] synthesized the CoCrFeMnNi alloy by MA and vacuum HPS. The mechanical alloying afforded nanocrystalline powders composed of an FCC matrix and minor amounts of BCC and amorphous phases. After vacuum fusion, the BCC phase virtually disappeared, simultaneously with the precipitation of σ-phases and $M_{23}C_6$ carbides. An increase in the sintering temperature resulted in grain growth in the precipitated phases. When the sintering temperature increased from 700 to 1000 °C, the strain-to-failure increased from 4.4 to 38.2%, while the yield strength decreased from 1682 to 774 MPa.

Yim *et al.*[62] obtained the CoCrFeMnNi alloy by pressing of mechanically alloyed powders using static and shock wave compaction followed by pressureless sintering. The microstructure evolution and mechanical properties were analyzed using optical microscopy, scanning electron microscopy, finite element simulation and tensile tests. The alloy consisted of an FCC phase with a minor amount of ZrO_2 after milling and sintering. The presence of ZrO_2 was caused by contamination during milling, which promoted the formation of the composite microstructure after sintering. The static compaction of the alloyed powders resulted in an increase in the compaction density up to ~85–88% as pressure increased to 1–3 GPa, while the shock wave compaction of the alloyed powders provided a high relative density (~95%) and the presence of only small isolated pores. After sintering, the shock wave compacted samples were characterized by almost full densification (~99.5%), smaller gran size and better mechanical properties (for example, the yield strength was ~630 MPa with uniform strain distribution) than statically compacted samples.

Tian *et al.*[63] synthesized a coating of equiatomic CrMnFeCoNi alloy on a steel Q235 substrate using the MA method. The fabrication of the coating of this HEA included two stages: first, a powder with a high degree of mixing was prepared, then it was placed on a substrate and annealed for 10 h. Finally, a strong HEA coating was formed. The CrMnFeCoNi powder and the final coating were solid solutions with a single FCC phase. The 180 μm-thick coating had good adhesion to the substrate, and the elements in the coating were uniformly distributed. The results of this study indicated that the CrMnFeCoNi coating has a higher corrosion resistance than the substrate.

Mechanical alloying was used to obtain non-equiatomic $Co_{35}Ni_{30}Fe_{20}Mn_{10}Cr_5$ high-entropy alloy with a low chromium content dispersed with various amounts of Y_2O_3 nanoparticles.[64] The solid solution phase was formed after long-term alloying for 16 h. It was assumed that the added Y_2O_3 particles served as the nucleation sites for chromium oxide particles, which were uniformly distributed in the bulk and accounted for high values of hardness and elastic modulus.

Szklarz *et al.*[65] investigated the corrosion properties in a chloride medium for the CoNiFeMnCr alloy obtained by mechanical alloying of pure powders of chromium, manganese, iron, cobalt and nickel combined with hot isostatic pressing (1000 °C, 15 min, 150 bar). In addition, the authors studied the composite of the initial HEA with SiC nanoparticles; the addition of 5 mass % of SiC improved the mechanical properties (hardness, yield strength) and increased the corrosion resistance of the material.

Alijani *et al.*[66] investigated the magnetic properties of the FeCoNiMnV high-entropy alloy synthesized by ball milling. According to X-ray diffraction data, FCC and BCC phases co-existed during milling. In addition, vanadium-enriched σ-phase was found in the milled samples. The obtained powders can be considered as a semi-hard magnetic material. The highest saturation magnetization of 100 emu g^{-1} was found for the powder milled for 48 h.

The MoNbTaTiV refractory alloy has been studied.[67] The mechanically alloyed powder with a uniform distribution of chemical elements and average grain size of < 15 nm, obtained by milling for 40 h, exhibited high thermal stability at 1200 °C. A study of mechanically alloyed CoFeNi, CoFeNiCr, CoFeNiCrMn and CoFeNiCrMnAl powders showed [68] that increase in the number of elements from 3 to 6 was accompanied by a change in the sintering kinetics: slow grain growth, decrease in the compaction rate and increase in the activation energy of sintering were observed. The trend toward increasing microhardness also attested to good mechanical properties of these alloys.

In order to increase the strength and hardness of HEAs, twelve Al-containing $FeCoCrNiMnAl_x$ alloys with various concentrations of transition metals were fabricated by MA and HPS methods and the effect of aluminium concentration on their microstructure and mechanical properties was elucidated.[55] It was found that Al-containing alloys consisted of FCC matrices or (FCC + BCC) phases, a small amount of $M_7C_3 + M_{23}C_6$ carbides (where M = Cr, Mn, Fe) and Al_2O_3 oxide. As the concentration of aluminium increased, the crystal structure of the solid solution changed from FCC to BCC. The addition of aluminium clearly strengthened the alloys, especially those containing (FCC + BCC) phases of the solid solution. For example, the yield strength, compressive strength and hardness of the $FeCoCrNiMnAl_{0.7}$ alloy reached values of 2230, 2552 MPa and 622 HV, respectively, which was mainly attributed to a small grain size.

The equiatomic CuNiCoZnAl high-entropy alloy was obtained [56] using two MA procedures. If the balls in the mill were of equal radius, the alloy was not formed even after 50-h alloying. The use of balls of different size and increase in the milling velocity resulted in successful synthesis of the alloy, particularly, a single-phase solid FCC solution without signs of an amorphous phase or intermetallic compounds.

The effect of the amount of zinc on the crystal structure and phase formation of the $AlCoCrCuFeZn_x$ alloy obtained by mechanical alloying was studied by Murali *et al.*[57] Both crystalline and non-equilibrium nanocrystalline samples with crystallite size < 10 nm were synthesized.

Sun *et al.*[58] used MA and HPS methods to design a new type of composite based on the $Fe_{18}Ni_{23}Co_{25}Cr_{21}Mo_8WNb_3C_2$ high-entropy alloy. First, a mixture of amorphous powders of chromium and molybdenum was prepared by MA; then other powdered elements (Fe, Ni, Co, W, Nb and C) were added and milling gave a HEA powder consisting of single-phase austenite (γ). The composite sintered by HPS contained the austenite A matrix phase and M_6C carbide as the second phase. The precip-

itation process that took place during sintering can be described as $\gamma \rightarrow A + M_6C$. At room temperature, the ultimate tensile strength and relative elongation were ~1452 MPa and ~3.9%, respectively; at 650 °C, these values were ~795 MPa and ~13.3%.

Oleszak *et al.*[59] investigated the phase composition and thermal stability of the equimolar WMoNbZrV alloy that they synthesized using MA. A nanocrystalline BCC solid solution with crystallite size of 10 nm and lattice parameter of 3.1687 Å was formed. The lattice deformation amounting to 0.58% decreased to 0.20% as the sample was heated to 700 °C, while the crystallite size did not change, which is indicative of good thermal stability of this nanocrystalline solid solution.

The effect of addition of elemental Co, Cu and Ag on the microstructure and thermal and magnetic properties of mechanically alloyed FeSiBAlNi HEAs (basic composition) was studied in detail by Xu *et al.*[60] The amorphous FeSiBAlNi(Co, Cu, Ag) alloys were obtained. The addition of cobalt and copper reduced the time of formation of fully amorphous phase. The final product of milling of FeSiBAlNiAg consisted of an amorphous phase and FCC nanocrystals. The addition of cobalt improved the thermal stability of the basic alloy, while the addition of copper and silver impaired the thermal stability. In addition, milled HEAs were semi-hard magnetic materials. The authors discussed the mechanisms of phase formation in the amorphous state and in solid solution and the microstructure–magnetic property relationship, which has to be known for the development of new alloys.

2.2. Spark plasma sintering

The synthesis by spark plasma sintering is used either to supplement the mechanical alloying or to improve properties of known materials. For example, relatively well studied equiatomic CrMnFeCoNi alloy was used[69] for the first time as an auxiliary agent for spark plasma sintering of B_4C ceramics in the temperature range of 1500–2100 °C. The mechanical properties of the B_4C-5 vol.% HEA ceramic and mechanisms of densification of this ceramic during SPS were studied. The ceramic of this composition sintered at the optimized temperature of 1950 °C exhibited an attractive set of properties, particularly, the relative density of 99.27%, microhardness of 3427 HV and a rupture strength of 619 MPa (the last-mentioned value is 37% higher than that of the most pure B_4C ceramic).

Pan *et al.*[70] used MA and SPS processes to synthesize refractory HEAs of compositions $Nb_{25}Mo_{25}Ta_{25}W_{25}$ and $Ti_8Nb_{23}Mo_{23}Ta_{23}W_{23}$. Ball milling gave single-phase BCC nanocrystallites with a size of ~10 nm. After SPS, the grain size of both alloys was <1 μm. The compressive yield strength, failure strain and Vickers hardness of the bulk $Nb_{25}Mo_{25}Ta_{25}W_{25}$ alloy were 2460 MPa, 16.8% and 7.78 GPa, respectively, which is substantially higher than these characteristics of an alloy of the same composition obtained by VAM. The addition of titanium may improve compression behaviour. Indeed, in the case of $Ti_8Nb_{23}Mo_{23}Ta_{23}W_{23}$, the fracture strain and the peak compressive stress unexpectedly increased by 56.5 and 10.7%, respectively.

The bulk CoCrFeMnNi high-entropy alloy was completely densified using the SPS process.[77] The powder of this alloy was first milled at low temperature, which was followed by short-term planetary milling. An X-ray diffraction study showed the presence of one bulk stable phase both during milling and during sintering. The CoCrFeMnNi alloys prepared by MA and SPS had a higher hardness than the alloys treated by usual melting and casting processes.

In order to use HEAs for manufacturing high-strength mechanical parts, Kanyane *et al.*[78] studied a new equiatomic TiAlMoSiW alloy obtained by SPS for the effect of the sintering temperature on its properties. The samples prepared at high sintering temperature (800, 900 and 1000 °C) had enhanced microhardness and densification.

The synthesis and evaluation of mechanical properties of non-equiatomic plastic single-phase $Ni_{1.5}Co_{1.5}CrFeTi_{0.5}$ HEA were reported by Moravcik *et al.*[79] Excellent properties of this HEA were demonstrated: in particular, the bend strength was 2593 MPa, the tensile strength was 1384 MPa, the tensile elongation to rupture was 4.01% and the elastic modulus was 216 GPa. These characteristics were higher than those of the conventional cast HEAs. This alloy was obtained by combining MA process in a planetary ball mill and SPS (for powder compaction). The samples consisted of a single-phase solid solution with an FCC structure composed of very small grains and oxide inclusions inherited from the initial raw material powder.

New $AlFeCuCrMg_x$ high-entropy alloys ($x = 0$, 0.5, 1, 1.7) were synthesized[80] by MA process followed by SPS compaction. The formation of two BCC phases in the AlFeCuCr alloy and more complex structures in the $AlFeCuCrMg_x$ alloys containing AlFe and Cu_2Mg type phases was established. The inclusion of magnesium markedly affected hardness, which increased to the peak value of 853 HV for $AlFeCuCrMg_{0.5}$ and decreased to 533 HV for $AlFeCuCrMg_{1.7}$.

The induction melting and combination of MA and SPS methods at temperatures of 800 and 1000 °C were used[81] to obtain the equiatomic CoCrFeNiMn alloy with a high entropy. The cast alloy had a much coarser microstructure and poorer mechanical properties than the alloy obtained by 8-h mechanical alloying and plasma sintering. The alloy sintered at 1000 °C reached a hardness of 424 ± 7 HV, while that compacted at 800 °C had a lower hardness of 352 ± 12 HV. Both alloys demonstrated good thermal stability, which was confirmed by insignificant change in the hardness during 100-hour annealing at 400 and 600 °C. These alloys were also superior in the compression and stress–strain tests up to a temperature of 600 °C.

The phase and structural transformations in the samples of equiatomic AlCuNiFeCr alloy obtained by MA, annealing and SPS have been studied.[82] It was shown that the nanocrystalline alloy of this composition synthesized by the MA method consisted of a supersaturated solid solution with a BCC structure. After annealing and spark plasma sintering at 800 °C, the alloy consisted of three phases — one major solid solution with a *B*2 structure, one FCC solution (25 mass %) and the $(Cr, Fe)_{23}C_6$ phase (8 mass %). The Vickers hardness of the sintered AlCuNiFeCr alloy was 8.35 GPa, while compressive strength at room temperature reached 1960 MPa.

Examination of samples of the equiatomic TiAlMoSiNi high-entropy alloy manufactured by the SPS process, with outstanding wear resistance characteristics and oxidative properties, showed the presence of BCC and FCC phases with intermetallic $TiSi_2$ and Ni_2Si_2 inclusions.[83] The 1000 °C sample showed the highest densification of 98.8%, microhardness of 612 HV, friction coefficient of 0.23 μm and also high oxidation stability.

Mechanically alloyed AlCoCrCuFeNi powders were used as binding components for SPS manufacture of WC–HEA composite materials.[84] The effects of sintering duration and temperature and the content of binding component on the microstructure and mechanical properties of the resulting material were studied. The advantages of HEA as a binder over cobalt was holding down of the growth of WC grains: an increase in the content of the binder retarded diffusion and decreased the WC average grain size. A good set of mechanical properties was established after sintering of a sample containing 10 mass % HEA at 1250 °C and at 30 MPa for 5 min.

Pohan *et al.*[71] considered the phase evolution in samples of $Al_{0.3}$CoCrFeMnNi high-entropy alloy obtained by combined MA and SPS processes. The mechanical alloying of the powders resulted only in the FCC phase. However spark plasma sintering gave ordered *B*2 precipitates and chromium carbide precipitates. Optimization of the sintering temperature showed the highest densification and hardness values and high compressive yield strength (979 ± 20 MPa) and ductility (39 ± 3%) to be attained at 900 °C. Grain boundary strengthening together with dispersion strenghening in the presence of carbides and *B*2 particles appears to make the crucial contribution to the improved properties of the alloys.

The understanding of the alloying mechanism is crucial for the development of two-phase HEAs. It was shown that addition of iron influences the microstructure, phase evolution and mechanical properties of the $(AlCoCrFeNi)_{100-x}Fe_x$ alloys (x = 5, 15, 20) prepared by mixing of iron and AlCoCrFeNi powders followed by MA and SPS processes. After compaction, all alloys had a two-phase structure (FCC + BCC). As the iron content increased from 0 to 20 at.%, the volume percentage of the FCC phase changed from 31.5 to 67.8%, while the size of enriched (with ion or chromium) precipitate decreased from 62 to 31 nm. The failure strain increased from 14.9 to 29.9% with increasing iron content (due to the change in the structure), while the compressive strength decreased from 1961.2 to 1380 MPa and the yield strength decreased from 1702.8 to 899.8 MPa. The excellent combination of strength and ductility inherent in this alloy is due to two-phase structure. Good mechanical properties of this HEA can be attained by adjusting the iron content.

The spark plasma sintering method holds great potential for the production of HEAs. Heating rate is a process parameter that is critically important for optimizing microstructure with the goal to enhance the mechanical properties of HEAs. The role of this factor was elucidated[73] for the AlCoCrFeNi alloy. Phase composition, microstructural textures and mechanical properties were studied. It was found that the FCC phase is formed at BCC grain boundaries, while the σ-phase is deposited at the *B*2/BCC interface irrespective of the heating rate. The Vickers hardness and wear resistance decreased with increasing heating rate; the compressive strength and the corresponding plastic strain reached the maximum values of 2752.0 ± 48 MPa and 26.5 ± 1.3%, respectively, at a heating rate of 150 °C min^{-1}.

The MoNbTaTiV refractory high-entropy alloy with ultrafine grains and homogeneous microstructure was successfully synthesized by MA and SPS processes.[74] The authors systematically studied the microstructure evolution, mechanical properties and strengthening mechanisms for alloy samples. Nanocrystalline powders containing a BCC phase were formed after 40-hour MA process. Then the powders were spark plasma sintered in the temperature range of 1500–1700 °C. The bulk alloy sintered at 1600 °C consisted of the BCC matrix (average gain size of 0.58 μm) and a precipitated BCC phase (average particle size of 18 μm) and had a high microhardness of 542 HV, compressive yield strength of 2208 MPa, fracture strength of 3238 MPa and an acceptable plastic strain of 24.9% at room temperature. The enhanced mechanical characteristics of MoNbTaTiV were mainly due to grain boundary strengthening and solid solution strengthening.

Waseem *et al.*[75] considered methods of synthesis and characteristics of Ti_xWTaVCr high-entropy alloys meant for high-temperature and nuclear applications. Samples of Ti_xWTaVCr containing 0 to 7 at.% titanium were obtained by spark plasma sintering of a mixture of elemental powders at 1500 °C. Study of mechanical characteristics of the alloys showed that they were harder and stronger than some known HEAs. The alloy containing 7 at.% Ti also had a high oxidation stability in air at 1000 °C.

Nanocrystalline CoCrFeNi and CoCrFeMnNi high-entropy alloys were obtained by combining MA and SPS methods.[76] They were found to be single phases (have thermally stable FCC structure) contaminated with Cr_7C_3. Long-term diffusion growth of grains takes place in these alloys, since the activation energies for grain growth, which are 134 and 197 kJ mol^{-1} for CoCrFeNi and CoCrFeMnNi, respectively, are much lower than the activation energy of diffusion in them. The dependence of hardness on the grain size was measured for CoCrFeMnNi and found to obey a Hall–Petch type relation. The calculated strength coefficient proved to be 1.92 GPa, which is almost three times as high as the strength factor of a coarse-grained sample. The presence of carbides increases the hardness of these HEAs.

2.3. Bridgman method

The methods of HEA synthesis considered above results in micro- or nanocrystalline structures. The Bridgman method in which HEA single crystals are grown from a liquid is used much more rarely. For example, Ma *et al.*[85] successfully obtained single-crystalline $CoCrFeNiAl_{0.3}$ alloy using this approach and comprehensively studied its crystallographic orientation, tensile behaviour, fracture mechanism, hardness and elastic modulus. The growth of the single crystalline product was focused on the ⟨001⟩ direction. The high tensile ductility can be attributed to the less intense dislocation motion and the only one crystallographic orientation and, hence, less pronounced plastic strain incompatibility.

Microstructure and crystal orientation characteristics were determined for non-equiatomic $FeCoNiAl_{0.25}Si_{0.25}$ high-entropy alloy samples synthesized by the Bridgman method at various withdrawal velocities (30, 100 and 200 μm s^{-1}).[86] The morphological evolution that accompanied the crystal growth in samples prepared at different withdrawal velocities was almost the same: from equiaxial grains to columnar crystals. The grains had a magnetic anisotropy if the magnetic field was applied in different directions.

2.4. Vacuum arc melting

The arc melting process was used to prepare Cr_xAlFeCoNi high-entropy alloys with x = 0, 0.5, 1.0 and 1.5.[87] An X-ray diffraction study revealed the presence of three crystal structures — FCC, BCC and σ. *Ab initio* calculations of

the electronic structure and total energy were carried out using the KKR-CPA method,‡ which takes into account the chemical disorder effects. Theoretical analysis confirmed that the multiphase system was energetically more favourable than the single-phase one.

The $Al_xFeNiCrCo$ high-entropy alloys ($0 \leqslant x \leqslant 1.5$) obtained by sintering and arc melting of pure metal powders have been systematically studied.[88] In the two detected crystallographic structures, three phases with different stoichiometries were identified; the compositions and proportions of the phases were found to depend on the aluminium content in the HEA. The phase compositions of these alloys were very similar, but the microstructures were different: dendritic structure was observed for melted samples, while large regular grains were detected for sintered alloys.

Chen *et al.*[89] synthesized $Al_{0.4}CoCu_{0.6}NiSi_x$ high-entropy alloys (x = 0, 0.05, 0.1, 0.2) by VAM (Mx) and by fast quenching *via* copper injection (Ix). The influence of silicon admixture and fast cooling on these alloys was studied. According to the results, Mx had a (FCC + L12) structure, but at $x = 0.1$ and 0.2, it transformed into (FCC + L12 + minor BCC). The Ix alloys were shown to have a (FCC + L12) structure, except for the alloy with $x = 0.2$, which had the structure FCC + L12 + minor BCC. As the silicon content increased, the hardness of Mx increased from 193 to 334 HV, and the Ix hardness increased from 216 to 395 HV. The mechanism of alloy strengthening is related to the formation of BCC phase and solid solution and fine grain strenghtening. The strengthening effect was more pronounced for the BCC phase than for fine grains, while the fine grain strengthening was more pronounced than the solid solution strengthening.

The effect of boron on the microstructure and the mechanical behaviour of $AlFeCoNiB_x$ high-entropy alloys (x = 0, 0.05, 0.10, 0.15, 0.2) obtained by the VAM process was studied by Hou *et al.*[90] The addition of boron resulted in the transformation of the microstructure from pure *B*2-phase to (*B*2 + FCC) and then to the *B*2 + eutectic structure. The eutectic structure consisted of FCC1 and FCC2 phases. The FCC1 phase was rich in cobalt and nickel, and the FCC2 phase was rich in boron, iron and cobalt. As the boron concentration increased, the grain size of the *B*2 phase first decreased and then increased. The change in the boron content from 0 to 0.2 was accompanied by increase in the fracture strength and plastic strain from 850 to 2293 MPa and from 0.07 to 0.27, respectively. The increase in the yield strength was due to solid solution and fine grain strengthening by boron atoms, while increase in the ductility was caused by the formation of an FCC eutectic.

The equiatomic refractory NbZrTiCrAl high-entropy alloy was prepared by the VAM process.[91] Its microstructure and oxidation processes at 800, 1000 and 1200 °C were studied. The alloy mainly consisted of a single-phase solid solution with a BCC structure and non-uniform microstructure with dendritic and interdendritic regions. The alloy oxidation at 800 and 1000 °C followed second-order kinetics; protective properties were attributed to the formation of uniform dense complex oxides — $CrNbO_4$, ZrO_2, TiO_2, Al_2O_3 and $ZrNb_2O_7$. At 1200 °C, the oxidation kinetics became linear and the oxides formed acquired a layered structure, which probably accounts for the low stability of the alloy to prolonged oxidation at higher temperature.

‡ The Korringa – Kohn – Rostoker (KKR) method in the coherent potential approximation (CPA).

2.5. Additive manufacturing

The additive manufacturing is a relatively new and very promising approach for the synthesis of HEAs, as this allows the formation of uniform single-phase dense structures, which is important for some applications. For example, Yang *et al.*[92] studied the strength characteristics and applicability for 3D printing for the AlCrFeCoNi alloy obtained by this method. The equimolar powders synthesized by vacuum induction melting were sprayed in an inert gas, then a layer of the powder was deposited on stainless steel 304 by laser 3D-printing. The microstructure and wear resistance of the printed HEA layer were evaluated. During the synthesis and layer printing, only the BCC phase was detected. The printed alloy had a typical dendritic/interdendritic structure and had high hardness and wear resistance.

Although a variety of HEAs have been obtained, the possibility of using rare earth and refractory elements in combination with 3d transition metals and aluminium has not been studied. Sarswat *et al.*[93] used selective laser melting technique to manufacture several new hybrid HEAs ($AlCoFeNiV_{0.9}Sm_{0.1}$, $AlCoFeNiSm_{0.1}TiV_{0.9}$, $AlCoFeNiSm_{0.05}TiV_{0.95}Zr$) and AlCoFeNiTiVZr bulk metallic glass. A layer of the appropriate powder was deposited on the surface and melted by a laser; then it was hardened, and the operation was repeated pixel-by-pixel and layer-by-layer. Most of such alloys were single-phase solid solutions with a FCC structure and, as shown by *ab initio* calculations and experiments, they possessed excellent mechanical properties and corrosion resistance.

The $AlCoFeNiTiV_{0.9}Sm_{0.1}$ and $AlCoFeNiV_{0.9}Sm_{0.1}$ alloys synthesized by additive laser method were studied[94] in order to elucidate their resistance to harsh media at elevated temperatures. The drawbacks of other modern techniques for HEA production such as arc melting or spark plasma sintering are high energy consumption, the necessity of grain grinding and melting, and size restrictions. The laser additive method ensures flexibility in the design of HEAs, fast manufacturing and high quenching rates, which satisfies the requirements of many technologies. The phase analysis of the alloys tested in a harsh atmosphere at elevated temperatures showed the presence of only the FCC phase without considerable surface cracks. The additional CALPHAD modelling and DFT calculations confirmed the experimental results.

The main drawback of HEAs that show good mechanical properties, have a broad range of applications and are in demand in the market is their low ductility. The new $Ni_6Cr_4WFe_9Ti$ alloy with a fine-grain structure manufactured by Yang *et al.*[95] showed the fracture strength >970 MPa and a tensile elongation of up to ~12.2% at room temperature. The synthesis was performed by the additive method using the selective laser melting technique; this gave an optimal microstructure of fine grains with nanoparticles uniformly distributed in the matrix alloy. This procedure provided efficient removal of the impurities at grain boundaries and formation of a fine-grained material with high strength and ductility.

The above data indicate that HEAs are mainly prepared using various combinations of transition metals such as Fe, Co, Cr, Ni, Mn, Ti, V, Mo, Nb, Ta, W, Zr and Y. Often, Al, Cu, Zn, Si, B and Mg are added to attain enhanced characteristics (*e.g.*, higher yield strength); in some studies,

rare earth metals such as samarium have been used in HEAs. It was noted above that ~40 elements in various combinations (of five or more elements) can be potentially used to obtain a great variety of HEAs with excellent characteristics. Apparently, less than a thousand of HEAs have been investigated to date, which stimulates further development of synthesis and applications of these alloys.

Meanwhile, the experimental studies carried out, to some extent, by the trial and error method are costly and can give information only on a limited number of alloys. The synthesis of HEAs with enhanced performance characteristics requires combining different methods and search for the optimal parameters for industrial processes. This search is a sort of art and its results depend on the researcher s skills. Therefore, theoretical methods for prediction of promising alloys become more and more important.

3. Methods and results of computer simulation

The increase in the computing power of the modern electronic hardware extends the potential of computational methods, which enable both qualitative and quantitative prediction of the properties of materials. Computer simulation is especially relevant to HEAs, because high dimensionality of the compositional space markedly complicates experimental investigation of these systems. In addition to the prediction of properties, computer simulation can also be used to interpret experimental results. The large number of components that make up HEAs may give rise to various effects, which may perhaps be interpreted within the framework of atomistic simulation. In this Section, versatile computer simulation methods used in computational materials science, which are applicable to virtually any system, are addressed and examples of application of each method to particular HEAs are given.

This Section is arranged in the following way: first, the general statements of thermodynamics are considered, indicating that many phases can exist simultaneously in a multicomponent system; this is followed by semiempirical criteria of formation of single-phase disordered solid solutions in multicomponent systems based on pairwise enthalpies of mixing and on the difference between the sizes of atoms of elements. Usually, the calculation of these criteria is the initial stage of studies of new HEA compositions.

Atomistic simulation is a large and computational power-demanding class of computer simulation techniques, which has gained wide use in recent years. In this case, DFT calculations are used to determine the energy of an arbitrary atomic configuration.

Below we discuss a procedure for the generation of atomic configurations to reproduce most efficiently the complete atomic disorder inherent in an infinite disordered solid solution — special quasi-random structures. Using the knowledge on the electronic and nuclear subsystems (gained from DFT data), one can find forces acting on the nuclei and then numerically integrate the Newton equations to derive the nuclear trajectories. This is the essence of *ab initio* molecular dynamics, a fairly computationally costly method. In order to reduce the computational cost, the interaction of the nuclei (determined by their positions and electron density distribution) should be approximated by some interaction potential, *i.e.*, it is necessary to specify a potential energy surface. Relying on the *ab initio* data, it is possible to parameterize the potential energy surface. Here we consider both the traditional forms of potential energy surface such as embedded atom potential and a relatively new class of potentials based on artificial neural networks. The cluster expansion method can also be classified as an atomistic methods for calculation of the energy of a system of atoms; however, it is mainly suitable for crystals.

When the system energy as a function of coordinates of all atoms is known, it is possible to use statistical mechanics to calculate the free energy of the system and to perform Monte Carlo calculations. In turn, the data on the free energy can be used to construct phase diagrams by the CALPHAD method, which is mentioned in part 3.9.

Thus, each part of this Section is closely connected with the previous one. Indeed, special quasi-random structures are very important for DFT calculations, the results of *ab initio* molecular dynamics can be used to construct potentials of classical molecular dynamics, while the values calculated by statistical mechanics techniques, which are based on atomistic simulation results, form the grounds for constructing phase diagrams.

3.1. General statements of thermodynamics

Most metallurgical processes occur under isothermal-isobaric conditions; therefore, the Gibbs free energy is the most relevant thermodynamic function

$$G(N,p,T,\boldsymbol{\omega}) = E + pV - TS \tag{1}$$

where E is the internal energy of the system, p is pressure, V is volume, T is temperature, S is entropy, N is the number of atoms in the system, $\boldsymbol{\omega} = \{\omega_i\}_{i=1\ldots K}$ is a vector that takes on K values (K is the number of components in the system) equal to the atom fractions of i-th components.

Often, it is convenient to use the Helmholtz free energy

$$F(N,V,T,\boldsymbol{\omega}) = E - TS \tag{2}$$

Legendre transformation is utilized to pass from F to G.

Under isothermal-isobaric conditions, a thermodynamic system occurs in equilibium if its Gibbs energy is minimized. Each of the system components has its own chemical potential μ_i, which is determined by the relation

$$G = \sum_{i=1}^{K} \mu_i N_i \tag{3}$$

Here $N_i = \omega_i \mathrm{N}$ is the number of atoms of the i-th type. In the case of coexistence of several phases, all the foregoing applies separately to each of them. For example, for the J-th phase

$$G^J = \sum_{i=1}^{K} \mu_i^J \omega_i^J N^J \tag{4}$$

where μ_i^J is the chemical potential of the i-th component in the J-th phase, ω_i^J is the atomic fraction of the i-th component in the J-th phase, N^J is the number of atoms in the J-th phase.[96]

Coexistence of Φ phases, each being characterized by $K + 2$ variables (K atomic fractions or K chemical potentials, pressure and temperature), is possible if their chemical potentials and pressures and temperatures in each phase are equal. Thus, out of the total set of $\Phi(K + 2)$ variables $\{T^J; p^J; \{\mu_i^J\}_{i=1\ldots K}\}_{J=1\ldots\Phi}$, only $K + 2$ variables are independent, particularly temperature, pressure and the chemical potential of i-th component in any arbitrarily chosen phase. Hence, the superscript indicating the phase for a

chemical potential is no longer needed and, hence, the expression for the Gibbs energy of a multiphase multicomponent system takes on the form

$$G(N,p,T,\boldsymbol{\omega}) = \sum_{J=1}^{\Phi}\sum_{i=1}^{K}\mu_i\omega_i^J N^J \tag{5}$$

The Gibbs – Duhem equation obtained by combining Eqns (1) and (5) holds for each phase J

$$\sum_{i=1}^{K}\omega_i^J N^J \mathrm{d}\mu_i + S^J \mathrm{d}T - V^J \mathrm{d}p = 0 \tag{6}$$

Thus, the $K + 2$ variables that remained independent are subject to Φ constraints. Hence, only n variables can be varied independently

$$n = K + 2 - \Phi \tag{7}$$

This fact is known as the Gibbs phase rule,[97] which implies that the greater the number of components K in the system, the greater the number of phases that can coexist. When the temperature and pressure are fixed and the chemical potentials do not change (*i.e.*, when $n = 0$), at most $\Phi = K + 2$ phases can coexist.

The properties of a material are determined by the phase composition; therefore, it is necessary to know how to predict the phase composition corresponding to a definite component composition. Even in the case of equiatomic systems, it is hardly expedient to study experimentally various compositions of potential HEAs, and in the case of an arbitrary component ratio it is just impossible. Meanwhile, mathematical modelling and computer simulation techniques considerably narrow down the region in the space of compositions that should be chosen for further experimental investigations.

3.2. Semiempirical criteria

In most published sources, a multicomponent alloy is assigned to the class of HEAs if this alloy is a single-phase disordered solid solution.[29] Indeed, from the fundamental standpoint, the disordered solid solution phase has the highest configurational entropy of mixing among all other phase compositions.

Despite the fact that single-phase substitutional solid solutions do not always have the optimal properties, numerous semiempirical criteria have been developed particularly to divide all possible compositions into those that would form solid solutions and those that would exist as several phases.[98] A K-component system the composition of which is specified by vector $\boldsymbol{\omega}$ is described using a geometric parameter (δ), the enthalpy of mixing (ΔH_{mix}), generalized thermodynamic parameter (Ω) and the entropy of mixing (ΔS_{mix})

$$\delta = \sqrt{\sum_{i=1}^{K}\omega_i\left(1 - \frac{r_i}{\bar{r}}\right)^2} \tag{8}$$

where r_i is the atomic radius of the i-th component,

$$\bar{r} = \sum_{i=1}^{K}\omega_i r_i;$$

$$\Delta H_{\mathrm{mix}} = \sum_{i=1}^{K}\sum_{j=i+1}^{K} 4\Delta H_{ij}\omega_i\omega_j \tag{9}$$

where ΔH_{ij} is the enthalpy of mixing for a binary solid solution;

$$\Omega = \frac{T_{\mathrm{m}}\Delta S_{\mathrm{mix}}}{|\Delta H_{\mathrm{mix}}|} \tag{10}$$

$$T_{\mathrm{m}} = \sum_{i=1}^{K}\omega_i T_{\mathrm{m}i} \tag{10a}$$

where $T_{\mathrm{m}i}$ is the melting point of the i-th component.

Most often, ΔS_{mix} is determined using the expression for ideal configurational entropy of mixing. In the case of a disordered solid solution in which the probability of occupation of a lattice site with an atom of i-th component is proportional only to the concentration of this component, the entropy of mixing is determined by the Boltzmann formula

$$\Delta S_{\mathrm{mix}} = -R\sum_{i=1}^{K}\omega_i \ln(\omega_i) \tag{11}$$

Here $R = 8.31\ \mathrm{J\,mol^{-1}\,K^{-1}}$ is the universal gas constant. The criteria for the formation of a single-phase disordered solid solution are that the above parameters should be lower than some critical values or should fall into particular ranges the boundaries of which are derived from experimental data.

These values are not strict; moreover, various publications give different boundary values for these parameters (Table 2).

If the above criteria are met, then, considering the average number of valence electrons per atom, one can make an assumption about the crystal structure of the formed HEA. The formation of one or another crystal structure can be predicted relying on the number of valence electrons per atom in the i-th component called valence electron concentration (VEC)

$$\mathrm{VEC} = \sum_{i=1}^{K}\omega_i \mathrm{VEC}_i \tag{12}$$

It was ascertained[101] for a large number of HEAs that for VEC < 6.87, the BCC phase is stable, while for VEC > 8.00, the stable phase is FCC; if VEC is intermediate, the alloy contains both of the above phases. There are also high-entropy alloys with an HCP structure, *e.g.*, $AlLiMg_{0.5}ScTi_{1.5}$,[102] GdTbDyTmLu,[103] HoDyYGdTb,[104] in which VEC is approximately 3. Systems with high VEC can also contain HCP structures; for example, Takeuchi *et al.*[103] obtained $Ir_{26}Mo_{20}Rh_{22.5}Ru_{20}W_{11.5}$ and $Ir_{25.5}Mo_{20}Rh_{20}Ru_{25}W_{9.5}$ alloys with VEC of approximately 8.

The fact that different sources give different (in some cases, contradictory) criteria for the formation of HEAs means that detailed investigations using other, more sophisticated, methods are required.

Table 2. Semiempirical criteria for the formation of disordered solid solutions in multicomponent metallic systems.

δ (%)	ΔH_{mix}, kJ mol^{-1}	Ω	Ref.
< 5	−15 to 5	–	98
< 5	−15 to 5	$\gg 1$	99
< 4.27	−7.27 to 4	–	100

3.3. Density functional theory calculations at 0 K

The calculation of the crystal structure energy as a function of atom coordinates and types is important for evaluating the possibility of formation of particular phases and the structures and properties of these phases. Currently, this problem is solved, most often, using highly accurate DFT calculations.[105] According to this approach, the atomic nuclei are considered to be classical particles and are defined, in an N-atomic system, by a set of Cartesian coordinates (R) and charge numbers (Z) — $\{\mathbf{R}_i, Z_i\}_{i=1\ldots N}$; electrons are treated in terms of quantum mechanics. In the general case, a system containing n electrons is described by some many-electron wave function $\Psi(\mathbf{1}, \mathbf{2}, \ldots, \mathbf{n})$ where $\mathbf{i} = \{x_i, y_i, z_i, \sigma_i\}$ is a set of Cartesian and spin coordinates of the i-th electron, *i.e.*, by a function of $4n$ variables. Meanwhile, of practical interest is not the many-electron function itself, but rather electron density distribution

$$\rho(\mathbf{r_1}) = n \int |\Psi(\mathbf{1}, ..., \mathbf{N})|^2 \mathrm{d}\sigma_1 \mathbf{d2}...\mathbf{dN} \tag{13}$$

where integration is performed over the spin coordinate of the first electron and all coordinates of other electrons.

In the one-electron approximation, some one-electron wave functions (spin orbits), which are products of spatial orbitals $\varphi_i(\mathbf{r}_j)$ and spin functions $\gamma_i(\sigma_j)$, are considered

$$\{\psi_i(\mathbf{j}) = \varphi_i(\mathbf{r}_j)\gamma_i(\sigma_j)\}_{i,j=1\ldots N} \tag{14}$$

It is taken that $\varphi_i(\mathrm{r}_j)$ and $\gamma_i(\sigma_j)$ are functions of variables of only one electron, the wave function Ψ can be represented as a Slater determinant of functions ψ_i, while the electron density distribution function can be written in the following way:

$$\rho(\mathbf{r}) = \sum_{i=1}^{n} |\varphi_i(\mathbf{r})|^2 \tag{15}$$

According to DFT, the total energy of the electronic subsystem can be expressed as an electron density functional

$$E = E[\rho(\mathbf{r})] \tag{16}$$

The electron density is found using the Kohn–Sham equations for one-electron orbitals,[106] which are solved by self-consistent iteration procedure

$$\left(-\frac{1}{2}\nabla^2 - \sum_{m=1}^{N}\frac{Z_m}{|\mathbf{R}_m - \mathbf{r}|} + \int\frac{\rho(\mathbf{r}')\mathrm{d}\mathbf{r}'}{|\mathbf{r}' - \mathbf{r}|} + \varepsilon_{xc}\right)\varphi_i = \varepsilon_i\varphi_i \tag{17}$$

where ∇^2 is the Laplace operator, $\mathbf{R}_\mathrm{m}$ is the radius vector of the m-th nucleus, Z_m is the charge number of the m-th nucleus, $\mathbf{r}$ and $\mathbf{r}'$ are the spatial coordinates of electrons, φ_i is the i-th spatial orbital, ε_{xc} is the exchange correlation energy, ε_i is the orbital energy. The orbital functions are expanded in a pre-specified basis set; in the case of solids and liquids, plane-wave basis set is used most often.[107] The Kohn–Sham equations were derived by a variational method; hence, they provide electron density distribution function $\rho(\mathbf{r})$ corresponding to the minimum functional $E[\rho(\mathbf{r})]$. After calculation of the electron structure for particular positions of nuclei, it is possible to calculate the total energy of the system and then, by varying nuclear coordinates, an attempt should be made to minimize the system energy relative to them. Several minimization methods are used to self-consistently solve the Kohn–Sham equation and to find the energy minimum: conjugate gradient method,[108] Davidson algorithm,[109] RMM-DIIS [110, 111] and so on.

The density functional theory can be used either as a separate tool to calculate the energy of a particular atomic structure at temperature 0 K, or it can be combined with other methods that take into account the finite temperature effect and atomic dynamics.

3.4. Special quasi-random structures

For DFT calculations, it is necessary to specify the initial coordinates of each of N atoms and the type of atom (*i.e.*, the charge number Z). In the case of simple metals, this problem is solved rather easily: the atoms and atom positions in the unit cell are specified and then periodic boundary conditions are applied. Any ordered compound can be studied according to the same protocol, namely, one or several unit cells are subjected to periodic boundary conditions. In the case of disordered systems such as HEAs, there arises the problem of describing the maximum disorder by a finite number of atoms. On the one hand, it is clear that the greater the number of atoms in the supercell, the easier the simulation of an infinite disordered solid solution. However, the computational cost of DFT increases as n^3 where n is the number of valence electrons in the system (valence electrons are those for which the Kohn–Sham equations are solved). Thus, it is expedient to consider supercells with the maximum number of atoms for which the calculation takes a reasonable time. Modern software packages are applicable for systems containing 10^2–10^3 atoms. However, even considering a crystal supercell of only 100 atoms, for a five-component equiatomic alloy, one has $100!/(5 \times 20!)$ configurations of atoms at the supercell lattice sites, which evidently cannot be calculated. Some of these configurations would correspond to fully ordered structures, while some other would more closely reproduce the atomic disorder inherent in an infinite disordered solid solution.

Special quasi-random structures are those in which the atomic positions in the lattice sites reproduce most closely the specified correlation functions of an infinite disordered solid solution, for example, partial pair correlation functions. The SQS approach was developed by Zunger *et al.*,[112] who addressed the problem of atomistic simulation of a disordered binary compound. Whereas for small supercells, SQS can be generated by enumerating all possible configurations followed by selection of the most appropriate one, in the case of large supercells typical of HEAs, the simple enumeration is impossible. Currently, SQS for large supercells are generated using the stochastic method described by Van de Walle [113] and implemented in the mcsqs code of the ATAT (alloy theoretic automated toolkit) software package. A monograph [46] devoted to HEAs considers SQS for four- and five-component supercells of various sizes and structures (BCC, FCC, HCP), which can be used in DFT calculations.

The energy of ideal SQS should not depend on $K!$ — the number of permutations of the types of atoms in the system. The greater the number of atoms in a correctly generated SQS, the more closely this criterion is met. However, the nature of atoms and the crystal structure also affect the SQS sensitivity to permutations of the types of atoms. For example, Gao *et al.*[46] used SQS for CoCrFeNi, CoOsReRu and MoNbTaW characterized by FCC, HCP and BCC structures, respectively (Fig. 3). The enthalpies of formation

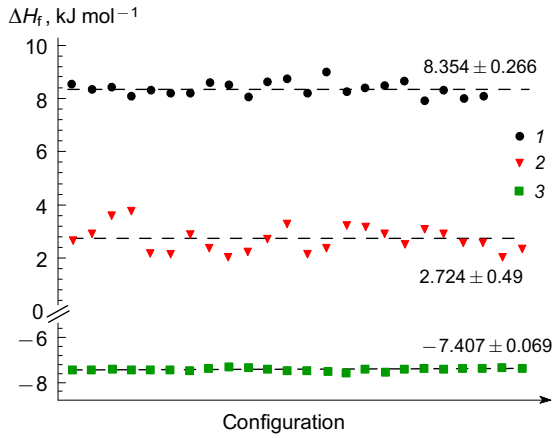


Figure 3. Enthalpy of formation as a function of atomic configuration for CoCrFeNi (*1*), CoOsReRu (*2*) and MoNbTaW (*3*).[46] Published with permission from Springer Nature.

for 4! = 24 permutations of types of atoms were calculated. It can be seen that SQS describes MoNbTaW best of all, while for the two other alloys, considerable deviations from the average enthalpy of formation were observed.

The use of SQS is significant for atomistic calculations of HEAs. By randomly positioning only a few hundreds of atoms accessible for DFT calculations in the lattice sites, one can get, for example, a very high scatter of the partial coordination numbers for pairs of atoms, which is not typical of an infinite disordered solid solution. Meanwhile, enumeration of a large number of random positions of atoms in the lattice sites is unfavourable from the computational cost standpoint, since atomistic methods do not possess a sufficient capacity for generating all possible permutations of hundreds of atoms.

3.5. *Ab initio* molecular dynamics

It was shown above that in DFT the atomic nuclei are considered as classical particles; hence, they can be described using classical Newton motion equations

$$\{\mathbf{F}_i = M_i \ddot{\mathbf{R}}_i\}_{i=1\ldots N} \tag{18}$$

where $\mathbf{F}_i$ is the total force acting on the i-th nucleus, M_i is the mass of the i-th nucleus. According to the Hellmann–Feynman theorem,[114] this force can be expressed as

$$\mathbf{F}_i = \sum_{j\neq i}^{N} \frac{Z_i Z_j}{|\mathbf{R}_{ij}|^3}\mathbf{R}_{ij} - \int \frac{Z_i \rho(\mathbf{r})}{|\mathbf{R}_i - \mathbf{r}|^3}(\mathbf{R}_i - \mathbf{r})\mathrm{d}\mathbf{r} \tag{19}$$

where $\mathbf{R}_{ij} = \mathbf{R}_j - \mathbf{R}_i$.

The electron density distribution function is calculated by DFT. If the initial positions and velocities of the nuclei are known, by integrating equations of motion using some numerical method (*e.g.*, the Verlet method[115]), one can obtain the trajectories of nuclei. This approach to studying the time evolution of a system of atoms is called *ab initio* molecular dynamics. This method can be used to determine the trajectories of atoms both in solids and in liquids. However, due to relatively low productivity, this method is not used very often to simulate the dynamics of solids, because the relaxation times for them are rather long. However, AIMD is employed to simulate multicomponent melts, in particular, to predict the possibility of formation of a single-phase disordered substitutional solid solution by analyzing the partial radial distribution functions for multicomponent melts (Figs 4 and 5).[116] One such function $g_{\alpha\beta}(r)$ is the number of pairs between type α and β atoms located at a distance from r to $r + \mathrm{d}r$ divided by the volume of the spherical layer $4\pi r_2 \mathrm{d}r$ and normalized to the average pair density

$$g_{\alpha\beta}(r) = \frac{V}{N_\alpha(N_\beta - \delta_{\alpha\beta})}\sum_{i=1}^{N_\alpha}\sum_{\substack{j=1\\(i\neq j \text{ if } \alpha=\beta)}}^{N_\beta}\frac{\delta(|\mathbf{r}-\mathbf{r}_{ij}|)}{4\pi r^2 \mathrm{d}r} \tag{20}$$

where V is the supercell volume, N_i is the number of the i-th component atoms in the supercell, $\delta_{\alpha\beta}$ is the Kronecker delta symbol, $\mathrm{d}r$ is a spatial network step, $\delta(|\mathbf{r}-\mathbf{r}_{ij}|)$ is a function equal to unity when $0 < |\mathbf{r}-\mathbf{r}_{ij}| < \mathrm{d}r$ and equal to zero in all other cases.

The partial radial distribution functions for different pairs of atoms are considerably different (see Fig. 4), which attests to low probability of formation of a disordered substitutional solid solution. Indeed, Singh *et al.*,[19] found precipitates enriched in Cu, Al–Ni and Cr–Fe in the AlCoCrFeNi alloy, which is consistent with the data shown in Fig. 4.

The HfNbTaTiZr alloy has long been considered to be a single-phase BCC solid solution;[46] however, later[117,118] it was found that a second HCP phase was formed during annealing. Nevertheless, such inclusions appear only after a 10-hour annealing at 600 °C, while in the cast state, this alloy is actually a single-phase disordered solid solution,

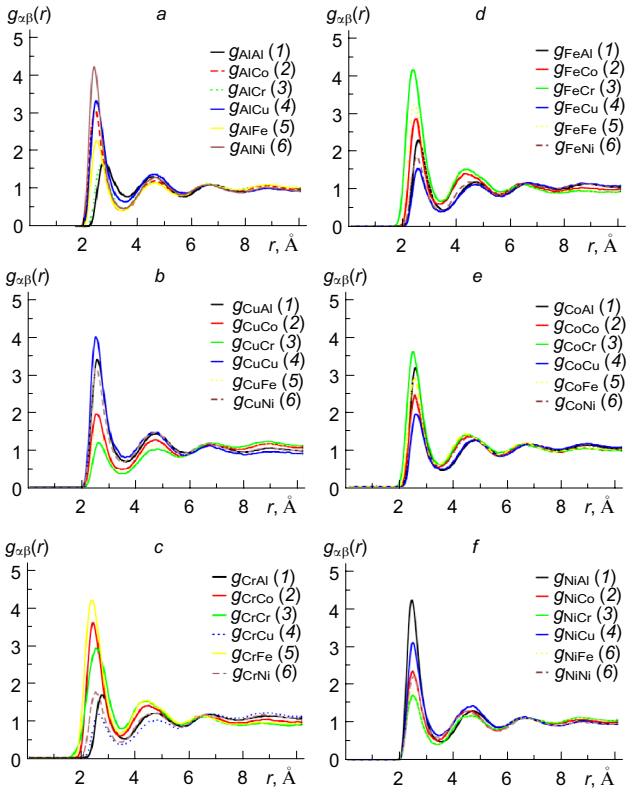


Figure 4. Partial radial distribution functions of pairs of atoms α and β of $Al_{1.3}CoCrCuFeNi$ melt in a 200-atom supercell at a temperature of 1873 K obtained during 30 ps. α = Al (*a*), Cu (*b*), Cr (*c*), Fe (*d*), Co (*e*), Ni (*f*); β = Al (*1*), Co (*2*), Cr (*3*), Cu (*4*), Fe (*5*), Ni (*6*).[116]

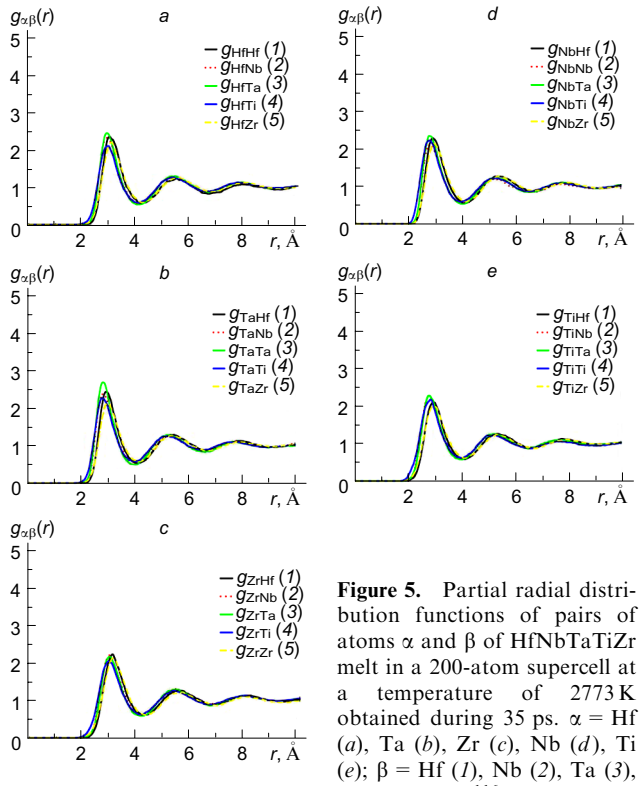


Figure 5. Partial radial distribution functions of pairs of atoms α and β of HfNbTaTiZr melt in a 200-atom supercell at a temperature of 2773 K obtained during 35 ps. α = Hf (*a*), Ta (*b*), Zr (*c*), Nb (*d*), Ti (*e*); β = Hf (*1*), Nb (*2*), Ta (*3*), Ti (*4*), Zr (*5*). [116]

which is in line with the form of the partial radial distribution functions (see Fig. 5).

In addition to structural properties characterized by radial distribution functions, it is possible to calculate dynamic characteristics of materials by AIMD. For example, in the case of liquids, the productivity of this method is quite sufficient for determining the diffusion coefficients for particular sorts of atoms (D_a). D_a can be calculated using the Green–Kubo relation [119, 120]

$$D_a = \frac{\Delta t}{3N_a(T_{\max} - T_{\mathrm{VACF}})} \int_0^{T_{\mathrm{vacf}}} \sum_{i=1}^{N_a} \sum_{t_m=0}^{T_{\max}-T_{\mathrm{vacf}}} \mathbf{v}_i(t_m)\mathbf{v}_i(t+t_m)\mathrm{d}t \quad (21)$$

where Δt is the time step of molecular dynamics; N_a is the number of atoms of sort a; $T_{\max}$ is the maximum time over which the statistical data were acquired; T_{VACF} is the integration time of the velocity autocorrelation function (VACF), $\mathbf{v}_i(t)$ is the velocity of the i-th atom at time point t.

The D_a value can be calculated using the slope of the linear segment in the time dependence of the mean square displacement of sort a atoms (MSD_a) [121]

$$\mathrm{MSD}_a(t) = \frac{\Delta t}{N_a(T_{\max} - T_{\mathrm{MSD}})} \sum_{i=1}^{N_a} \sum_{t_m=0}^{T_{\max}-T_{\mathrm{MSD}}} [\mathbf{r}_i(t_m + t) - \mathbf{r}_i(t)]^2 \quad (22)$$

where T_{MSD} is the maximum time of MSD measurement, $\mathbf{r}_i(t)$ is the radius vector of the i-th atom at the time point t.

The velocity autocorrelation function and mean-square displacements for atoms of various sorts in an HfNbTaTiZr melt are shown in Fig. 6.[122] The diffusion coefficients calculated from these data obey the following trend: D_a decreases with increasing mass and size of sort a atom, which agrees with the results of Gao and Alman [116] for this alloy.

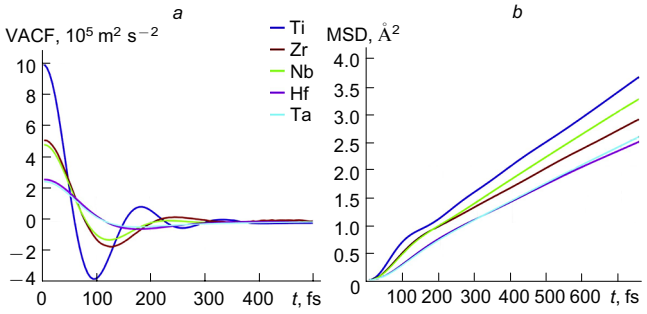


Figure 6. Variation of the velocity autocorrelation function (*a*) and mean-square displacements (*b*) for various atoms in HfNbTaTiZr melt at a temperature of 2773 K.[122] Published with permission from Elsevier.

Thus, using the AIMD method, it is possible to predict whether or not a system of a specified chemical composition would exist as a disordered substitutional solid solution during crystallization by considering the partial radial distribution functions and, indirectly, by considering the dependence of the diffusion coefficient on the atom mass and size.

It is noteworthy that the complexity of AIMD calculations for HEAs does not increase with increasing number of components in the system; the computational cost depends mainly on the number of electrons in the cell. However, acquisition of statistical data for partial radial distribution functions in a K-component system of the same quality as for radial distribution functions in a simple system requires $\sim K^2$ times more MD steps. Thus, in the case of HEAs, the AIMD productivity is quite a severe problem, which motivates the creation and development of classical models of potential energy surfaces for these alloys.

3.6. Classical molecular dynamics

The main drawbacks of AIMD are low productivity and nonlinear (with respect to the number of atoms or, more precisely, electrons) increase in the computational time. The main computational cost of this method falls to the self-consistent DFT calculation of the electronic subsystem. However, the forces acting on nuclei are unambiguously determined by positions of other nuclei. If one generates a function of $3N$ variables — the potential energy surface, which can be differentiated with respect to coordinates of the i-th nucleus to give the force acting on this nucleus, the problem turns into a problem of motion of N interacting particles, which is solved in terms of classical MD. The *a priori* specification of the potential energy surface obviates the necessity to calculate the electronic subsystem; therefore, the terms nucleus and atom are equivalent in the classical MD.

It was noted above that the classical MD calculation eliminates the necessity to carry out a DFT calculation for every new position of the atoms. Therefore, the classical MD method has a markedly higher productivity. The introduction of cutoff radii for interaction between the atoms also leads to a linear dependence of the computational time on the number of atoms.[123] Owing to high productivity of the classical MD method, it is possible to obtain statistically significant results even for solids. The main complexity of this method is to choose the interaction potential between the atoms (or, which is equivalent, to

specify the potential energy surface). The simplest pair interaction potentials such as the Lennard-Jones potential are rarely applied to real systems and to quantitative calculations; they are more often used for model systems to interpret some phenomena at a qualitative level.[123] For more accurate calculations, many-body potentials are used such as embedded atom model/method (EAM), which is often utilized in the modelling of metals. In this case, the potential energy surface is determined by the following expression:[124]

$$E_{\text{tot}} = \sum_i F_i\left(\sum_{j\neq i}\rho_j(r_{ij})\right) + \frac{1}{2}\sum_i\sum_{j\neq i}\varphi_{ij}(r_{ij}) \qquad (23)$$

where F_i is the embedding function of an i-th atom, $\rho_j(r_{ij})$ is the contribution to the electron density of a j-th atom at distance r_{ij} from its position, r_{ij} is the distance between atoms i and j, φ_{ij} is the pair interaction function.

It is noteworthy that in the general case, functions F and ρ can be different for different types of atoms, while φ_{ij} can be different for different pairs of atoms. Thus, for example, to specify the EAM potential of a five-component system, it is necessary to specify 25 functions: 5 embedding functions, 5 electron density functions and 15 pair potential functions.

Most of potentials used in the classical MD have an invariable functional form, which allows easy interpretation of the physical meaning of the potentials; however, as a consequence, it is often impossible to predict the experimental or AIMD values of interest even upon exhaustive enumeration of all possible parameters of the potential. For multicomponent systems such as HEAs, one more problem arises, namely, even in the case of simplest pair interactions in a K-component system, it is necessary to specify $K(K+1)/2$ interactions. This brings about the necessity of substantiated choice of a large number of interaction parameters, which is a fairly complicated task.

Recent years have witnessed active development of the approach to generating interatomic interaction potentials using high-dimensional artificial neural networks. Classical molecular dynamics using these potentials allows one to simulate the DFT values of energies and forces to an accuracy of up to 0.1 meV per atom and 10 meV Å^{-1}, respectively. Furthermore, the productivity of the classical MD method with neural network potentials is several orders higher than the AIMD productivity. The main idea of construction of these potentials in relation to a three-atom system is shown schematically in Fig. 7.[125]

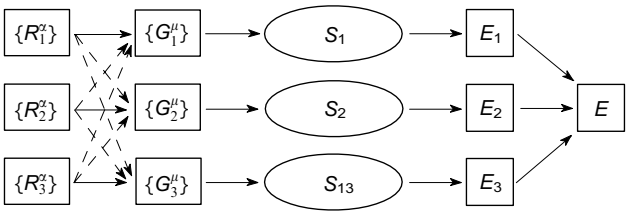


Figure 7. Schematic of the implementation of high-dimensional artificial neural networks. The coordinates of three atoms $\{R_1^\alpha\}$ are converted to the set of $\{G_2^\mu\}$ values to preserve the system symmetry. These values are used as inputs of atomic neural networks S_i, which give E_i, the fictitious energy of the i-th atom, at the output.[125] Published with permission from the American Physical Society.

The DFT data such as configuration, system energy in the given configuration and forces acting on each atom in the given configuration often serve as training sets. The coordinates of each atom are taken from the training set as the input data for the neural network potential. Then the atom coordinates are subjected to a number of transformations aimed at the retention of the translational and rotational symmetry of the system. Thus, the rotation and translation of the system should not change its energy. After that, the transformed coordinates are supplied to the input of atomic neural networks. The atomic neural networks for the j-th type of atoms are identical; therefore, the permutation of two atoms of the same type does not change the energy of the system. The output value of each atomic neural network is E_i, that is, the fictitious atomic energy of the i-th atom. The output value of the high-dimensional neural network (HDNN) is the sum

$$E_{\text{HDNN}} = \sum_{j=1}^{N} E_i \qquad (24)$$

which, in terms of the given approach, corresponds to the potential energy surface of the system.

Since E_{HDNN} is an analytical (although fairly sophisticated) function of atom coordinates, its partial derivatives with respect to all atom coordinates (*i.e.*, forces acting on atoms) are known. The energies and forces are determined by a large set of parameters: weight coefficients in atomic neural networks. These parameters are selected by minimizing the penalty function containing root-mean-square deviations of the neural network-calculated forces and energies from the values found by AIMD.

The above-described approach was implemented in the n2p2 software package.[126] A similar approach is DeePMD,[127] which differs from n2p2 mainly in the procedure of transformations of Cartesian coordinates to local atomic environment descriptors. In the context of machine learning, mention should also be made of the methods using moment tensor potential (MTP)[128] and spectral neighbour analysis potential (SNAP[9]),[129] the method developed by Dolgirev *et al.*[130] and so-called on-the-fly machine learning method, which generates an interatomic potential *via* AIMD calculations.[131]

Balyakin *et al.*[132] employed the n2p2 method to develop the interatomic interaction potential for the VZrNbHfTa system. A comparison of the partial radial distribution functions obtained using n2p2 and AIMD approaches demonstrated that the developed potential fairly adequately describes the structural properties. The diffusion coefficients calculated by the two methods were not equal, but quite close to each other (Fig. 8). The authors attributed this difference to insufficient statistics and to the effect of small size of the AIMD cell on the calculated values.

Thus, some approaches (such as machine learning potentials) that can describe potential energy surfaces of HEAs to a sufficient accuracy, despite the HEA complexity, have been developed to date. The use of classical MD with precise potentials neutralizes the errors of AIMD calculations associated with insufficient statistics, which is once again important for studying HEAs, because analysis of the atomic trajectories in multicomponent systems requires determination of partial correlation functions (one-body: MSD and VACF; two-body: partial radial distribution function, *etc.*); the greater the number of components in the system and the higher the order of the correlation

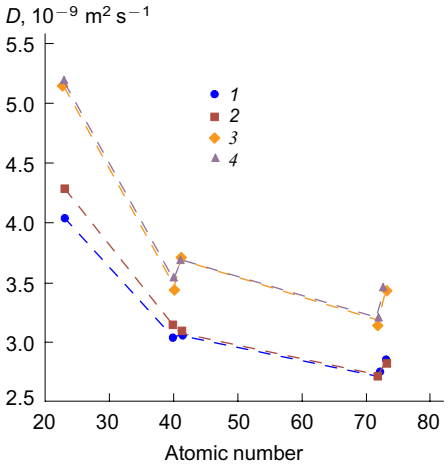


Figure 8. Diffusion coefficient as a function of the atomic number of the element in VZrNbHfTa melt at a temperature of 2500 K. The calculations were performed by AIMD (*1*, *2*) and HDNNP (*3*, *4*) using the Green–Kubo relation (*1*, *3*) and mean-square displacement of atoms (*2*, *4*).[132]

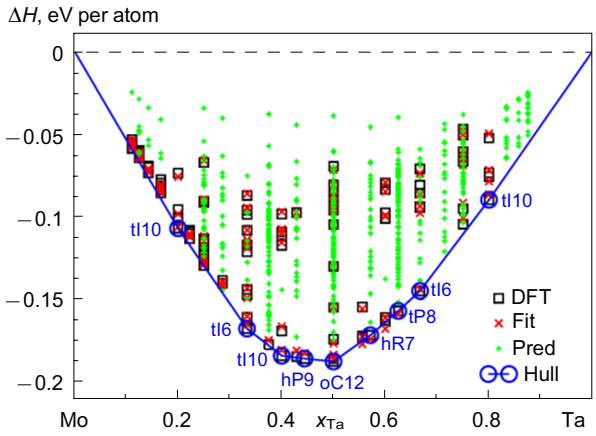


Figure 9. Enthalpies of formation of binary compounds in the Mo–Ta subsystem at 0 K.[137] Designations: DFT stands for density functional theory calculations; Fit stands for cluster expansion calculations (parameters of which were found from approximation of DFT calculations) for the same structures for which DFT calculations were carried out; Pred are enthalpies predicted by cluster expansion for other (not calculated by DFT) structures; Hull is a convex shell with applied stable structures of the Mo–Ta subsystem designated by Pearson symbols. Published with permission from Springer Nature.

function, the greater the number of statistical data needed for its correct calculation.

3.7. Cluster expansion method

The cluster expansion method is based on the idea that some scalar parameter of the system, most often energy (E), is expressed as a function of system configuration. This method is based on a lattice model; hence, it is mainly applicable to crystalline substances. If there is a crystalline system of N equivalent units containing K components, the configuration of such system can be described by a vector in an N-dimensional space

$$\boldsymbol{\sigma} = \{\sigma_1, \ldots, \sigma_N\} \tag{25}$$

where σ_i can take on K different values depending on which type of atom occupies the i-th lattice point, *e.g.*, $m, \ldots 0, \ldots -m$, if the system contains an odd number of types of atoms (*i.e.*, $K = 2m + 1$), or $m, \ldots, 1, -1, \ldots, -m$, if $K = 2m$, where m is an integer. In the described method, each i-th point is assigned with a set of K functions. Most often, Chebyshev polynomials $\{\Theta_s(\sigma_i)\}_{s=0\ldots K-1}$, where s is the polynomial order, are used as such sets. Then the notion of cluster $\{\Theta_s(\sigma_i)\}_{s=0\ldots K-1}$, s as a set of points is introduced

$$\boldsymbol{\alpha} = \{\mathbf{n}_1, \mathbf{n}_2, \ldots, \mathbf{n}_{|\alpha|}\} \tag{25a}$$

Each cluster is matched to a set of cluster functions

$$\Phi^s_{\boldsymbol{\alpha}} = \prod_{i=1}^{|\alpha|} \Theta_{s_i}(\sigma_i) \tag{25b}$$

where the product is taken over all points incorporated in the cluster $\boldsymbol{\alpha}$, while s_i can take on values from 1 to $(K-1)$. It is noteworthy that if s_i is zero in at least one case, then a subcluster rather than the whole cluster $\boldsymbol{\alpha}$ is considered.

It can be shown that any function with configuration σ (in particular, the energy per atom) can be expressed in the following way:

$$E(\boldsymbol{\sigma}) = \sum_{\boldsymbol{\alpha}} \sum_{s} m_{\boldsymbol{\alpha}} J^{(s)}_{\boldsymbol{\alpha}} \bar{\Phi}^{(s)}_{\boldsymbol{\alpha}}(\boldsymbol{\sigma}) \tag{26}$$

where m_α is the number of clusters $\boldsymbol{\alpha}$ per atom; $J^{(s)}_{\boldsymbol{\alpha}}$ are expansion coefficients; $\bar{\Phi}^{(s)}_{\boldsymbol{\alpha}}(\boldsymbol{\sigma})$ is the average value of the cluster function obtained by averaging over all clusters $\boldsymbol{\alpha}$ at a given configuration, *i.e.*, at definite σ. The expression for energy can be exact if the entire crystal is used as the maximum cluster; however, in practice, the desired accuracy can be achieved even for relatively small maximum clusters.[133]

The unknowns in the expansion of the energy are the coefficients $J^{(s)}_{\boldsymbol{\alpha}}$ — so-called effective cluster interactions. A number of software packages, *e.g.*, ATAT,[134] CLEASE,[135] UNCLE [136] and other, have now been developed for computerized calculations by the cluster expansion method; the results for DFT calculations of a small number of configurations (this number is small in comparison with the total number of all possible configurations) are used as the input information. The subsequent minimization of the penalty function containing the squared energy differences found *via* DFT calculations and *via* the cluster expansion method results in the data on effective cluster interactions. This provides the possibility of calculating the energy of an arbitrary atomic configuration.

For example, the application of the cluster expansion method [137] to the Mo–Nb–Ta–W system resulted in the prediction of the $A2 \rightarrow B2$ phase transition upon temperature rise. The calculations were based on cluster expansion data for binary compounds (Fig. 9).

3.8. Free energy calculation

While studying HEAs, it is important to consider the finite temperature effects, because entropy is present in the expression of free energy as a multiplier of temperature. These effects can be considered by analysis of free energy; so far, the internal energy of the system was mainly mentioned.

We will consider the Helmholtz free energy $F(N,V,T,\boldsymbol{\omega})$ and outline the procedure of calculation of free energy of the multicomponent disordered solid solution used by Feng *et al.*[138]

First of all, we will represent $F(N,V,T,\boldsymbol{\omega})$ as a sum of independent terms

$$F_{\text{tot}} = F_{\text{conf}} + F_{\text{el}} + F_{\text{vib}} \tag{27}$$

where F_{conf}, F_{el} and F_{vib} are the configurational, electronic and vibrational contributions to the free energy.

For a crystalline solid in a configuration space, it is possible to distinguish sites that correspond to particular relaxed positions of atoms of various types in the vicinity of ideal crystal lattice points. These sites can be described by the vector $\boldsymbol{\sigma}$ with the dimensionality equal to the number of sites in the considered supercell. Then the configurational part of the Helmholtz free energy can be written as follows:

$$F_{\text{conf}} = -kT\ln\left[\sum_{\sigma}\exp\left(-\frac{E(\boldsymbol{\sigma})}{kT}\right)\right] \tag{28}$$

The energy $E(\boldsymbol{\sigma})$ can be calculated by any available method (DFT, classical potentials, cluster expansion, *etc.*). However, for a disordered solid solution, the number of terms of summation is enormous even at relatively small supercell size; therefore, for considering the disordered state, it is possible to take one representative structure, for example, a special quasi-random structure, and calculate the configurational free energy as

$$F_{\text{conf}} = E_{\text{SOS}}^{T=0\,K} - TS_{\text{conf}} \tag{29}$$

The S_{conf} value can be found, in particular, by the Boltzmann formula. The subsequent calculation is done for the same supercell.

The electronic free energy is found from the following expressions

$$F_{\text{el}} = U_{\text{el}} - TS_{\text{el}} \tag{30}$$

$$U_{\text{el}} = \int ED(E)\left[f_{T,\mu}(E) - f_{0,E_f}(E)\right]\mathrm{d}E \tag{31}$$

$$S_{\text{el}} = -k\int D(E)\left[f_{T,\mu}(E)\ln\left(f_{T,\mu}(E)\right) + \right. \\ \left. +\left(1-f_{T,\mu}(E)\right)\ln\left(1-f_{T,\mu}(E)\right)\right]\mathrm{d}E \tag{32}$$

where $f_{T,\mu}(E)$ is the Fermi–Dirac function, $D(E)$ is the density of states derived from DFT calculations, μ is the chemical potential determined by the normalization relation

$$N_{\text{el}} = \int D(E)f_{T,\mu}(E)\mathrm{d}E \tag{33}$$

The vibrational component of the free energy is determined in the harmonic approximation for the same supercell from the vibrational state density $g(\omega)$, which is also derived from DFT calculations,

$$F_{\text{vib}} = kT\int g(\omega)\ln\left(2\,\mathrm{sh}\frac{\hbar\omega}{2kT}\right)\mathrm{d}\omega \tag{34}$$

$$\omega = 2\pi\nu \tag{34a}$$

As indicated above, transition from $F(N,V,T)$ to $G(N,p,T)$ is performed by the Legendre transformations

$$G(N,p,T) = F(N,V(p),T) + pV(N,T) \tag{35}$$

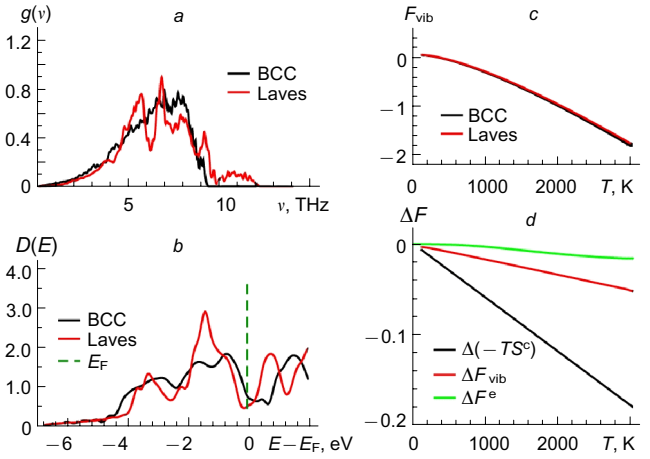


Figure 10. Variation of the density of vibrational states (*a*), density of electronic states (*b*), vibrational free energy (*c*) and contributions to the free energy upon transition of the CrMoNbV alloy from the Laves phase to a disordered BCC solid solution (*d*).[138] Designations: E_{F} is the Fermi energy, S^{c} is configurational entropy, F_{vib} is vibrational Helmholtz free energy, F^{e} is the electronic Helmholtz free energy.

For example, Feng *et al.*[138] calculated the configurational, vibrational and electronic contributions to the change in the free energy for the transition of the CrMoNbV alloy from a Laves phase to a disordered solid solution with a BCC structure (Fig. 10).

The thermodynamic stability of the phase under these conditions is determined by the free energy; therefore, the free energy calculation is highly important, for example, for constructing phase diagrams for one or another system. A specific feature of HEAs in this respect is that in addition to the vibrational and electronic contributions, it is necessary to include the configurational contribution to the entropy.

3.9. Monte Carlo method

The Monte Carlo method is often used to calculate the average thermodynamic values; this allows rather fast movement in the configuration space of the system. We will describe the simplest implementation of the Monte Carlo method. Consider the canonical ensemble (NVT). An arbitrary structure is described by the set of numbers $\{x_i, y_i, z_i, n_i\}_{i\,=\,1\,\ldots\,N}$ (here n_i is the sort of the i-th atom). Having chosen the initial structure (for example, by randomly distributing the atoms among a primitive cubic lattice sites), we will designate the system state by A_0 and calculate the potential energy $U(A_0)$ of this system. Then the following transformations are done for the first atom

$$x_1 \to x_1 + \delta r_{\max} rnd \tag{36}$$

$$y_1 \to y_1 + \delta r_{\max} rnd \tag{37}$$

$$z_1 \to z_1 + \delta r_{\max} rnd \tag{38}$$

where $\delta r_{\max}$ is the maximum displacement along the Cartesian axes, rnd is a random number in the range from -1 to 1. These transformations bring the system into a new state A_1 with the potential energy $U(A_1)$. Then, if $U(A_1) \leqslant U(A_0)$, the state A_1 is accepted. Then the next transformation (for particle number 2) takes place from the state A_1. Meanwhile, if $U(A_1) > U(A_0)$, the state A_1 is accepted with the probability

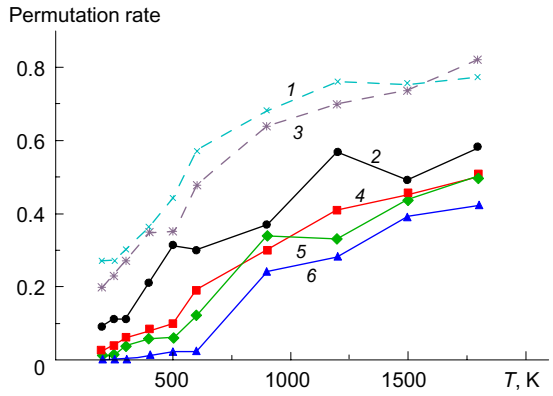


Figure 11. Temperature dependences of the atom permutation rates for Ta–Nb (*1*), Nb–W (*2*), W–Mo (*3*), Ta–W (*4*), Nb–Mo (*5*) and Ta–Mo (*6*) pairs in the Mo–Nb–Ta–W system.[139] Published with permission from Springer Nature.

$$p_{01} = \exp\left(\frac{U(A_0) - U(A_1)}{kT}\right) \quad (39)$$

This procedure is repeated in the same way for all particles from 1 to N. The potential energy of the system can be found using either *ab initio* methods or classical interaction potentials.

When the number of components in the crystal $K > 1$, then, instead of the random displacement, it is possible to exchange positions of atoms i and j provided that their sorts are different. The criterion of switching from one state to another remains the same. It is noteworthy that if the original crystalline state is relaxed in some way, then permutation of two atoms of different sorts will, most likely, lead to an unrelaxed state. In order to solve this problem, before every permutation of atoms, it is necessary to minimize the energy, for example, by the conjugate gradient method. The atoms in crystals oscillate around their equilibrium positions; the character of these oscillations is determined by temperature and by the potential energy surface. Simple permutations of atoms between crystal lattice sites cannot bring the system to those points of the configuration space that are reachable *via* thermal vibrations. In order to bring the system to these points, Monte Carlo and MD methods are combined. The main idea of this combination is that several MD steps are performed between Monte Carlo permutations: for example, alternation of Monte Carlo testing with ten AIMD steps was used.[139] This made it possible to identify pairs of atoms in the Mo–Nb–Ta–W system for which the exchange occurs more easily and elucidate the temperature dependence of the exchange rate (Fig. 11).

3.10. Phase diagram calculation method

The method of phase diagram calculation is based on theoretical and/or experimental data on the phases. Virtually all procedures mentioned above can be used to construct phase diagrams; the required experimental information is mainly provided by calorimetric measurements and determination of chemical potentials.[140]

The quality of CALPHAD calculations is determined by the used database (experimental or theoretical). The modern software implementing the CALPHAD procedure is available both on a free basis (Open Calphad, PyCALPHAD) and on a commercial basis (FactSage, MTDATA, PANDAT, Thermo-Calc, NUCLEA/GEMINI, *etc.*). The TCHEA1 database meant for HEAs, which includes data on binary and ternary intermetallic compounds and various solid solutions for 15 elements, was reported.[141] Currently, this database contains information about compounds of 26 elements, including multicomponent solid solutions.

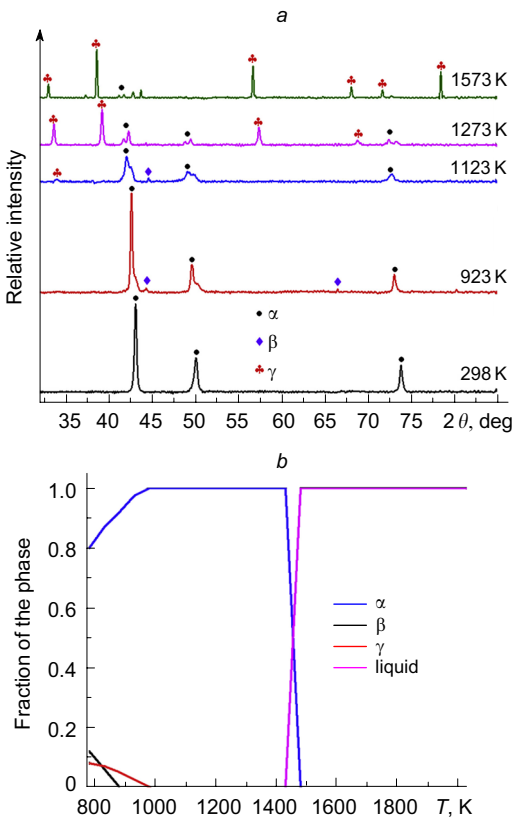


Figure 12. X-Ray diffraction patterns of CoCuFeMnNi (*a*) and results of CALPHAD simulation of the phase composition at various temperatures (*b*).[142] Published with permission from Elsevier.

The applicability of this approach to HEAs was demonstrated, for example, by Sonkusare *et al.*[142] The CALPHAD method in combination with the first version of TCHEA database was used to predict the phase composition of the CoCuFeMnNi alloy, the experimental X-ray diffraction patterns of which at various temperatures are depicted in Fig. 12*a*. It can be seen that α-phase (FCC1 solid solution) predominates at room temperature; after temperature rise to 900 K, the β-phase (BCC solid solution) appears; as the temperature further increases, the γ-phase (FCC2 solid solution) starts to predominate. The results of thermodynamic modelling by the CALPHAD method are shown in Fig. 12*b*. Comparison of Figs 12*a* and 12*b* indicates that agreement between the experimental and calculated results consists in the correct prediction of phases existing in this temperature range and the temperature range in which the BCC phase exists.

4. Heat-, corrosion- and oxidation-resistant materials and coatings

A promising application of HEAs is their use as heat- and oxidation resistant materials and coatings. By heat resistance is meant the ability of materials to operate without

destruction or noticeable residual strain under a load at elevated temperature, while oxidation resistance (scale resistance) is the ability of an alloy to resist oxidation at high temperatures. The first HEAs were based on refractory elements: Ti, Zr, Hf, Cr, Al, Si, Co and Ni. Some of the alloys had only four basic components, while some other alloys contained elements with concentrations > 35% and were not single-phase systems. These alloys, which do not fall under the traditional definition of HEAs, are called refractory complex concentrated alloys (RCCA).[143, 144] We use a less strict definition, namely, multicomponent metallic systems with high concentrations of basic components.

4.1. Phase composition and microstructure

The HEA concept implies a single-phase disordered solid solution; however, the best mechanical properties do not always correspond to particularly this phase composition. In some cases, the desired mechanical properties are provided by a complex microstructure with two or more phases. A detailed review of studies dealing with refractory HEAs published from 2010 to 2018 was reported by Senkov *et al.*[144] The results of studies of dozens refractory HEAs were reported in recent years; most of these alloys were single-phase solid solutions with BCC structure such as AlCoCrFeNi,[145] CrFeMoV,[146] WNbMoTaV,[147] HfNbTiZr,[148] NbTaTiV, NbTaTiW, NbTaTiVW,[149] $Re_{0.5}$NbMoTaW,[150] HfNbTaTiZrW, HfNbTaTiZrMoW,[151] MoNbTaTiV,[74] NbZrTiCrAl,[91] CrMoVW,[152] TiZrNbTa,[153] VNbMoTaW,[154] $TiZrHfNbTaMo_{0.25-0.75}$ [155] and $Ti_{50}Nb_{30}Cr_{10}V_{10}$.[156] Some of the refractory HEAs were mixtures of phases, which contained Laves phases, *e.g.*, $Al_{0.5}CrMoNbTiZr_{0.5}$,[157] NbMoTaWVCr,[158] CrMoNbWTi-C,[159] $AlNbTiVZr_{0.5}$,[160] CrMoNbTiVWZr,[161] $Al_{20}Cr_{10}Nb_{15}Ti_{20}V_{25}Zr_{10}$ [162] and CrNbTiZrAl.[163] When non-metals such as carbon or silicon were added to the compositions, carbide and silicide phases appeared, *e.g.*, CrMoNbWTi-C (Ref. 159) and $HfNbTiVSi_{0.5}$.[164]

Some refractory HEAs have a dendritic structure in which dendrites are often enriched in particular elements. The dendrites can be enriched in chromium (in AlCoCrFeNi),[145] in tantalum and niobium (NbTaTiV),[149] tantalum and tungsten (NbTaTiW),[149] tungsten, tantalum and niobium (HfNbTaTiZrW),[151] niobium and titanium (NbZrTiCrAl),[91] molybdenum and tungsten (CrMoVW),[152] niobium, tantalum and molybdenum ($TiZrHfNbTaMo_{0.25-0.75}$) [155] and niobium ($Ti_{50}Nb_{30}Cr_{10}V_{10}$).[156]

Using information available from the published sources mentioned in this part of the review, we constructed a three-dimensional diagram (Fig. 13), in which the number of RCCAs can be correlated with the number of components and phases. According to this diagram, the increase in the entropy of mixing of an ideal solid solution with a definite number of components following an increase in the number of components does not always ensure the formation of a single-phase system. For example, it can be seen that in the case of six-component compositions, there are more two-phase systems than single-phase ones.

4.2. Mechanical characteristics

The properties investigated most often for refractory HEAs are hardness and/or compressive strength.[75, 146–152, 154–160, 162–170] The yield strength as a function of testing temperature and the regions occupied by refractory HEAs that are described by Senkov *et al.*[144] are shown in Fig. 14.

It can be seen that strength characteristics of HEAs obey more beneficial temperature dependences than those of known commercial alloys, *e.g.*, INCONEL 718. However, it is necessary to mention that over the last two years, no significant progress was attained in the synthesis of HEAs possessing good high-temperature strength characteristics. In addition. most of strength tests were carried out at room temperature, and certain advances were made. Raza *et al.*[146] found a yield strength in the 2730 to 3552 MPa range for the group of $Al_xCrFeMoV$ alloys ($x = 0-0.6$) at room temperature. These alloys are lightweight, which ensures a very high specific yield strength equal to 512 MPa $cm^3\ g^{-1}$.

Apart from the strength characteristics, Vickers microhardness was studied for many alloys, with the typical values being approximately 5–10 GPa. Out of the considered bulk HEAs, the highest hardness was found for VNbMoTaW.[154] The authors attributed this result to the fine-grain structure of thia alloy and solid solution strengthening.

The studies devoted to the fatigue and creep properties of refractory HEAs are more rare. As an example of studying the fatigue properties of a refractory HEA, consider a paper by Guennec *et al.*[170] addressing the fatigue endurance of HfNbTaTiZr. The authors showed that this BCC alloy has a relatively high ratio of the fatigue endurance to the

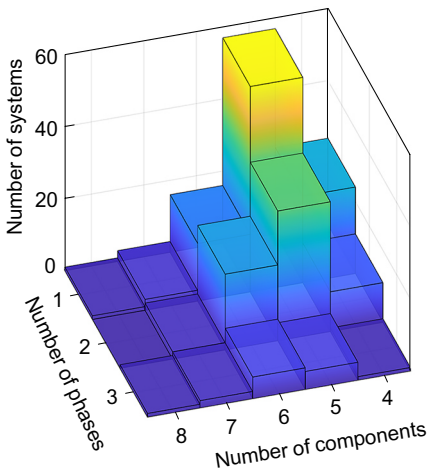


Figure 13. Diagram relating the numbers of components, phases and refractory HEAs. The Figure was created by the authors using data of Ref. 144 and other publications considered in Section 4.1.

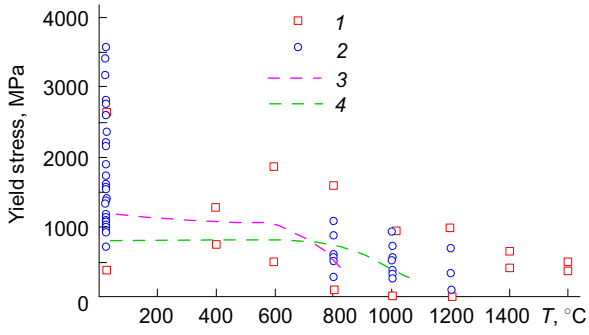


Figure 14. Temperature dependences of the strength properties for several refractory HEAs. The Figure was created by the authors using data of a review [144] (*1*) and publications [75, 146–148, 150–152, 154–160, 162, 163, 165–170] (*2*); (*3*) INCONEL 718 alloy; (*4*) Mag M247 alloy.

ultimate tensile strength in comparison with traditional alloys, bulk metallic glasses or FCC HEAs. The creep behaviour of $Al_xCoCrFeNi$, $Ni_{47.9}Al_{10.2}Co_{16.9}Cr_{7.4}Fe_{8.9}Ti_{5.8}Mo_{0.9}Nb_{1.2}W_{0.4}C_{0.4}$ and $AlTiVNbZr_{0.25}$ high-entropy alloys at elevated temperature have been studied in Refs 171–173, respectively.

4.3. Corrosion resistance

A material meant for long-term operation at elevated temperature should not only possess beneficial strength characteristics but also be chemically inert towards the environment (most often, surrounding gases), *i.e.*, it should be corrosion resistant. Thus, in addition to high-temperature mechanical properties, the ability of HEAs to resist corrosion at high temperature is also of interest.

Most often, corrosion is due to reaction between the metal and air oxygen. The oxidation stability is evaluated by the thermogravimetric method, which shows the time variation of the sample mass in an oxygen-containing atmosphere at a specified temperature. The ratio of the sample mass gain to the area of sample contact with the atmosphere can serve as a quantitative characteristic of the oxidation stability of the material. In addition, the shape of the curve for the variation of the sample mass can provide information on the oxidation mechanisms. There are two most frequent oxidation regimes: linear [proportional to time (t)] and parabolic (proportional to $t^{1/2}$) ones.

The data on HEAs that have been investigated for oxidation behaviour at elevated temperature are summarized in Table 3.

The resistance to high-temperature oxidation is associated with the formation of a continuous protective oxide layer at the metal/gas interface. This layer is formed most efficiently by Cr_2O_3, Al_2O_3 and SiO_2. In the presence of a protective layer, the oxidation regime is parabolic (this is more desirable), *i.e.*, the reaction proceeds *via* the diffusion of metal and oxygen atoms in the formed oxide layer. If the protective layer is porous, oxygen atoms easily get to the metal surface and the oxidation follows a linear regime; in this case, the oxidation rate does not depend on the oxide layer thickness. Since HEAs are multicomponent, the oxidation often gives complex oxides.

It is noteworthy that the oxidation kinetics is described most often by a parabolic (or nearly parabolic) law. However, opposite examples are also given in a review.[144] This attests to a considerable progress made in recent years in the development of HEAs resistant to high-temperature oxidation. This progress would have been impossible without numerous systematic studies.

Some papers deal with the effect of particular elements on the high-temperature oxidation behaviour of matetials. In particular, for $Ni_2FeCoCrAl_x$ alloy, the increase in x from 0 to 1 was accompanied by a considerable decrease in the oxidation rate.[185] A beneficial effect of aluminium was also indicated in other studies.[176, 178, 179, 191, 192, 194, 196–198] It was shown[174–176, 186] that the oxidation rate decreases upon the addition of silicon to HEAs (see Table 3). The resistance to high-temperature oxidation was found to increase with increasing copper content in the $AlCoCu_xCrFeNi$ alloy[193] and chromium content in the $FeCr_xCoNiB$ alloy[188] and with decreasing iron content in $Fe_x(CoCrMnNi)_{100-x}$.[187] The addition of niobium improves the resistance of $CoCrFeMnNiNb_x$ to the oxidation at 700–800 °C; however, it decreases at higher temperatures.[189] An adverse influence of molybdenum on the high-temperature oxidation resistance was noted;[177, 179] this was caused by the fact that molybdenum oxide is evaporated from the metal surface, giving rise to pores, which let in oxygen of the medium. Gorr *et al.*[174] noted the adverse effect of vanadium.

Depending on the temperature, the oxidation kinetics can change. For example, in the temperature range of 800–1000 °C, parabolic oxidation kinetics is implemented for NbZrTiCrAl, while at 1200 °C, the oxidation follows linear kinetics.[91] Despite the very high testing temperature (1400 °C), the oxidation regime of $Cr_{17.6}Al_{20.3}Mo_{15.2}Nb_{2.9}Si_{13.4}Ta_{5.4}Ti$ remained parabolic, and the specific mass gain over 100 hours of oxidation was only 18 mg cm^{-2} (Ref. 195). The so high oxidation resistance was attributed to the formation of a mullite layer — $Al_{4+2x}Si_{2-2x}O_{10-x}$ ($x = 0.26–0.27$).

In addition to the studies of HEA behaviour in a hot oxygen-containing atmosphere, the corrosion resistance of HEAs was also studied in other gas media, *e.g.*, in a CO_2-CO mixture at elevated temperatures,[199] and in aqueous solutions with various concentrations of NaCl,[200–209] NaOH [145, 203] and H_2SO_4.[145, 202, 203] The use of HEA coatings can substantially increase the wear resistance and corrosion resistance of a manufactured article. Apart from the specified strength and hardness characteristics and stability in harsh media, protective coatings should have good adhesion to the substrate material.

Coatings made of high-entropy alloys based on transition metals have been investigated.[210–214] Transition metals that are most often used for this purpose are Co, Cr, Fe and Ni.[212, 215–281] The most popular substrate materials are various brands of steels. Silicon, copper and titanium alloys are used somewhat less often. Quite a few multicomponent coatings are high-entropy nitrides.[216, 219, 220, 248, 259, 266, 277, 282] Apart from nitrogen, other non-metal components can be present, *e.g.*, silicon,[216–218, 234, 243, 246, 248, 250, 259, 265, 270, 276, 280] tungsten carbide[283] and graphene oxide.[252–254]

The large number of papers dealing with HEA coatings, comparable with the number of publications addressing bulk alloys, attests to good prospects for the development of this research area. Indeed, using minor HEA additives, it is possible to increase hardness, strength, wear resistance and corrosion resistance of manufactured articles almost in all cases. Nevertheless, as in the case of bulk HEAs, high-temperature studies of the mechanical properties of HEA coatings were not systematic. The relevant experiments were carried out only in some cases. For example, Ye *et al.*[280] studied the hardness of the $Al_xFeCoNiCuCr$ coating on an AISI 1045 steel substrate in the temperature range of 200–800 °C. High-temperature wear testing of $FeCoCrNiMnAl_x$ and FeCrCoNiSiB coatings was carried out by Shu *et al.*[243] and Cui *et al.*,[276] respectively. Study of the high-temperature oxidation resistance of $FeCoCrNiMnAl_x$ (Ref. 237) and $MoFe_xCrTiWAlNb_y$ (Ref. 276) showed that in the former case, the protective film was mainly Al_2O_3, while in the latter case, it was a mixture of many oxides — Fe_2O_3, FeO, Cr_2O_3, MoO_3, WO_3, Nb_2O_5 and Al_2O_3.

A considerable portion of publications address the electrochemical corrosion in aqueous solutions of salts, acids and alkalis. For example, the amorphous VAlTiCrSi high-entropy film[250] deposited on steel 304 increased the absolute magnitude of the corrosion potential and decreased the corrosion current density in artificial seawater. The authors attributed the good corrosion resistance of these films to their amorphous structure and composition. The amorphous structure precludes the formation of a

Table 3. Data on HEA resistance to high-temperature oxidation.

Alloy	T, °C	t, h	Mass gain, mg cm^{-2}	Oxidation regime	Oxides	Ref.
NbMoCrTiAl	1100	48	8.3	Parabolic	Cr_2O_3, Al_2O_3	174
NbMoCrTiAl + 1% Si	1100	48	6.4	Parabolic → linear	Cr_2O_3, Al_2O_3	174
$NbCrMoAl_{0.5}Ti$	1300	20	150	Linear	TiO_2	175
$NbCrMoAl_{0.5}V$	1300	20	345	Linear	$CrNbO_4$	175
$NbCrMoAl_{0.5}TiV$	1300	20	265	Linear	TiO_2	175
$NbCrMoAl_{0.5}TiVSi_{0.3}$	1300	20	198	Linear	TiO_2	175
FeCoNiCrAl	900	45	0.25	Parabolic	Al_2O_3, $FeAl_2O_4$	176
FeCoNiCrMn	900	45	3.3	Parabolic	Mn_2O_3, Mn_3O_4, Cr_2O_3	176
FeCoNiCrSi	900	45	0.45	Parabolic	Cr_2O_3, SiO_2	176
$Al_{0.5}CrNbTiZr_{0.5}$	1000	50	24	Linear	Al_2O_3, CrO_2, $CrNbO_4$	177
CoCrCuFeNi	1000	100	1.31	Parabolic	Cr_2O_3, (CoNiCu)O, spinel	178
$Al_{0.5}CoCrCuFeNi$	1000	100	0.73	Parabolic	Al_2O_3, Cr_2O_3, spinel	178
AlCoCrCuFeNi	1000	100	0.32	Parabolic	Al_2O_3, Cr_2O_3, spinel	178
$Al_{1.5}CoCrCuFeNi$	1000	100	0.26	Parabolic	Al_2O_3, Cr_2O_3, spinel	178
$Al_2CoCrCuFeNi$	1000	100	0.24	Parabolic	Al_2O_3, Cr_2O_3, spinel	178
$TiNbTa_{0.5}Zr$	1000	40	120	Parabolic	Al_2O_3	179
$TiNbTa_{0.5}ZrAl$	1000	40	42	Parabolic	Al_2O_3	179
$TiNbTa_{0.5}ZrAlMo_{0.5}$	1000	40	150	Linear	MoO_3	179
$Al_{0.6}CrFeCoNi$	900	100	0.64	Parabolic	Cr_2O, spinel, Al_2O_3	180
$Al_{0.6}CrFeCoNiSi_{0.3}$	900	100	0.66	Parabolic	Cr_2O, spinel, Al_2O_3	180
CrMnFeCoNi	1100	24	9	Parabolic	Cr_2O_3, Mn_3O_4	181
MoWAlCrTi	1000	40	8	Parabolic	Cr_2O_3, Al_2O_3, TiO_2, WO_3	182
NbCrVWTa	800	72	285	Parabolic	–	183
FeCoNiCrMn	900	45	2.4	Parabolic	Mn_3O_4, Cr_3O_3, Cr_2O_3	184
$Ni_2FeCoCrAl_{0.5}$	900	49	0.4	Parabolic	Al_2O_3	185
$FeCoNiCrSi_{0.5}$	900	49	0.5	Parabolic	Cr_2O_3, SiO_2	186
FeCoCrMnNi	1100	49	19	Parabolic	Mn_3O_4, Fe_3O_4, $NiCr_2O_4$, $CoMn_2O_4$, $CrMn_{1.5}O_4$	187
$FeCoCr_3NiB$	900	50	3	Parabolic	Cr_2O_3	188
CoCrFeMnNi	900	100	2.9	Parabolic	–	189
$CoCrFeMnNiNb_{0.25}$	900	200	3.1	Parabolic	Mn_2O_3, Mn_3O_4	189
$AlCrFeNiTiMn_{0.5}$	900	100	1.7	Linear	TiO_2, Al_2O_3, Mn_2O_3	190
AlCrFeNiTi	900	100	1.3	–	TiO_2, Al_2O_3	190
$Al_{0.7}CoCrFeNi$	1100	200	0.5	Parabolic	Al_2O_3, Cr_2O_3, NiO, $NiCr_2O_4$	191
$Al_{0.3}CoCrFeNi$	1100	200	1.1	Parabolic	Al_2O_3, Cr_2O_3, NiO, $NiCr_2O_4$	191
$Al_{1.5}CoCrFeNiTi_{0.5}$	1100	100	0.9	Parabolic	$(Al_{0.9}Cr_{0.1})_2O_3$	192
AlCoCrCuFeNi	1000	100	0.2	Parabolic	Al_2O_3	193
$Al_2CoCrFeNiMn$	900	100	1	Parabolic	Cr_2O_3, Al_2O_3, Mn_3O_4, Mn,Ni, $(Cr,Fe,Al)_2O_4$	194
AlNbTiZr	1000	3	13.8	Parabolic	$AlNbO_4$, Ti_2ZrO_6	168
NbZrTiCrAl	1200	50	183	Linear	$CrNbO_4$, ZrO_2	91
$Cr_{17.6}Al_{20.3}Mo_{15.2}Nb_{2.9}$, $Si_{13.4}Ta_{5.4}Ti$	1400	100	18	Parabolic	Cr_2O_3, $Al_{4+2x}Si_{2-2x}O_{10-x}$ ($x = 0.26-0.27$)	195

Note. The presented data were obtained at the highest temperature among those used in experiments.

large number of galvanic microcells on the coating surface, while the presence of some elements such as aluminium, chromium or silicon enables the formation of protective films of oxides of theseelements.

5. Radiation-resistant materials and coatings

By radiation resistance is meant the ability of a material to retain its mechanical, physical and chemical properties under irradiation (an important factor is preservation of the integrity and density of the material being irradiated) and the ability of finished products made of this material to preserve their shape and size. Any material is damaged by radiation to one or another extent as a result of parallel or successive process stages that are listed below. The first stage is interaction of radiation with the matter accompanied by induced excitation of electrons and phonons, photoelectric effect, ionization of atoms, displacement of atoms from their equilibrium positions to interstices, vacancies or positions of other atoms, isotope transformations, *etc*.

In the second stage, the energy is transferred from the primarily excited electrons, phonons and displaced atoms to other atoms, which often induces cascade processes. The final stage is the relaxation and thermalization to give radiation defects stable at the irradiation temperature. Simple radiation-induced point defects include vacancies, interstitial atoms and substitution atoms. In addition, complex defects often arise, *e.g.*, defect clusters — aggregates of interstitial atoms and/or vacancies. As a rule, radiation-induced defects are thermodynamically non-equilibrium; therefore, upon temperature rise, they can migrate over the material, disappear or agglomerate to give larger and more complex defects. These processes take place both during the irradiation and during post-radiation annealing.

The radiation resistance of elements has been studied modt thoroughly, but they are rarely used in materials. The radiation resistance of HEAs has started to be studied only recently, but this characteristic is expected to be high, because the structure of these alloys is disordered. These expectations are based on the known radiation resistance of other disordered systems. Indeed, owing to the high degree of disorder and high concentration of structural vacancies, highly non-stoichiometric interstitial compounds and their solid solutions — the hardest and the most refractory known compounds — have high radiation resistance.[284, 285] The radiation resistance of non-stoichiometric compounds containing vacancies in one sublattice or in simultaneously two sublattices was studied for transition metal monocarbides[286] and monoxides.[287]

An understanding why atomically disordered materials are resistant to radiation can be gained from comparing their behaviour under irradiation with the behaviour of perfectly ordered single crystal stoichiometric compounds, which have no homogeneity regions. This study was carried out in relation to silicon carbide using irradiation with high-energy electrons at a low temperature.[288] It was shown that materials with high degree of ordering are more prone to destruction under high-energy radiation, since they cannot accumulate large numbers of atomic structure defects. Meanwhile, materials that already contain structural defects can withstand more defects, as they have developed relaxation mechanisms. Moreover, an increase in the degree of disorder results in higher stability of these materials due to increasing entropy. Therefore, it is reasonable to expect that high-entropy materials with a high degree of disorder of chemical elements would be resistant to radiation.

Indeed, it was shown by MD calculations[289] that CoCrFeMnNi HEA accumulates less radiation damage during irradiation than nickel with FCC structure and pure iron with BCC structure. In this HEA, the defects generated under irradiation are located in a relatively confined space because of high energy of migration of interstitial atoms and the absence of displacement cascades, which leads to efficient recombination and small number of residual defects. In addition, the instability of defect clusters caused by crystal lattice distortions further increases the rate of recombination of residual defects and delays the growth of defect clusters. The delay of accumulation of radiation defects results in increasing radiation resistance of the CoCrFeMnNi alloy. The retarded accumulation of radiation damages for this HEA is caused by distortion of the crystal lattice due to its multicomponent nature.

High tolerance to the radiation damage can also be expected for other multielement alloys. The theoretical predictions were confirmed experimentally. It was shown[290–292] that HEAs are less sensitive to irradiation than conventional alloys. In particular, the radiation-induced swelling[293, 294] and the formation of dislocation loops[293, 295] decreased. It was shown in a comparative experiment[296] that swelling of the NiCoFeCrMn high-entropy alloy was only 0.2%, whereas swelling of pure nickel was 6.7% under the same conditions. Zhang and co-workers[296–298] suggested that owing to the increased lattice deformations in HEAs, the diffusion of defects is retarded, the motion of dislocations is prevented and the motion of interstitial defect clusters in the ⟨110⟩ crystallographic direction of the FCC lattice is suppressed. These factors facilitate recombination of the interstitial defects with vacancies.

Irradiation changes the physicomechanical properties of HEA, in particular, irradiation-induced creep appears in the nanostructured material.[299] The irradiation of NiCoFeCrMn with a high-energy (2.6 meV) Ag^{3+} ion flux at a dose rate of 1.5×10^{-3} dpa s^{-1} at 100 °C promotes transition from the relaxation regime to the regime in which the concentration of defect traps is insufficient and creep appears. The intense creep induced by irradiation at low temperature prevails over the thermal creep up to 650 °C. The authors[299] also demonstrated that the HEA nanograin size slightly affects the defect recombination. This conclusion requires further verification and more detailed studies of nanocrystalline HEAs.

According to Komarov *et al.*,[300, 301] radiation-resistant materials such as high-entropy nanostructured nitrides of transition metals — titanium, hafnium, zirconium, vanadium and niobium — are most promising as coatings for fuel element jackets of nuclear reactor cores and for the first walls of nuclear fusion reactors (tokamaks and stellarators). The authors irradiated the (Ti,Hf,Zr,V,Nb)N coatings with helium ions with an energy of 500 keV in the fluency range from 5×10^{16} to 3×10^{17} ions per cm^2 and examined their composition, structure and properties before and after irradiation. After irradiation, no changes in the elemental composition, structure or phase composition were detected in the coatings (apart from the decrease in the crystallite size to nanoscale values). Therefore, it was concluded that these materials are suitable as coatings of nuclear fuel elements.

More evidence in favour of using HEA coatings for materials of nuclear technology can be found in publications[291, 302, 303] considering a useful feature of HEAs, namely, the tolerance to the variation of chemical composition without a change in the microstructure. This enables fine tuning of HEA properties, which is important for both external and internal hot parts of nuclear fusion reactors. Vanadium-containing HEAs were considered[304] as promising materials for fusion reactors; using these materials, it is possible to decrease the amount of radioactive waste. The homogenized VCrMn and VCrMnTi alloys, which were not used previously for this purpose, were prepared and characterized. It was found that their single-phase BCC solid solutions can successfully dissolve a large concentration of vanadium, which is a low-activation element. Thus, HEA coatings can be very useful for power engineering applications.

6. Materials and coatings for biomedicine

Materials for biomedical applications are very important for both patient treatment and development of procedures for studying human body structure and functioning in the

normal and pathological states as well as for development of diagnostic methods. Medicine is a field of knowledge and practice, which, on the one hand, uses almost everything that was created by nature and, on the other hand, sets relevant problems for fundamental science. A basic challenge is development of new materials that meet various demands of medicine. Since the development of biomedicine, a theoretical science, is associated with studying the details of functioning of a human body and processes occurring at cellular and intracellular levels, it is necessary to design innovative non-toxic biocompatible materials.

The progress of modern medicinal chemistry is related to the design and efficient and selective synthesis of new pharmaceutical agents. This research field is very broad and it can hardly be described, even superficially, within the framework of this review. Therefore, we will consider only one aspect related to the use of disordered non-stoichiometric materials;[305] HEAs are likely to be used for this purpose in the future. Rempel and Valeeva [305] compared the results of application of ordered stoichiometric and disordered non-stoichiometric titanium dioxides to catalyze the cross-coupling reactions for the synthesis of new organic molecules, which are needed for the development of modern medicinal products, in particular antiviral agents. It was shown that disordered TiO_{2-x} is better than ordered TiO_2 for the visible light-induced (without involvement of the ultraviolet range) synthesis of medicinal products. Owing to the appearance of the impurity energy level in the disordered material, visible light photons are absorbed in the energy gap giving rise to electrons and holes, which catalyze the cross-coupling of heteroarenes. By introducing other metals into the titanium sublattice and nitrogen and carbon into the oxygen sublattice of TiO_2, it is possible to obtain a disordered high-entropy material, which would be an even more efficient photocatalyst than the disordered non-stoichiometric titanium dioxide. This is quite probable because a multicomponent solid solution can be tuned to the particular absorption wavelength that is needed for selective and efficient photocatalysis of the desired organic reaction.

Currently, surgeries often involve implantation of metallic structures into the patient s body, and to attach these structures, artificial foreign materials are introduced. These materials can injure the surrounding biological tissues. One way to increase the adaptability of the body to these materials is the use of HEA coatings that show the shape memory effect. Another way is to employ bioresorbable materials, *e.g.*, artificial bones [306–310] based on multicomponent composites. The most promising modern approach is to combine alloys and coatings made of composite materials.[306]

Using nanotechnologies, new functional nanocomposites can be designed from known compounds. For example, a considerable number of phosphates crystallize in the $CaO-P_2O$ system, some of them being used in medicine. A widely used phosphate — synthetic hydroxyapatite (HAP) $Ca_{10}(PO_4)_6(OH)$ — is used to replace bone defects and to coat implants in order to improve the connection with bone tissue. However, the application of HAP-based bioceramics is restricted by insufficiently high mechanical properties such as strength and cracking resistance. The mechanical properties of the bioceramics can be improved by adding zirconium, titanium and titanium dioxide.[306, 311–313] Titanium and its oxides have good biocompatibility, and when added to bioceramics, they not only increase their strength and crack resistance,[311] but also endow materials with photocatalytic activity [311] and bactericidal properties. It was shown [313] that the HAP/TiO_2 composite induces efficient degradation of pentachlorophenol, while the HAP/Ti nanocomposite [311] can be applied to eliminate dyes from aqueous solutions. According to Farzin *et al.*,[314] nanostructured composite materials based on HAP show a higher biological activity than similar compositions with micrometre-sized particles. Thus, the research field dealing with biomedical composite materials follows a trend towards the design of multielement high-entropy systems.

High-entropy alloys that are used as coatings on implants can also perform useful functions. For example, such coatings can suppress the dissolution and leaching of elements hazardous for human health that are present in composite materials. Interesting results concerning the inhibition of leaching were obtained by Chang *et al.*[315] The selective leaching and surface properties were studied in relation to FCC structured CoNiCr, FeCoNiCr and FeCoNiCrPd medium- and high-entropy alloys. On the basis of experimental results, the authors drew conclusions about the potential of these materials for biomedicine. Selective leaching showed that the concentration of cobalt and nickel ions released from CoNiCr, FeCoNiCr and FeCoNiCrPd was higher than the concentration of chromium, iron and palladium ions. The relatively high rate of selective leaching of cobalt and nickel was attributed to the presence of large amounts of cobalt and nickel metals near the alloy surface, comparable with the amounts of nickel and cobalt in the oxidized state. However, most of chromium and iron ions near the alloy surface were in their highest passive oxidation states rather than in the corresponding metallic states. Owing to remarkably high corrosion resistance and exceptionally low rate of selective leaching, FeCoNiCrPd high-entropy alloys are better suited for biomedical applications than the CoNiCr and FeCoNiCr medium-entropy alloys. The beneficial properties of FeCoNiCrPd were attributed to the fact that highly inert palladium metal and PdO are mainly present on the alloy surface, despite the fact that the content of palladium in the equiatomic FeCoNiCrPd alloy is only 20%.

Highly interesting and important results concerning coatings for biomedical purposes were obtained by Braic *et al.*,[316] who described a method for the preparation of multielement nitride and carbide coatings, (TiZrNbHfTa)N and (TiZrNbHfTa)C, on the Ti_6Al_4V alloy by co-sputtering of transition metal targets (titanium, zirconium, niobium, hafnium and tantalum) in a reactive atmosphere. The coatings were characterized by elemental and phase composition, crystalline structure, morphology, residual stress, hardness, friction performance, corrosion resistance and cell viability. All coatings were found to form only ideal FCC solid solutions with predominant (111) orientation and crystallite size from 7.2 to 13.5 nm. These coatings were subjected to a compressive stress from 0.8 to 1.6 GPa. The carbide coating with the highest carbon content (the carbon to metal ratio was $\sim$1.3) had the highest hardness ($\sim$31 GPa), the best friction coefficient (0.12) and the highest wear resistance (0.2×10^{-6} mm^3 N^{-1} m^{-1}) when measured in model biological fluids. Testing of the viability of biological cells demonstrated that osteoblast cells felt well on the high-entropy coating of the Ti_6Al_4V alloy; a very high percentage of live cells was detected on this surface after a 72-hour incubation.

The early studies were continued by development of a biomaterial that contained analogous transition metals, but was neither carbide nor nitride. Todai *et al.*[317] described a metallic biomaterial — equiatomic TiNbTaZrMo alloy. While developing the biomaterial, the authors were guided by the main principles of the construction of HEAs, considering a number of parameters such as ΔH_{mix}, Ω, δ and VEC. The BCC solid solution phases with different lattice constants were obtained by casting and in the annealed state. The synthesized HEA showed relatively high strength and deformability and very high biocompatibility compared with that of pure titanium. Thus, the study demonstrated good prospects for using HEAs as metallic biomaterials.

Edalati *et al.*[318] rightly indicated that most of publications are devoted to the mechanical properties of HEAs, while only few studies address their biocompatibility. Therefore, they determined the biocompatibility of the alloys, apart from their mechanical properties. The authors chose the TiAlFeCoNi high-entropy alloy, which had a ultrahigh Vickers hardness, low elastic modulus determined by nanoindentation, and superior activity for cell viability and cytotoxicity according to the MTT assay data (colorimetric assay for determining the metabolic activity of cells). A sample of this alloy was processed by high-pressure torsion with the goal of increasing its hardness as a result of formation of nanograins and dislocations and order–disorder transitions. After this processing, the TiAlFeCoNi alloy with the L21-BCC crystal structure had a 170–580% higher hardness and 260–1020% higher metabolic activity compared to known biomaterials — titanium and Ti-6Al-7Nb, respectively. Thus, the experiment showed a high potential of HEAs for biomedical applications.

The successful result obtained by Todai *et al.*,[317] who used a primitive approach to the formation of HEAs, is an incentive for using theoretical studies to predict the properties. In this respect, it is necessary to mention a purely theoretical study,[319] which considers many HEAs and makes a profound analysis of their electronic structure, interatomic interactions on the basis of quantum mechanics principles and total and partial density of states. The authors chose seven elements (Ti, Nb, Ta, V, Zr, Hf, Mo) and predicted, using their approach, the properties of three biocompatible multicomponent alloys. Most likely, such an approach should prevail for the development of functional materials using HEAs.

7. Properties and applications of protective coatings based on high-entropy alloys

Owing to the microcrystalline structure and high stress in the crystal lattice, high-entropy alloys can have enhanced strength in combination with oxidation and corrosion resistance. In view of the above, the application of HEAs for the production of coatings, in particular by plasma spraying is a promising trend. The two most popular high-entropy coatings are nitrides and carbides. To date, HEA nitride coatings have been most studied, while carbide coatings have been little investigated.[40] This is due to the fact that nitride coatings exhibit fairly high physicomechanical properties.

A number of publications [320–322] considered TiVCrZrY, AlCrTaTiZr AlCrNbSiTiV and AlMoNbSiTaTiVZr coatings deposited by plasma sputtering of a target obtained by arc melting. The effect of process parameters on the physicomechanical properties of the coatings have been studied.[216, 320, 321, 323] Liang *et al.*[323] and Huang and Yeh [324] discussed data on the effect of annealing on the variation of hardness and Young modulus of AlCrNbSiTiVN HEA nitride coatings. According to X-ray diffraction data, the structural characteristics of the coatings did not change even after annealing at 1000 °C. The possible explanation is that the FCC lattice of the coating is stable due to the high-entropy effect. Even at 900 °C, the hardness virtually did not change, while at higher temperature it somewhat decreased; the Young modulus increased with increasing temperature to reach a maximum at 900 °C and then also decreased. This may be attributed to the formation of a thin ($\sim$20 nm) oxide layer on the coating surface.

Liang *et al.*[323] studied the effect of the substrate temperature, which changed from room temperature to 450 °C, on the physicomechanical properties of the TiVCrZrHfN coating. As the substrate temperature was raised, the percentages of elements and the phase composition of the coating remained invariable (only one stable FCC phase was detected); however, grain sizes changed and the hardness and Young modulus increased. This is due to the fact that temperature rise leads to higher mobility of atoms in the surface layer of the coating, which thus has less voids and becomes more compact.

Te Hsueh *et al.*[216] investigated the effect of nitrogen concentration and the substrate bias potential on the mechanical characteristics and phase composition of the $(AlCrSiTiZr)_{100-x}N_x$ HEA nitride coatings. Study of the phase composition demonstrated that at nitrogen concentrations of 0 and 5%, the films were amorphous. The diffraction peak broadening observed with increasing concentration of nitrogen attests to increasing degree of atomic disorder in the coating. In other words, an increase in the nitrogen concentration can be considered as a factor that destroys the amorphous structure of the coating. A similar effect was also observed in another study [325] dealing with nitride films. The hardness of the coatings increased from 11.5 to 17 GPa as the concentration of nitrogen changed from 0 to 5%, decreased 16 GPa when the nitrogen concentration was 15%, and remained invariable for nitrogen concentration of 30%. The Young modulus varied in approximately the same way. The indicated variation of hardness may be attributable to the influence of nitrogen concentration and modifications of the crystal structure of the coating.

Lee *et al.*[326] investigated the effect of the direct current bias on the microstructure, residual stress and the hardness of TiVCrZrTaN coating obtained by reactive high-frequency magnetron sputtering. It was shown that at a voltage <100 V, the (111) crystallographic orientation predominated, while at 100 and 120 V, the prevailing orientation was (200). As the applied voltage increased, the roughness decreased. Upon the increase in the voltage from 0 to 100 V, the hardness also increased, while when the bias voltage was >100 V, it sharply decreased. The effect of nitrogen concentration on the structure and properties of the HEA nitrides was studied. For example, it was shown [327] that increase in the nitrogen concentration was accompanied by a change in the coating structure from amorphous alloy to nanocomposite and even to crystalline nitride; simultaneously, the hardness increased from 13 to 30 GPa.

One more promising method used to prepare protective coatings is detonation spraying. This technology is based on

the processes of interaction of the sprayed particles with the gas medium and substrate surface.[328, 329] The regularities of these processes are determined by the spraying technique,[330] size and shape of the powder particles [331] and the physico-mechanical properties of the sprayed material and the substrate.[332] It is worth noting that the detonation combined multilayer coatings based on chromium carbide, tantalum carbide and chromium nickelide, as well as HEAs are promising for modification of the working surfaces of parts and assemblies operating at elevated temperatures in harsh media. Yin *et al.*[245] used for the first time the solid-state cold spraying to prepare a HEA coating of the FeCoNiCrMn alloy. The results of the experiment showed that this method, which completely preserves the phase composition of HEAs without any transformations, can be used to deposit thick-layer coatings with low porosity. The results indicate that the grains of the coating substantially changed with respect to the grains of the initial HEA powder as a result of dynamic recrystallization in the highly strained intergrain region. Due to the enhanced dislocation density at grain boundaries, the HEA coating was markedly harder than the as-received HEA powder. A tribological study showed that the FeCoNiCrMn HEA coating obtained by the solid-state cold spraying is characterized by a lower wear rate than the coatings of the same HEA deposited by laser cladding.

8. Note added in proof

More than half a year passed since this review was accepted for publication. During this period, the research in this field has actively developed, and new publications appeared. Thus the Cantor alloy, CoCrFeMnNi, which has been seemingly thoroughly studied since 2004, was used as the investigation object in several works. For example, the effect of the ionizing radiation on CoCrFeMnNi and amorphization of this HEA under extreme loads were studied by Zhang *et al.*[333] and Zhao *et al.*,[334] respectively. A machine learning potential for CoCrFeMnNi for the use in molecular dynamics was obtained.[335] The Cantor alloy was used [336] as a diffusion binder between titanium and copper, which prevented the formation of intermetallic compounds that deteriorate the properties of the interface.

The search of new HEA compositions and applications is also in progress. The single-phase TaZrHfMoSc solid solution with high strength at elevated temperature was produced;[337] and the $(Cr_{0.2}Mn_{0.2}Fe_{0.2}Co_{0.2}Mo_{0.2})B$ monoboride, promising for shielding of electromagnetic interferences, was synthesized.[338] A high-entropy ceramic aerogel, $(Sm_{0.2}Eu_{0.2}Tb_{0.2}Dy_{0.2}Lu_{0.2})_2Zr_2O_7$, possessing a very low heat conductivity, was reported.[339] A composite based on graphene and (AlCrCuFeNi)O high-entropy oxide showed catalytic properties in relation to the Fenton reaction.[340]

Several specialized publications appeared in this period. A review [341] is devoted to the mechanical properties of high-entropy alloys; the authors consider the general approaches to the design of HEAs, mechanisms of deformation and strengthening and some properties such as creep, fracture and fatigue. The attention in the review is focused on mechanical effects at micro-, submicro- and nanometre levels. This might be the first systematic review of HEAs.

Some reviews addressing specific applications of HEAs appeared. A publication [342] is devoted to the practical aspects of HEA use in additive manufacturing. Methods for preparation of the powder feedstock for 3D printing from HEAs are considered; it was noted that for HEAs with moderate melting points of components, gas atomization of the metal can be successfully used to obtain a powder of spherical HEA particles. However, in the case of refractory alloys (*e.g.*, WTaMoNbVand TaNbHfZrTi), it is necessary to combine mechanical mixing and plasma treatment methods. The review also addresses a number of manufacturing technique such as direct laser deposition, selective laser melting, selective electron beam melting and the liquid ink technique, which was successfully used to manufacture articles from CoCrFeNi.

A review [343] considers the application of HEAs in nuclear industry. It was noted that it is still unclear whether the especially high resistance to radiation damage is a general feature of HEAs. It was assumed, in particular, that diffusion and lattice distortion are unlikely to be more important than in conventional alloys (*i.e.*, diffusion in HEAs can hardly be abnormally slow and the lattice distortion can hardly be abnormally high). Nevertheless, some properties such as low thermal conductivity caused by the compositional complexity of HEAs can indeed increase the radiation resistance.

The biomedical aspect of application of high-entropy alloys has been considered in a review.[344] It was noted that the number of various HEAs is currently enormous, but only some of them are applicable as biomaterials. Even those HEAs that are considered as an alternative to the existing biomaterials (mainly titanium-containing systems) and that have better mechanical properties than conventional biomedical alloys have not yet been systematically investigated, in particular, to elucidate their biocompatibility.

Hydrogen storage applications of HEAs are addressed in a review.[345] The authors emphasized that, because of large dimensionality of the composition space for HEAs, simulation methods such as CALPHAD and *ab initio* calculations, are highly important. These approaches are necessary to narrow down the search area for suitable compositions that can be used in hydrogen energy engineering. High-entropy alloys that form BCC solid solutions (*e.g.*, $Ti_{0.325}V_{0.275}Zr_{0.125}Nb_{0.275}$ and TiVCrNb) are most appropriate for hydrogen storage.

Mention should be made of high interest in the catalytic applications of HEAs, as indicated by reviews of 2021–2022 devoted only to the catalytic properties of HEAs.[346–351]

Thus, the interest in classical HEAs (*e.g.*, the Cantor alloy) is still retained: new applications are proposed for them, their behaviour under extreme conditions is being studied and they are used as model systems for calculations. Specialists continue active search for novel HEA compositions; the research covers not only metallic HEAs, but also high-entropy carbides, nitrides, oxides and borides. Unlike early works, which were mainly devoted to mechanical properties of HEAs under various conditions, now increasing attention is devoted to the use of HEAs in additive manufacturing technologies, nuclear industry, medicine, hydrogen energy engineering and catalysis, as the amount of research material accumulated to date is enough for specialized reviews. Thus, high-entropy alloys are no longer purely construction materials, but they attract increasing interest for their functional properties. This is evidenced by a review [352] considering HEA application as functional materials in a number of fields including environmental protection, hydrogen storage, electromagnetic protection,

thermoelectricity, radiation protection, magnetocaloric applications, superconductivity, catalysis and shape memory applications.

9. Conclusion

Currently, several hundred HEA compositions are known and their structures and some properties (mainly mechanical properties) have been studied. However, no systematic studies of the physicochemical behaviour and performance characteristics of HEAs over a wide temperature range have been performed as yet. These studies represent a promising scientific and practical problem.

The versatile simulation methods considered in this review are applicable to various classes of compounds. However, due to specific composition, HEAs are a sort of challenge to these methods, thus stimulating their further development. For example, for considering the atomic disorder in crystalline HEAs, large supercells are reuired for DFT calculations, which markedly increases the computational time. The generation of special quasi-random structures is markedly complicated with increasing number of HEA components, so is verification of their adequacy. The number of calculations for verification of special quasi-random structures increases as the factorial of the number of components.

Development of the classical potentials for HEAs is a sophisticated problem, since it requires substantiated selection of many interaction parameters. A certain progress was attained owing to the use of machine learning methods to generate neural network potentials. Study of structural correlation functions for liquids, such as partial radial distribution functions, also requires larger space-and-time scales in the case of multicomponent systems compared to simple systems. Investigation of HEAs using cluster expansion method requires a large number of clusters and training structures, while the Monte Carlo scanning of configuration space requires more time than is needed for simple systems owing to higher dimensionality of HEA configuration space. However, all these problems are quantitative rather than conceptual, and they are being gradually solved by increasing the computing power, improving computational algorithms and using simplifications and techniques. This makes it possible to carry out fundamental research of multicomponent systems and to incorporate these calculations into the process of HEA development.

The use of HEAs as heat and oxidation resistant materials is fairly promising. The results of numerous studies showed that high-temperature strengths is higher for some HEAs than for commercial nickel superalloys. However, fatigue, wear resistance and creep tests of bulk HEAs are still few in number. Considerable attention is paid to high-temperature oxidation of various alloys. Owing to the formation of oxide films, the oxidation kinetics of many HEAs is parabolic, that is, determined by slow diffusion processes in the solid oxide film.

The most promising HEA application is the manufacture of protective coatings. This is indicated by not only more extensive studies in this area, but also by the total number of works devoted to HEA application as coatings. Indeed, the complexity of the synthesis of bulk HEAs and high cost of some components restrict their practical use. Meanwhile, methods for the synthesis of coatings such as laser or plasma cladding do not require generation and maintenance of high temperature in a large space (which is necessary for manufacturing bulk HEAs), which can result in the formation of coatings containing even very refractory metals (*e.g.*, molybdenum).

High-entropy alloys are promising for nuclear and fusion power engineering, since they have high radiation resistance and are applicable for the production of coatings for fuel element jackets and first walls of fusion reactors (tokamaks and stellarators).

Extensive use of HEAs in modern biomedicine is considered, ranging from catalysis of the preparation of new medicinal products or cleaning of surfaces from viruses and bacteria to coatings of metallic implants to increase their biocompatibility with the tissues and fluids of living organisms.

Due to the lack of integrated interdisciplinary studies on the choice of compositions for fabrication of protective coatings taking account of the supersonic plasma spraying technique, the influence of chemical and phase composition of materials on the physicomechanical and performance properties of the coatings, development of efficient and inexpensive methods for sputtering of protective coatings with improved characteristics and expansion of the range of these coatings are relevant tasks.

This review was prepared within the framework of the state assignment of IMET UB RAS and was supported by the Russian Foundation for Basic Research (Project No. 19-13-50348 Ekspansia).

10. List of abbreviations and symbols

AIMD — *ab initio* molecular dynamics,
CALPHAD — calculation of phase diagrams,
CCA — complex concentrated alloys,
DFT — density functional theory,
EAM — embedded atom model/method,
HAP — hydroxyapatite,
HEA — high-entropy alloy,
HPS — hot pressing sintering,
MA — mechanical alloying,
MD — molecular dynamics,
MPEA — multi-principal element alloy,
MSD_a — mean square displacement of sort a atoms,
RCCA — refractory complex concentrated alloys,
RHEA — refractory high-entropy alloys,
SIA — self-interstitial atom,
SQS — special quasi-random structures,
SPS — spark plasma sintering,
VAM — vacuum arc melting,
VACF — velocity autocorrelation function,
VEC — valence electron concentration,
D_a — diffusion coefficient of sort a atoms,
E — internal energy of the system,
F — Helmholtz energy,
F_i — total force acting on the i-th nucleus,
F_{el} — electronic contribution to free energy,
F_{conf} — configurational contribution to free energy,
F_{vib} — vibrational contribution to free energy,
G — Gibbs energy,
K — number of components in the system,
N_a — number of sort a atoms,
N — total number of atoms in the system,
N_i — number of atoms of i-th type,
p — pressure,
r_i — atomic radius of i-th component,
S — entropy of the system,

T — temperature,
T_{mi} — melting point of i-th component,
V — volume,
Z — nuclear charge of an atom,
δ — geometric parameter,
ΔH_{mix} — enthalpy of mixing,
ΔS_{mix} — entropy of mixing,
μ_i — chemical potential of i-th component,
$\rho(\mathbf{r})$ —electron density distribution,
φ_{ij} — pair interaction function,
Φ — total number of phases in the system,
Ψ — many-electron wave function,
ψ — one-electron wave function,
Ω — generalized thermodynamic parameters,
$\boldsymbol{\omega} = \{\omega_i\}_{i=1\ldots K}$ — vector taking on K values.

11. References

1. J.W.Yeh, S.K.Chen, S.J.Lin, J.Y.Gan, T.S.Chin, T.T.Shun, C.H.Tsau, S.Y.Chang. *Adv. Eng. Mater.*, **6**, 299 (2004)
2. T.K.Chen, T.T.Shun, J.W.Yeh, M.S.Wong. *Surf. Coat. Technol.*, **188**–**189**, 193 (2004)
3. C.Y.Hsu, J.W.Yeh, S.K.Chen, T.T.Shun. *Metall. Mater. Trans. A*, **35**, 1465 (2004)
4. P.-K.Huang, J.-W.Yeh, T.-T.Shun, S.-K.Chen. *Adv. Eng. Mater.*, **6**, 74 (2004)
5. J.W.Yeh, S.K.Chen, J.Y.Gan, S.J.Lin, T.S.Chin, T.T.Shun, C.H.Tsau, S.Y.Chang. *Metall. Mater. Trans. A*, **35**, 2533 (2004)
6. B.Cantor, I.T.H.Chang, P.Knight, A.J.B.Vincent. *Mater. Sci. Eng. A*, **375**–**377**, 213 (2004)
7. S.Ranganathan. *Curr. Sci.*, **85**, 1404 (2003)
8. M.H.Tsai, J.W.Yeh. *Mater. Res. Lett.*, **2**, 107 (2014)
9. Y.H.Hsu, S.W.Chen, J.W.Yeh. Master's Thesis, National Tsing Hua University, Hsinchu, 1996
10. B.Cantor. *Entropy*, **16**, 4749 (2014)
11. B.Cantor, I.T.Chang, P.Knight. In *The 11th International Conference on Rapidly Quenched and Metastable Materials*. Amsterdam, 2004. P. 213
12. A.J.Vincent. *A Study of three Multicomponent Alloys. BSc Part II Thesis*. University of Sussex, Sussex, UK, 1981
13. P.Knight. *BCs Part II Thesis*. University of Oxford, Oxford, UK, 1995
14. Patent US 2002/0159914A1 (2000)
15. C.J.Tong, Y.L.Chen, S.K.Chen, J.W.Yeh, T.T.Shun, C.H.Tsau, S.J.Lin, S.Y.Chang. *Metall. Mater. Trans. A*, **36**, 881 (2005)
16. J.-W.Yeh, Y.L.Chen, S.J.Lin, S.K.Chen. *Mater. Sci. Forum*, **560**, 1 (2007)
17. C.C.Tung, J.W.Yeh, T.Tsung Shun, S.K.Chen, Y.S.Huang, H.C.Chen. *Mater. Lett.*, **61**, 1 (2007)
18. X.F.Wang, Y.Zhang, Y.Qiao, G.L.Chen. *Intermetallics*, **15**, 357 (2007)
19. S.Singh, N.Wanderka, B.S.Murty, U.Glatzel, J.Banhart. *Acta Mater.*, **59**, 182 (2011)
20. C.J.Tong, M.R.Chen, S.K.Chen, J.W.Yeh, T.T.Shun, S.J.Lin, S.Y.Chang. *Metall. Mater. Trans. A*, **36**, 1263 (2005)
21. M.F.Del Grosso, G.Bozzolo, H.O.Mosca. *J. Alloys Compd.*, **534**, 25 (2012)
22. D.Miracle, J.Miller, O.Senkov, C.Woodward, M.Uchic, J.Tiley. *Entropy*, **16**, 494 (2014)
23. M.V.Ivchenko, V.G.Pushin, N.Wanderka. *Zh. Techn. Fiz.*, **84**, 57 (2014)
24. G.A.Salishchev, M.A.Tikhonovsky, D.G.Shaysultanov, N.D.Stepanov, A.V.Kuznetsov, I.V.Kolodiy, A.S.Tortika, O.N.Senkov. *J. Alloys Compd.*, **591**, 11 (2014)
25. M.A.Laktionova, E.D.Tabachnikova, Z.Tang, P.K.Lianu. *Fiz. Nizkikh Temperatur*, **39**, 814 (2013)
26. I.V.Petrzhik, A.O.Volkhonskii, V.N.Anikin, M.I.Petrzhik, D.E.Derevtsova. *Fiz. Khim. Obrabot. Mater.*, 37 (4), 37 (2010)
27. D.Wang, A.Fernandez-Martinez. *Science*, **337**, 812 (2012)
28. N.D.Stepanov, D.G.Shaysultanov, G.A.Salishchev, M.A.Tikhonovsky, E.E.Oleynik, A.S.Tortika, O.N.Senkov. *J. Alloys Compd.*, **628**, 170 (2015)
29. F.Otto, Y.Yang, H.Bei, E.P.George. *Acta Mater.*, **61**, 2628 (2013)
30. U.S.Hsu, U.D.Hung, J.W.Yeh, S.K.Chen, Y.S.Huang, C.C.Yang. *Mater. Sci. Eng. A*, **460**–**461**, 403 (2007)
31. Z.Y.Sun, J.Zhang, J.B.Zhu, J.C.Li. *Arab. J. Sci. Eng.*, **39**, 8247 (2014)
32. B.S.Li, Y.P.Wang, M.X.Ren, C.Yang, H.Z.Fu. *Mater. Sci. Eng. A*, **498**, 482 (2008)
33. X.Yang, Y.Zhang. *Mater. Chem. Phys.*, **132**, 233 (2012)
34. S.Guo, Q. Hu, C.Ng, C.T.Liu. *Intermetallics*, **41**, 96 (2013)
35. M.G.Poletti, L.Battezzati. *Acta Mater.*, **75**, 297 (2014)
36. F.Tian, L.K.Varga, N.Chen, J.Shen, L.Vitos. *Intermetallics*, **58**, 1 (2015)
37. D.B.Miracle, O.N.Senkov. *Acta Mater.*, **122**, 448 (2017)
38. Y.Zhang, T.T.Zuo, Z.Tang, M.C.Gao, K.A.Dahmen, P.K.Liaw, Z.P.Lu. *Prog. Mater. Sci.*, **61**, 1 (2014)
39. E.J.Pickering, N.G.Jones. *Int. Mater. Rev.*, **61**, 183 (2016)
40. A.D.Pogrebnjak, A.A.Bagdasaryan, I.V.Yakushchenko, V.M.Beresnev. *Russ. Chem. Rev.*, **83**, 1027 (2014)
41. E.Lewin. *J. Appl. Phys.*, **127**, 160901 (2020)
42. J.Li, Y.Huang, X.Meng, Y.Xie. *Adv. Eng. Mater.*, **21**, 1900343 (2019)
43. W.Li, P.Liu, P.K.Liaw. *Mater. Res. Lett.*, **6**, 199 (2018)
44. X.H.Yan, J.S.Li, W.R.Zhang, Y.Zhang. *Mater. Chem. Phys.*, **210**, 12 (2018)
45. B.S.Murty, S.Ranganathan, J.W.Yeh, P.P.Bhattacharjee. *High-Entropy Alloys*. (Amsterdam: Elsevier, 2019)
46. M.C.Gao, P.K.Liaw, J.W.Yeh, Y.Zhang. *High-Entropy Alloys: Fundamentals and Applications*. (Springer International Publishing, 2016)
47. *The 3rd International Conference on High Entropy Materials (ICHEM-2020)*. (Berlin, 2020); https://www.ichem2020.uni-bayreuth.de/en/index.html (last Access 25.05.2022)
48. *International Conference on High Entropy Alloys (ICHEA-2021)*. (Graz, Austria, 2021); http://conferencefora.org/Conference/22713/ICHEA (last Access 25.05.2022)
49. *Wordl Congress on High Entropy Alloys (HEA-2019)*. (Seattle, Washington, USA, 2019); https://www.tms.org/hea2019 (last Access 25.05.2022)
50. *The 2nd Wordl Congress on High Entropy Alloys (HEA-2021)*. (Charlotte, Nort Carolina, USA, 2021); https://www.tms.org/hea2021 (last Access 25.05.2022)
51. *III Mezhdunarodnaya Shkola-Konferentsiya 'Poluchenue, Struktura i Svoistva Vysokoentrapiinykh Materialov', IMET UB RAS, 2021;*
(The III International Conference and School 'Synthesis, Structure, and Properties of High-Entropy Materials' Institute of Metallurgy, Ural Branch of the Russian Academy of Sciences, Ekaterinburg, Russia); http://shea.bsu.edu.ru/shea (last Access 25.05.2022)
52. S.Uporov, V.Bykov, S.Pryanichnikov, A.Shubin, N.Uporova. *Intermetallics*, **83**, 1 (2017)
53. X.Liu, H.Cheng, Z.Li, H.Wang, F.Chang, W.Wang, Q.Tang, P.Dai. *Vacuum*, **165**, 297 (2019)
54. A.Kilmametov, R.Kulagin, A.Mazilkin, S.Seils, T.Boll, M.Heilmaier, H.Hahn. *Scr. Mater.*, **158**, 29 (2019)
55. H.Cheng, X.Liu, Q.Tang, W.Wang, X.Yan, P.Dai. *J. Alloys Compd.*, **775**, 742 (2019)
56. F.Salemi, M.H.Abbasi, F.Karimzadeh. *J. Alloys Compd.*, **685**, 278 (2016)
57. M.Murali, S.P.K.Babu, B.J.Krishna, A.Vallimanalan. *Prog. Nat. Sci. Mater. Int.*, **26**, 380 (2016)

58. C.Sun, P.Li, S.Xi, Y.Zhou, S.Li, X.Yang. *Mater. Sci. Eng. A*, **728**, 144 (2018)
59. D.Oleszak, A.Antolak-Dudka, T.Kulik. *Mater. Lett.*, **232**, 160 (2018)
60. J.Xu, C.Shang, W.Ge, H.Jia, P.K.Liaw, Y.Wang. *Adv. Powder Technol.*, **27**, 1418 (2016)
61. H.Cheng, Y.C.Xie, Q.H.Tang, C.Rao, P.Q.Dai. *Trans. Nonferrous Met. Soc. China (Engl. Ed.)*, **28**, 1360 (2018)
62. D.Yim, W.Kim, S.Praveen, M.J.Jang, J.W.Bae, J.Moon, E.Kim, S.J.Hong, H.S.Kim. *Mater. Sci. Eng. A*, **708**, 291 (2017)
63. Y.Tian, C.Lu, Y.Shen, X.Feng. *Surf. Interfaces*, **15**, 135 (2019)
64. C.L.Chen, Suprianto. *Intermetallics*, **113**, 106570 (2019)
65. Z.Szklarz, J.Lekki, P.Bobrowski, M.B.Szklarz, Ł.Rogal. *Mater. Chem. Phys.*, **215**, 385 (2018)
66. F.Alijani, M.Reihanian, K.Gheisari. *J.Alloys Compd.*, **773**, 623 (2019)
67. G.Wang, Q.Liu, J.Yang, X.Li, X.Sui, Y.Gu, Y.Liu. *Int. J. Refract. Met. Hard Mater.*, **84**, 104988 (2019)
68. R.B.Mane, B.B.Panigrahi. *Mater. Lett.*, **217**, 131 (2018)
69. M.Zhang, R.Li, T.Yuan, X.Feng, L.Li, S.Xie, Q.Weng. *Powder Technol.*, **343**, 58 (2019)
70. J.Pan, T.Dai, T.Lu, X.Ni, J.Dai, M.Li. *Mater. Sci. Eng. A*, **738**, 362 (2018)
71. R.M.Pohan, B.Gwalani, J.Lee, T.Alam, J.Y.Hwang, H.J.Ryu, R.Banerjee, S.H.Hong. *Mater. Chem. Phys.*, **210**, 62 (2018)
72. L.Guo, D.Xiao, W.Wu, S.Ni, M.Song. *Intermetallics*, **103**, 1 (2018)
73. S.Xie, R.Li, T.Yuan, L.Zhou, M.Zhang, M.Wang, P.Niu, P.Cao, C.Chen. *Mater. Charact.*, **154**, 169 (2019)
74. Q.Liu, G.Wang, X.Sui, Y.Liu, X.Li, J.Yang. *J. Mater. Sci. Technol.*, **35**, 2600 (2019)
75. O.A.Waseem, J.Lee, H.M.Lee, H.J.Ryu. *Mater. Chem. Phys.*, **210**, 87 (2018)
76. M.Vaidya, A.Anupam, J.V.Bharadwaj, C.Srivastava, B.S.Murty. *J.Alloys Compd.*, **791**, 1114 (2019)
77. M.Laurent-Brocq, P.A.Goujon, J.Monnier, B.Villeroy, L.Perrière, R.Pirès, G.Garcin. *J. Alloys Compd.*, **780**, 856 (2019)
78. L.R.Kanyane, A.P.I.Popoola, N.Malatji, M.B.Shongwe. *Proc. Manuf.*, **35**, 968 (2019)
79. I.Moravcik, J.Cizek, J.Zapletal, Z.Kovacova, J.Vesely, P.Minarik, M.Kitzmantel, E.Neubauer, I.Dlouhy. *Mater. Des.*, **119**, 141 (2017)
80. O.Maulik, D.Kumar, S.Kumar, D.M.Fabijanic, V.Kumar. *Intermetallics*, **77**, 46 (2016)
81. F.Průša, A.Šenková, V.Kučera, J.Čapek, D.Vojtěch. *Mater. Sci. Eng. A*, **734**, 341 (2018)
82. A.I.Yurkova, V.V.Cherniavsky, V.Bolbut, M.Krüger, I.Bogomol. *J. Alloys Compd.*, **786**, 139 (2019)
83. L.R.Kanyane, N.Malatji, A.P.I.Popoola, O.S.I.Fayomi. *Res. Phys.*, **14**, 102465 (2019)
84. W.Luo, Y.Liu, Y.Luo, M.Wu. *J. Alloys Compd.*, **754**, 163 (2018)
85. S.G.Ma, S.F.Zhang, J.W.Qiao, Z.H.Wang, M.C.Gao, Z.M.Jiao, H.J.Yang, Y.Zhang. *Intermetallics*, **54**, 104 (2014)
86. T.Zuo, X.Yang, P.K.Liaw, Y.Zhang. *Intermetallics*, **67**, 171 (2015)
87. J.Cieslak, J.Tobola, J.Przewoznik, K.Berent, U. Dahlborg, J.Cornide, S.Mehraban, N.Lavery, M.Calvo-Dahlborg. *J. Alloys Compd.*, **801**, 511 (2019)
88. J.Cieslak, J.Tobola, K.Berent, M.Marciszko. *J. Alloys Compd.*, **740**, 264 (2018)
89. Y.Chen, S.Zhu, X.Wang, B.Yang, G.Han, L.Qiu. *Vacuum*, **150**, 84 (2018)
90. L.Hou, J.Hui, Y.Yao, J.Chen, J.Liu. *Vacuum*, **164**, 212 (2019)
91. P.Zhang, Y.Li, Z.Chen, J.Zhang, B.Shen. *Vacuum*, **162**, 20 (2019)
92. S.Yang, Z.Liu, J.Pi. *Mater. Lett.*, **261**, 127004 (2020)
93. P.K.Sarswat, S.Sarkar, A.Murali, W.Huang, W.Tan, M.L.Free. *Appl. Surf. Sci.*, **476**, 242 (2019)
94. S.Sarkar, P.K.Sarswat, M.L.Free. *Addit. Manuf.*, **30**, 100902 (2019)
95. X.Yang, Y.Zhou, S.Xi, Z.Chen, P.Wei, C.He, T.Li, Y.Gao, H.Wu. *Mater. Sci. Eng. A*, **767**, 138394 (2019)
96. M.Widom. *J. Mater. Res.*, **33**, 2881 (2018)
97. J.Gibbs. *The Scientific Papers*. (New York: Dover Publications, 1961)
98. Y.Zhang, Y.J.Zhou, J.P.Lin, G.L.Chen, P.K.Liaw. *Adv. Eng. Mater.*, **10**, 534 (2008)
99. Y.Zhang, Z.P.Lu, S.G.Ma, P.K.Liaw, Z.Tang, Y.Q.Cheng, M.C.Gao. *MRS Commun.*, **4**, 57 (2014)
100. L.Jiang, Y.P.Lu, H.Jiang, T.M.Wang, B.N.Wei, Z.Q.Cao, T.J.Li. *Mater. Sci. Technol. (UK)*, **32**, 588 (2016)
101. S.Guo, C.Ng, J.Lu, C.T.Liu. *J. Appl. Phys.*, **109**, 103505 (2011)
102. K.M.Youssef, A.J.Zaddach, C.Niu, D.L.Irving, C.C.Koch. *Mater. Res. Lett.*, **3**, 95 (2015)
103. A.Takeuchi, K.Amiya, T.Wada, K.Yubuta, W.Zhang. *JOM*, **66**, 1984 (2014)
104. P.F.Yu, L.J.Zhang, J.L.Ning, M.Z.Ma, X.Y.Zhang, Y.C.Li, P.K.Liaw, G.Li, R.P.Liu. *Mater. Lett.*, **196**, 137 (2017)
105. R.G.Parr. In *Horizons of Quantum Chemistry: Proceedings of the 3rd International Congress of Quantum Chemistry Held at Kyoto, Japan*. (Dordrecht: Springer Netherlands, 1980). P. 5
106. W.Kohn, L.J.Sham. *Phys. Rev.*, **140**, A1133 (1965)
107. G.Kresse, J.Furthmüller. *Comput. Mater. Sci.*, **6**, 15 (1996)
108. M.P.Teter, M.C.Payne, D.C.Allan. *Phys. Rev. B*, **40**, 12255 (1989)
109. *Methods in Computational Molecular Physics*. (Eds G.H.F.Diercksen, S.Wilson). (Dordrecht: Springer Netherlands, 1983)
110. D.M.Wood, A.Zunger. *J. Phys. A*, **18**, 1343 (1985)
111. P.Pulay. *Chem. Phys. Lett.*, **73**, 393 (1980)
112. A.Zunger, S.H.Wei, L.G.Ferreira, J.E.Bernard. *Phys. Rev. Lett.*, **65**, 353 (1990)
113. A.Van De Walle, P.Tiwary, M.De Jong, D.L.Olmsted, M.Asta, A.Dick, D.Shin, Y.Wang, L.Q.Chen, Z.K.Liu. *Calphad Comput. Coupling Phase Diagrams Thermochem.*, **42**, 13 (2013)
114. R.P.Feynman. *Phys. Rev.*, **56**, 340 (1939)
115. L.Verlet. *Phys. Rev.*, **159**, 98 (1967)
116. M.Gao, D.Alman. *Entropy*, **15**, 4504 (2013)
117. N.D.Stepanov, N.Y.Yurchenko, S.V.Zherebtsov, M.A.Tikhonovsky, G.A.Salishchev. *Mater. Lett.*, **211**, 87 (2018)
118. S.Y.Chen, Y.Tong, K.K.Tseng, J.W.Yeh, J.D.Poplawsky, J.G.Wen, M.C.Gao, G.Kim, W.Chen, Y.Ren, R.Feng, W.D.Li, P.K.Liaw. *Scr. Mater.*, **158**, 50 (2019)
119. M.S.Green. *J. Chem. Phys.*, **22**, 398 (1954)
120. R.Kubo. *J. Phys. Soc. Jpn.*, **12**, 570 (1957)
121. A.Einstein. *Ann. Phys.*, **322**, 549 (1905)
122. I.A.Balyakin, B.R.Gelchinski, A.A.Rempel. *Mater. Today Commun.*, **21**, 100627 (2019)
123. S.Mahajan. *Encyclopedia of Materials: Science and Technology*. (1st Edn.). (Oxford: Pergamon, 2001)
124. M.S.Daw, M.I.Baskes. *Phys. Rev. B*, **29**, 6443 (1984)
125. J.Behler, M.Parrinello. *Phys. Rev. Lett.*, **98**, 146401 (2007)
126. A.Singraber, T.Morawietz, J.Behler, C.Dellago. *J. Chem. Theory Comput.*, **15**, 3075 (2019)
127. H.Wang, L.Zhang, J.Han, W.E.*Comput. Phys. Commun.*, **228**, 178 (2018)
128. A.V.Shapeev. *Multiscale Model. Simul.*, **14**, 1153 (2016)
129. A.P.Thompson, L.P.Swiler, C.R.Trott, S.M.Foiles, G.J.Tucker. *J. Comput. Phys.*, **285**, 316 (2015)
130. P.E.Dolgirev, I.A.Kruglov, A.R.Oganov. *AIP Adv.*, **6**, 085318 (2016)
131. R.Jinnouchi, F.Karsai, G.Kresse. *Phys. Rev. B*, **100**, 014105 (2019)

132. I.A.Balyakin, A.A.Yuryev, B.R.Gelchinski, A.A.Rempel. *J. Phys. Condens. Matter*, **32**, 214006 (2020)
133. J.M.Sanchez, F.Ducastelle, D.Gratias. *Phys. A: Stat. Mech. Appl.*, **128**, 334 (1984)
134. A.Van de Walle, M.Asta, G.Ceder. *Calphad Comput. Coupling Phase Diagrams Thermochem.*, **26**, 539 (2002)
135. J.H.Chang, D.Kleiven, M.Melander, J.Akola, J.M.Garcia-Lastra, T.Vegge. *J. Phys.: Condens. Matter*, **31**, 325901 (2019)
136. D.Lerch, O.Wieckhorst, G.L.W.Hart, R.W.Forcade, S.Müller. *Model. Simul. Mater. Sci. Eng.*, **17**, 055003 (2009)
137. W.P.Huhn, M.Widom. *JOM*, **65**, 1772 (2013)
138. R.Feng, P.K.Liaw, M.C.Gao, M.Widom. *Comput. Mater.*, **3**, 50 (2017)
139. M.Widom, W.P.Huhn, S.Maiti, W.Steurer. *Metall. Mater. Trans. A*, **45**, 196 (2014)
140. H.L.Lukas.*Computational Thermodynamics: the Calphad Method.* (Cambridge: Cambridge University Press, 2007)
141. H.L.Chen, H.Mao, Q.Chen. *Mater. Chem. Phys.*, **210**, 279 (2018)
142. R.Sonkusare, P.Divya Janani, N.P.Gurao, S.Sarkar, S.Sen, K.G.Pradeep, K.Biswas. *Mater. Chem. Phys.*, **210**, 269 (2018)
143. O.N.Senkov, G.B.Wilks, D.B.Miracle, C.P.Chuang, P.K.Liaw. *Intermetallics*, **18**, 1758 (2010)
144. O.N.Senkov, D.B.Miracle, K.J.Chaput, J.P.Couzinie. *J. Mater. Res.*, **33**, 3092 (2018)
145. S.Jiang, Z.Lin, H.Xu, Y.Sun. *J. Alloys Compd.*, **741**, 826 (2018)
146. A.Raza, H.J.Ryu, S.H.Hong. *Mater. Des.*, **157**, 97 (2018)
147. B.Kang, J.Lee, H.J.Ryu, S.H.Hong. *Mater. Sci. Eng. A*, **712**, 616 (2018)
148. W.Wang, Z.Zhang, J.Niu, H.Wu, S.Zhai, Y.Wang. *Mater. Today Commun.*, **16**, 242 (2018)
149. H.W.Yao, J.W.Qiao, M.C.Gao, J.A.Hawk, S.G.Ma, H.F.Zhou, Y.Zhang. *Mater. Sci. Eng. A*, **674**, 203 (2016)
150. J.Zhang, Y.Hu, Q.Wei, Y.Xiao, P.Chen, G.Luo, Q.Shen. *J. Alloys Compd.*, **827**, 154301 (2020)
151. M.Wang, Z.Ma, Z.Xu, X.Cheng. *J. Alloys Compd.*, **803**, 778 (2019)
152. D.Ikeuchi, D.J.M.King, K.J.Laws, A.J.Knowles, R.D.Aughterson, G.R.Lumpkin, E.G.Obbard. *Scr. Mater.*, **158**, 141 (2019)
153. V.T.Nguyen, M.Qian, Z.Shi, T.Song, L.Huang, J.Zou. *Intermetallics*, **101**, 39 (2018)
154. S.W.Xin, M.Zhang, T.T.Yang, Y.Y.Zhao, B.R.Sun, T.D.Shen. *J. Alloys Compd.*, **769**, 597 (2018)
155. S.Zhang, Z.Wang, H.J.Yang, J.W.Qiao, Z.H.Wang, Y.C.Wu. *Intermetallics*, **121**, 106699 (2020)
156. E.S.Panina, N.Y.Yurchenko, S.V.Zherebtsov, M.A.Tikhonovsky, M.V.Mishunin, N.D.Stepanov. *Mater. Sci. Eng. A*, **786**, 139409 (2020)
157. O.A.Waseem, H.J.Ryu. *J. Alloys Compd.*, **845**, 155700 (2020)
158. Y.Long, X.Liang, K.Su, H.Peng, X.Li. *J. Alloys Compd.*, **780**, 607 (2019)
159. S.Lv, Y.Zu, G.Chen, X.Fu, W.Zhou. *J. Alloys Compd.*, **788**, 1256 (2019)
160. N.D.Stepanov, N.Y.Yurchenko, A.O.Gridneva, S.V.Zherebtsov, Y.V.Ivanisenko, G.A.Salishchev. *Mater. Sci. Eng. A*, **716**, 308 (2018)
161. M.G.Poletti, C.M.McCaughey, G.Fiore, R.Goodall, L.Battezzati. *Int. J.Refract. Met. Hard Mater.*, **76**, 128 (2018)
162. N.Yurchenko, E.Panina, M.Tikhonovsky, G.Salishchev, S.Zherebtsov, N.Stepanov. *Mater. Lett.*, **264**, 127372 (2020)
163. M.Zhu, L.Yao, Y.Liu, M.Zhang, K.Li, Z.Jian. *Mater. Lett.*, **272**, 127869 (2020)
164. Y.Zhang, Y.Liu, Y.Li, X.Chen, H.Zhang. *Mater. Lett.*, **174**, 82 (2016)
165. O.N.Senkov, J.K.Jensen, A.L.Pilchak, D.B.Miracle, H.L.Fraser. *Mater. Des.*, **139**, 498 (2018)
166. V.Soni, B.Gwalani, T.Alam, S.Dasari, Y.Zheng, O.N.Senkov, D.Miracle, R.Banerjee. *Acta Mater.*, **185**, 89 (2020)
167. S.Laube, H.Chen, A.Kauffmann, S.Schellert, F.Müller, B.Gorr, J.Müller, B.Butz, H.J.Christ, M.Heilmaier. *J. Alloys Compd.*, **823**, 153805 (2020)
168. J.Jayaraj, P.Thirathipviwat, J.Han, A.Gebert. *Intermetallics*, **100**, 9 (2018)
169. Y.Cao, Y.Liu, Y.Li, B.Liu, A.Fu, Y.Nie. *Int. J.Refract. Met. Hard Mater.*, **86**, 105132 (2020)
170. B.Guennec, V.Kentheswaran, L.Perrière, A.Ueno, I.Guillot, J.P.Couzinié, G.Dirras. *Materialia*, **4**, 348 (2018)
171. T.Cao, J.Shang, J.Zhao, C.Cheng, R.Wang, H.Wang. *Mater. Lett.*, **164**, 344 (2016)
172. T.K.Tsao, A.C.Yeh, C.M.Kuo, K.Kakehi, H.Murakami, J.W.Yeh, S.R.Jian. *Sci. Rep.*, **7**, 12658 (2017)
173. P.Kral, W.Blum, J.Dvorak, N.Yurchenko, N.Stepanov, S.Zherebtsov, L.Kuncicka, M.Kvapilova, V.Sklenicka. *Mater. Sci. Eng. A*, **783**, 139291 (2020)
174. B.Gorr, F.Mueller, H.J.Christ, T.Mueller, H.Chen, A.Kauffmann, M.Heilmaier. *J. Alloys Compd.*, **688**, 468 (2016)
175. C.M.Liu, H.M.Wang, S.Q.Zhang, H.B.Tang, A.L.Zhang. *J. Alloys Compd.*, **583**, 162 (2014)
176. W.Kai, C.C.Li, F.P.Cheng, K.P.Chu, R.T.Huang, L.W.Tsay, J.J.Kai. *Corros. Sci.*, **121**, 116 (2017)
177. O.A.Waseem, H.J.Ryu. *J. Alloys Compd.*, **828**, 154427 (2020)
178. Y.Y.Liu, Z.Chen, Y.Z.Chen, J.C.Shi, Z.Y.Wang, S.Wang, F.Liu. *Vacuum*, **169**, 108837 (2019)
179. Y.kui Cao, Y.Liu, B.Liu, W.D.Zhang, J.W.Wang, M.Du. *Trans. Nonferrous Met. Soc. China (Engl. Ed.)*, **29**, 1476 (2019)
180. L.Chen, Z.Zhou, Z.Tan, D.He, K.Bobzin, L.Zhao, M.Öte, T.Königstein. *J. Alloys Compd.*, **764**, 845 (2018)
181. Y.K.Kim, Y.A.Joo, H.S.Kim, K.A.Lee. *Intermetallics*, **98**, 45 (2018)
182. B.Gorr, M.Azim, H.J.Christ, T.Mueller, D.Schliephake, M.Heilmaier. *J. Alloys Compd.*, **624**, 270 (2015)
183. S.K.Varma, F.Sanchez, S.Moncayo, C.V.Ramana. *J. Mater. Sci. Technol.*, **38**, 189 (2020)
184. W.Kai, C.C.Li, F.P.Cheng, K.P.Chu, R.T.Huang, L.W.Tsay, J.J.Kai. *Corros. Sci.*, **108**, 209 (2016)
185. W.Kai, F.P.Cheng, Y.R.Lin, C.W.Chuang, R.T.Huang, D.Chen, J.J.Kai, C.T.Liu, C.J.Wang. *J. Alloys Compd.*, **836**, 155518 (2020)
186. W.Kai, F.P.Cheng, C.Y.Liao, C.C.Li, R.T.Huang, J.J.Kai. *Mater. Chem. Phys.*, **210**, 362 (2018)
187. M.P.Agustianingrum, F.H.Latief, N.Park, U.Lee. *Intermetallics*, **120**, 106757 (2020)
188. F.Chang, B.Cai, C.Zhang, B.Huang, S.Li, P.Dai. *Surf. Coat. Technol.*, **359**, 132 (2019)
189. D.Huang, J.Lu, Y.Zhuang, C.Tian, Y.Li. *Corros. Sci.*, **158**, 108088 (2019)
190. Z.S.Nong, Y.N.Lei, J.C.Zhu. *Intermetallics*, **101**, 144 (2018)
191. A.Mohanty, J.K.Sampreeth, O.Bembalge, J.Y.Hascoet, S.Marya, R.J.Immanuel, S.K.Panigrahi. *Surf. Coat. Technol.*, **380**, 125028 (2019)
192. S.Wang, Z.Chen, P.Zhang, K.Zhang, C.L.Chen, B.L.Shen. *Vacuum*, **163**, 263 (2019)
193. J.Dąbrowa, G.Cieślak, M.Stygar, K.Mroczka, K.Berent, T.Kulik, M.Danielewski. *Intermetallics*, **84**, 52 (2017)
194. F.Ye, Z.Jiao, S.Yan, L.Guo, L.Feng, J.Yu. *Vacuum*, **174**, 109178 (2020)
195. K.C.Lo, H.Murakami, J.W.Yeh, A.C.Yeh. *Intermetallics*, **119**, 106711 (2020)
196. S.Sheikh, L.Gan, T.K.Tsao, H.Murakami, S.Shafeie, S.Guo. *Intermetallics*, **103**, 40 (2018)
197. J.Lu, Y.Chen, H.Zhang, L.Li, L.Fu, X.Zhao, F.Guo, P.Xiao. *Corros. Sci.*, **170**, 108691 (2020)
198. T.M.Butler, M.L.Weaver. *J. Alloys Compd.*, **674**, 229 (2016)
199. W.Kai, F.C.Chien, F.P.Cheng, R.T.Huang, J.J.Kai, C.T.Liu. *Corros. Sci.*, **153**, 150 (2019)

200. Y.Y.Chen, U.T.Hong, H.C.Shih, J.W.Yeh, T.Duval. *Corros. Sci.*, **47**, 2679 (2005)
201. Y.J.Hsu, W.C.Chiang, J.K.Wu. *Mater. Chem. Phys.*, **92**, 112 (2005)
202. C.P.Lee, C.C.Chang, Y.Y.Chen, J.W.Yeh, H.C.Shih. *Corros. Sci.*, **50**, 2053 (2008)
203. Y.L.Chou, J.W.Yeh, H.C.Shih. *Corros. Sci.*, **52**, 2571 (2010)
204. Y.L.Chou, Y.C.Wang, J.W.Yeh, H.C.Shih. *Corros. Sci.*, **52**, 3481 (2010)
205. C.M.Lin, H.L.Tsai. *Intermetallics*, **19**, 288 (2011)
206. X.W.Qiu, Y.P.Zhang, L.He, C.G.Liu. *J. Alloys Compd.*, **549**, 195 (2013)
207. Y.X.Liu, C.Q.Cheng, J.L.Shang, R.Wang, P.Li, J.Zhao. *Trans. Nonferrous Met. Soc. China (Engl. Ed.)*, **25**, 1341 (2015)
208. Y.Shi, B.Yang, X.Xie, J.Brechtl, K.A.Dahmen, P.K.Liaw. *Corros. Sci.*, **119**, 33 (2017)
209. T.Fujieda, H.Shiratori, K.Kuwabara, M.Hirota, T.Kato, K.Yamanaka, Y.Koizumi, A.Chiba, S.Watanabe. *Mater. Lett.*, **189**, 148 (2017)
210. M.Zhang, X.Zhou, X.Yu, J.Li. *Surf. Coat. Technol.*, **311**, 321 (2017)
211. Y.Guo, Q.Liu. *Intermetallics*, **102**, 78 (2018)
212. S.B.Hung, C.J.Wang, Y.Y.Chen, J.W.Lee, C.L.Li. *Surf. Coat. Technol.*, **375**, 802 (2019)
213. B.Song, Y.Li, Z.Cong, Y.Li, Z.Song, J.Chen. *J. Alloys Compd.*, **797**, 1025 (2019)
214. M.A.Tunes, V.M.Vishnyakov. *Mater. Des.*, **170**, 107692 (2019)
215. H.Wang, Q.Liu, Y.Guo, H.Lan. *Intermetallics*, **115**, 106613 (2019)
216. H.Te Hsueh, W.J.Shen, M.H.Tsai, J.W.Yeh. *Surf. Coat. Technol.*, **206**, 4106 (2012)
217. W.J.Shen, M.H.Tsai, Y.S.Chang, J.W.Yeh. *Thin Solid Films*, **520**, 6183 (2012)
218. C.W.Tsai, S.W.Lai, K.H.Cheng, M.H.Tsai, A.Davison, C.H.Tsau, J.W.Yeh. *Thin Solid Films*, **520**, 2613 (2012)
219. L.Liu, J.B.Zhu, C.Hou, J.C.Li, Q.Jiang. *Mater. Des.*, **46**, 675 (2013)
220. X.W.Qiu, C.G.Liu. *J. Alloys Compd.*, **553**, 216 (2013)
221. J.B.Cheng, X.B.Liang, B.S.Xu. *Surf. Coat. Technol.*, **240**, 184 (2014)
222. V.Soare, M.Burada, I.Constantin, D.Mitricə, V.Bədiliţə, A.Caragea, M.Târcolea. *Appl. Surf. Sci.*, **358**, 533 (2015)
223. J.Cheng, D.Liu, X.Liang, Y.Chen. *Surf. Coat. Technol.*, **281**, 109 (2015)
224. B.R.Braeckman, D.Depla. *J. Alloys Compd.*, **646**, 810 (2015)
225. Y.Ma, G.J.Peng, D.H.Wen, T.H.Zhang. *Mater. Sci. Eng. A*, **621**, 111 (2015)
226. R.Chen, Z.Cai, J.Pu, Z.Lu, S.Chen, S.Zheng, C.Zeng. *J. Alloys Compd.*, **827**, 153836 (2020)
227. C.Shang, E.Axinte, J.Sun, X.Li, P.Li, J.Du, P.Qiao, Y.Wang. *Mater. Des.*, **117**, 193 (2017)
228. Z.Cai, Y.Wang, X.Cui, G.Jin, Y.Li, Z.Liu, M.Dong. *Surf. Coat. Technol.*, **330**, 163 (2017)
229. Q.Ye, K.Feng, Z.Li, F.Lu, R.Li, J.Huang, Y.Wu. *Appl. Surf. Sci.*, **396**, 1420 (2017)
230. C.L.Wu, S.Zhang, C.H.Zhang, H.Zhang, S.Y.Dong. *J. Alloys Compd.*, **698**, 761 (2017)
231. C.L.Wu, S.Zhang, C.H.Zhang, H.Zhang, S.Y.Dong. *Surf. Coat. Technol.*, **315**, 368 (2017)
232. W.Ge, B.Wu, S.Wang, S.Xu, C.Shang, Z.Zhang, Y.Wang. *Adv. Powder Technol.*, **28**, 2556 (2017)
233. X.W.Qiu, M.J.Wu, C.G.Liu, Y.P.Zhang, C.X.Huang. *J. Alloys Compd.*, **708**, 353 (2017)
234. C.L.Wu, S.Zhang, C.H.Zhang, J.Chen, S.Y.Dong. *Opt. Laser Technol.*, **94**, 68 (2017)
235. N.Ley, S.S.Joshi, B.Zhang, Y.H.Ho, N.B.Dahotre, M.L.Young. *Surf. Coat. Technol.*, **348**, 150 (2018)
236. Q.Fang, Y.Chen, J.Li, Y.Liu, Y.Liu. *Phys. B: Condens. Matter*, **550**, 112 (2018)
237. Y.Guo, H.Wang, Q.Liu. *J. Alloys Compd.*, **834**, 155147 (2020)
238. Y.Guo, X.Shang, Q.Liu. *Surf. Coat. Technol.*, **344**, 353 (2018)
239. Z.Cai, X.Cui, Z.Liu, Y.Li, M.Dong, G.Jin. *Opt. Laser Technol.*, **99**, 276 (2018)
240. C.Ni, Y.Shi, J.Liu, G.Huang. *Opt. Laser Technol.*, **105**, 257 (2018)
241. G.Jin, Z.Cai, Y.Guan, X.Cui, Z.Liu, Y.Li, M.Dong, D.Zhang. *Appl. Surf. Sci.*, **445**, 113 (2018)
242. W.Zhang, R.Tang, Z.B.Yang, C.H.Liu, H.Chang, J.J.Yang, J.L.Liao, Y.Y.Yang, N.Liu. *Surf. Coat. Technol.*, **347**, 13 (2018)
243. F.Y.Shu, S.Liu, H.Y.Zhao, W.X.He, S.H.Sui, J.Zhang, P.He, B.S.Xu. *J. Alloys Compd.*, **731**, 662 (2018)
244. A.Vallimanalan, S.P.Kumaresh Babu, S.Muthukumaran, M.Murali, V.Gaurav, R.Mahendran. *Mater. Today Proc.*, **27**, 2398 (2019)
245. S.Yin, W.Li, B.Song, X.Yan, M.Kuang, Y.Xu, K.Wen, R.Lupoi. *J. Mater. Sci. Technol.*, **35**, 1003 (2019)
246. F.Shu, B.Zhang, T.Liu, S.Sui, Y.Liu, P.He, B.Liu, B.Xu. *Surf. Coat. Technol.*, **358**, 667 (2019)
247. Y.Q.Jiang, J.Li, Y.F.Juan, Z.J.Lu, W.L.Jia. *J. Alloys Compd.*, **775**, 1 (2019)
248. C.H.Lin, J.G.Duh. *Surf. Coat. Technol.*, **203**, 558 (2008)
249. T.W.Lu, C.S.Feng, Z.Wang, K.W.Liao, Z.Y.Liu, Y.Z.Xie, J.G.Hu, W.B.Liao. *Appl. Surf. Sci.*, **494**, 72 (2019)
250. S.Zheng, Z.Cai, J.Pu, C.Zeng, S.Chen, R.Chen, L.Wang. *Appl. Surf. Sci.*, **483**, 870 (2019)
251. S.Zhao, L.X.He, X.X.Fan, C.H.Liu, J.P.Long, L.Wang, H.Chang, J.Wang, W.Zhang. *Surf. Coat. Technol.*, **375**, 215 (2019)
252. A.Aliyu, C.Srivastava. *Materialia*, **8**, 100459 (2019)
253. A.Aliyu, C.Srivastava. *Materialia*, **5**, 100249 (2019)
254. A.Aliyu, C.Srivastava. *Thin Solid Films*, **686**, 137434 (2019)
255. N.Tüten, D.Canadinc, A.Motallebzadeh, B.Bal. *Intermetallics*, **105**, 99 (2019)
256. G.H.Meng, N.A.Protasova, E.P.Kruglov, X.Lin, H.Xie, X.Ding. *J. Alloys Compd.*, **772**, 994 (2019)
257. S.Chen, Z.Cai, Z.Lu, J.Pu, R.Chen, S.Zheng, C.Mao, S.Chen. *Mater. Charact.*, **157**, 109887 (2019)
258. Z.Cui, Z.Qin, P.Dong, Y.Mi, D.Gong, W.Li. *Mater. Lett.*, **259**, 126769 (2020)
259. H.W.Chang, P.K.Huang, J.W.Yeh, A.Davison, C.H.Tsau, C.C.Yang. *Surf. Coat. Technol.*, **202**, 3360 (2008)
260. Q.Zeng, Y.Xu. *Mater. Today Commun.*, **24**, 101261 (2020)
261. Z.Gu, S.Xi, C.Sun. *J. Alloys Compd.*, **819**, 152986 (2020)
262. C.L.Chen, Suprianto. *Surf. Coat. Technol.*, **386**, 125443 (2020)
263. X.Qiu. *J. Mater. Res. Technol.*, **9**, 5127 (2020)
264. D.Zhao, T.Yamaguchi, J.Shu, T.Tokunaga, T.Danjo. *Appl. Surf. Sci.*, **517**, 145980 (2020)
265. J.K.Xiao, Y.Q.Wu, J.Chen, C.Zhang. *Wear*, **448 – 449**, 203209 (2020)
266. H.X.Guo, C.Y.He, X.L.Qiu, Y.Q.Shen, G.Liu, X.H.Gao. *Sol. Energy Mater. Sol. Cells*, **209**, 110444 (2020)
267. J.K.Xiao, H.Tan, Y.Q.Wu, J.Chen, C.Zhang. *Surf. Coat. Technol.*, **385**, 125430 (2020)
268. H.Liu, J.Liu, X.Li, P.Chen, H.Yang, J.Hao. *Surf. Coat. Technol.*, **392**, 125758 (2020)
269. Y.Zhang, T.Han, M.Xiao, Y.Shen. *Optik (Stuttg)*, **204**, 164168 (2020)
270. H.Zhang, Y.Pan, Y.He, H.Jiao. *Appl. Surf. Sci.*, **257**, 2259 (2011)
271. A.Anupam, R.S.Kottada, S.Kashyap, A.Meghwal, B.S.Murty, C.C.Berndt, A.S.M.Ang. *Appl. Surf. Sci.*, **505**, 144117 (2020)
272. K.Xiang, L.Y.Chen, L.Chai, N.Guo, H.Wang. *Appl. Surf. Sci.*, **517**, 146214 (2020)
273. Premlata, D.Singh, U.Pandel, R.K.Duchaniya. *Mater. Today Proc.*, **28**, 2411 (2020)

274. G.J.Zhang, Q.W.Tian, K.X.Yin, S.Q.Niu, M.H.Wu, W.W.Wang, Y.N.Wang, J.C.Huang. *Intermetallics*, **119**, 106722 (2020)
275. C.Sha, Z.Zhou, Z.Xie, P.Munroe. *Surf. Coat. Technol.*, **385**, 125435 (2020)
276. Y.Cui, J.Shen, S.M.Manladan, K.Geng, S.Hu. *Appl. Surf. Sci.*, **512**, 145736 (2020)
277. P.Cui, W.Li, P.Liu, K.Zhang, F.Ma, X.Chen, R.Feng, P.K.Liaw. *J. Alloys Compd.*, **834**, 155063 (2020)
278. C.Wang, J.Yu, Y.Yu, Y.Zhao, Y.Zhang, X.Han. *J. Mater. Res. Technol.*, **9**, 8482 (2020)
279. H.Zhang, Y.Pan, Y.Z.He. *Mater. Des.*, **32**, 1910 (2011)
280. X.Ye, M.Ma, Y.Cao, W.Liu, X.Ye, Y.Gu. *Phys. Proc.*, 303 (2011)
281. C.Huang, Y.Zhang, J.Shen, R.Vilar. *Surf. Coat. Technol.*, **206**, 1389 (2011)
282. W.Zhang, R.Tang, Z.B.Yang, C.H.Liu, H.Chang, J.J.Yang, J.L.Liao, Y.Y.Yang, N.Liu. *J. Nucl. Mater.*, **512**, 15 (2018)
283. Y.B.Peng, W.Zhang, T.C.Li, M.Y.Zhang, L.Wang, Y.Song, S.H.Hu, Y.Hu. *Int. J. Refract. Met. Hard Mater.*, **84**, 105044 (2019)
284. A.I.Gusev, A.A.Rempel, G.P.Shveikin. *Dokl. Akad. Nauk*, **357**, 490 (1997)
285. A.I.Gusev, A.A.Rempel, G.P.Shveikin. *Voprosy Atomnoi Nauki i Tekhniki. Ser. Materialovedenie i Novye Materialy*, **54**, 10 (1997)
286. A.A.Rempel, H.E.Schaefer, M.Forster, A.I.Girka. *Mater. Res. Soc. Symp. Proc.*, 299 (1994)
287. A.A.Rempel, W.Van Renterghem, A.A.Valeeva, M.Verwerft, S.Van Den Berghe. *Sci. Rep.*, **7**, 10769 (2017)
288. A.A.Rempel, W.Sprengel, K.Blaurock, K.J.Reichle, J.Major, H.E.Schaefer. *Phys. Rev. Lett.*, **89**, 185501 (2002)
289. H.S.Do, B.J.Lee. *Sci. Rep.*, **8**, 1 (2018)
290. C.Lu, T.Yang, K.Jin, G.Velisa, P.Xiu, M.Song, Q.Peng, F.Gao, Y.Zhang, H.Bei, W.J.Weber, L.Wang. *Mater. Res. Lett.*, **6**, 584 (2018)
291. S.Q.Xia, Z.Wang, T.F.Yang, Y.Zhang. *J. Iron Steel Res. Int.*, **22**, 879 (2015)
292. S.Q.Xia, X.Yang, T.F.Yang, S.Liu, Y.Zhang. *JOM*, **67**, 2340 (2015)
293. C.Lu, L.Niu, N.Chen, K.Jin, T.Yang, P.Xiu, Y.Zhang, F.Gao, H.Bei, S.Shi, M.R.He, I.M.Robertson, W.J.Weber, L.Wang. *Nat. Commun.*, **7**, 1 (2016)
294. K.Jin, C.Lu, L.M.Wang, J.Qu, W.J.Weber, Y.Zhang, H.Bei. *Scr. Mater.*, **119**, 65 (2016)
295. T.N.Yang, C.Lu, G.Velisa, K.Jin, P.Xiu, Y.Zhang, H.Bei, L.Wang. *Scr. Mater.*, **158**, 57 (2019)
296. Y.Zhang, G.M.Stocks, K.Jin, C.Lu, H.Bei, B.C.Sales, L.Wang, L.K.Béland, R.E.Stoller, G.D.Samolyuk, M.Caro, A.Caro, W.J.Weber. *Nat. Commun.*, **6**, 1 (2015)
297. Y.Zhang, K.Jin, H.Xue, C.Lu, R.J.Olsen, L.K.Beland, M.W.Ullah, S.Zhao, H.Bei, D.S.Aidhy, G.D.Samolyuk, L.Wang, M.Caro, A.Caro, G.M.Stocks, B.C.Larson, I.M.Robertson, A.A.Correa, W.J.Weber. *J. Mater. Res.*, **31**, 2363 (2016)
298. F.Granberg, K.Nordlund, M.W.Ullah, K.Jin, C.Lu, H.Bei, L.M.Wang, F.Djurabekova, W.J.Weber, Y.Zhang. *Phys. Rev. Lett.*, **116**, 135504 (2016)
299. G.S.Jawaharram, C.M.Barr, A.M.Monterrosa, K.Hattar, R.S.Averback, S.J.Dillon. *Acta Mater.*, **182**, 68 (2020)
300. F.F.Komarov, S.V.Konstantinov, A.D.Pogrebnyak. *Dokl. Akad. Nauk Belorusi*, **59**, 24 (2015)
301. F.F.Komarov, A.D.Pogrebnyak, S.V.Konstantinov. *Zh. Techn. Fiz.*, **85**, 105 (2015)
302. S.Zhao, Y.Zhang, W.J.Weber. In *Reference Module in Materials Science and Materials Engineering*. (Elsevier, 2020)
303. T.Egami, W.Guo, P.D.Rack, T.Nagase. *Metall. Mater. Transact.*, **45**, 180 (2014)
304. P.J.Barron, A.W.Carruthers, J.W.Fellowes, N.G.Jones, H.Dawson, E.J.Pickering. *Scr. Mater.*, **176**, 12 (2020)
305. A.A.Rempel, A.A.Valeeva. *Russ. Chem. Bull., Int. Ed.*, **68**, 2163 (2019)
306. S.M.Barinov, V.S.Komlev. *Biokeramika na Osnove Fosfatov Kal'tsiya (Bioceramics Based on Calcium Phosphates)*. (Moscow: Nauka, 2005)
307. S.V.Rempel, E.A.Bogdanova, A.A.Valeeva, H.Schroettner, N.A.Sabirzyanov, A.A.Rempel. *Inorg. Mater.*, **52**, 476 (2016)
308. S.V.Rempel, A.A.Valeeva, E.A.Bogdanova, H.Schroettner, N.A.Sabirzyanov, A.A.Rempel. *Mendeleev Commun.*, **26**, 543 (2016)
309. S.V.Rempel, A.A.Valeeva, E.A.Bogdanova, N.A.Sabirzyanov. *Lett. Mater.*, **7**, 170 (2017)
310. S.V.Rempel, D.A.Eselevich, A.A.Valeeva, A.A.Rempel. *Inorg. Mater.*, **54**, 898 (2018)
311. A.A.Egorov, V.V.Smirnov, V.S.Komlev, S.M.Barinov. *Onkokhirurgiya (Oncosurgery)*, **1**, 87 (2013)
312. M.Tsukada, M.Wakamura, N.Yoshida, T.Watanabe. *J. Mol. Catal. A: Chem.*, **338**, 18 (2011)
313. J.Xie, X.Meng, Z.Zhou, P.Li, L.Yao, L.Bian, X.Gao, Y.Wei. *Mater. Lett.*, **110**, 57 (2013)
314. A.Farzin, M.Ahmadian, M.H.Fathi. *Mater. Sci. Eng. C*, **33**, 2251 (2013)
315. S.H.Chang, S.K.Wu, B.S.Liao, C.H.Su. *Appl. Surf. Sci.*, **515**, 146044 (2020)
316. V.Braic, M.Balaceanu, M.Braic, A.Vladescu, S.Panseri, A.Russo. *J. Mech. Behav. Biomed. Mater.*, **10**, 197 (2012)
317. M.Todai, T.Nagase, T.Hori, A.Matsugaki, A.Sekita, T.Nakano. *Scr. Mater.*, **129**, 65 (2017)
318. P.Edalati, R.Floriano, Y.Tang, A.Mohammadi, K.D.Pereira, A.D.Luchessi, K.Edalati. *Mater. Sci. Eng. C*, **112**, 110908 (2020)
319. W.Y.Ching, S.San, J.Brechtl, R.Sakidja, M.Zhang, P.K.Liaw. *npj Comput. Mater.*, **6**, 1 (2020)
320. D.C.Tsai, Y.L.Huang, S.R.Lin, S.C.Liang, F.S.Shieu. *Appl. Surf. Sci.*, **257**, 1361 (2010)
321. C.H.Lai, M.H.Tsai, S.J.Lin, J.W.Yeh. *Surf. Coat. Technol.*, **201**, 6993 (2007)
322. P.K.Huang, J.W.Yeh. *Surf. Coat. Technol.*, **203**, 1891 (2009)
323. S.C.Liang, Z.C.Chang, D.C.Tsai, Y.C.Lin, H.S.Sung, M.J.Deng, F.S.Shieu. *Appl. Surf. Sci.*, **257**, 7709 (2011)
324. P.K.Huang, J.W.Yeh. *Thin Solid Films*, **518**, 180 (2009)
325. V.Dolique, A.L.Thomann, P.Brault, Y.Tessier, P.Gillon. *Mater. Chem. Phys.*, **117**, 142 (2009)
326. C.T.Lee, W.H.Cho, M.H.Shiao, C.N.Hsiao, K.S.Tang, C.C.Jaing. *Proc. Eng.*, **36**, 316 (2012)
327. S.Y.Chang, S.Y.Lin, Y.C.Huang, C.L.Wu. *Surf. Coat. Technol.*, **204**, 3307 (2010)
328. V.V.Kudinov, V.M.Ivanov. *Nanesenie Plazmoi Tugoplavkikh Pokrytii (Plasma Application of Refractory Coatings)*. (Moscow: Mashinostroenie, 1981)
329. Yu.A.Kharlamov, Yu.S.Borisov *Avtomaticheskaya Svarka*, (6), 19 (2001)
330. A.I.bushma, A.T.Zel'nichenko, I.V.Krivtsun. *Avtomaticheskaya Svarka*, (5), 14 (2004)
331. A.L.Borisova, L.I.Adeeva, V.Sladkov. *Avtomaticheskaya Svarka*, (4), 26 (1997)
332. V.V.Kudinov, P.Yu.Pekshev,, V.E.Belashchenko, O.P.Solonenko, V.A.Safiullin. *Nanesenie Pokrytii Plasmoi (Plasma Coating)* (Moscow: Nauka, 1990)
333. Z.Zhang, D.E.J.Armstrong, P.S Grant. *Prog. Mater. Sci.*, **123**, 100807 (2022)
334. S.Zhao, Z.Li, C.Zhu, W.Yang, Z.Zhang, D.E.J.Armstrong, P.S.Grant, R.O.Ritchie, V.A.Meyers. *Sci. Adv.*, **7**, 3108 (2021)
335. I.A.Balyakin, A.A Rempel. *Dokl. Phys. Chem.*, **502**, 11 (2022) 5021
336. W.Ding W, N.Liu , J.Fan, J.Cao, X.Wang. *Intermetallics*, **129**, 107027 (2021)
337. X.W.Nie, M.D.Cai, S.Cai. *Int. J. Refract. Met. Hard Mater.*, **98**, 105568 (2021)

338. H.Zhang, B.Zhao, F.Z.Dai, H.Xiang, Z.Zhang, Y.Zhou. *J. Mater. Sci. Technol.*, **77**, 58 (2021)
339. D.Liu, Y.Wang., F.Zhou, B.Xu, B.Lv. *Ceram. Int.*, 47, 29960 (2021)
340. C.T.Chiu, Y.J Teng., B.H.Dai, I.Y.Tsao, W.C.Lin, K.W.Wang, L.C.Hsu, Y.C.Chang, C.T.Li, H.T.Thai, C.Y.Chiang, W.H.Hung. *Mater. Chem. Phys.*, **275**, 125274 (2022)
341. W.Li, D.Xie, D.Li, Y.Zhang, Y.Gao, P.K.Liaw. *Prog. Mater. Sci.*, **118**, 100777 (2021)
342. A.Ostovari Moghaddam, N.A.Shaburova, M.N.Samodurova, A.Abdollahzadeh, E.A.Trofimov. *J. Mater. Sci. Technol.*, **77**, 131 (2021)
343. E.J.Pickering, A.W.Carruthers, P.J.Barron, S.C.Middleburgh, D.E.J.Armstrong, A.S.Gandy. *Entropy*, **23**, 98 (2021)
344. D.Castro, P.Jaeger, A.C.Baptista, J.P.Oliveira. *Metals*, **11**, 648 (2021)
345. F.Marques, M.Balcerzak, F.Winkelmann, G.Zepon, M.Felderhoff. *Energy Environ. Sci.*, 14, 5191 (2021)
346. K.N.Kumar, K.Biswas, J.-W.Yeh, S.Sharma, C.S.Tiwary. *Nano Energy*, **8**8, 106261 (2021)
347. H.Li, J.Lai, Z.Li, L.Wang. *Adv. Funct. Mater.*, **31**, 2106715 (2021)
348. J.K.Pedersen, T.A.A.Batchelor, D.Yan, L.E.J.Skjegstad, J.Rossmeisl. *Curr. Opin. Electrochem.*, **26**, 100651 (2021)
349. K.Li, W.Chen. *Mater. Today Energy*, **20**, 100638 (2021)
350. Y.Zhang, D.Wang, S.Wang. Small, **18**, 2104339 (2022)
351. T.Löffler, A Ludwig, J.Rossmeisl, W.Schuhmann. *Angew. Chem., Int. Ed.*, **60**, 26894 (2021)
352. X.Wang, W.Guo, Y.Fu. *J. Mater. Chem. A*, **9**, 663 (2021)